Regulation of microtubule sliding and its effect on mitotic spindle length in human retinal cells RPE-1

Ponjavić, Ivana

University of Zagreb

FACULTY OF SCIENCE
DEPARTMENT OF BIOLOGY

Ivana Ponjavić

REGULATION OF MICROTUBULE SLIDING AND ITS EFFECT ON MITOTIC SPINDLE LENGTH IN HUMAN RETINAL CELLS RPE-1

DOCTORAL THESIS

Zagreb, 2023.

University of Zagreb

PRIRODOSLOVNO-MATEMATIČKI FAKULTET
BIOLOŠKI ODSJEK

Ivana Ponjavić

REGULACIJA KLIZANJA MIKROTUBULA TE UTJECAJ NA DULJINU DIOBENOG VRETENA U STANICAMA RETINE ČOVJEKA RPE-1

DOKTORSKI RAD

Zagreb, 2023.

This work was done in laboratory of Iva M. Tolić, PhD, Senior Research Group Leader at Ruđer Bošković Institute, Zagreb, under supervision of Iva M. Tolić, PhD, Senior Research Group Leader. As a part of Postgraduate doctoral programme of Biology, this thesis is submitted for review to Department of Biology at Faculty of Science, University of Zagreb in order to achieve the academic degree Doctor of Biology.

Supervisor biography

Professor Iva M. Tolić was born in Zagreb, Croatia. She graduated Molecular biology at Faculty of Science, University of Zagreb, Croatia in 1996. During graduate studies, she worked as Research assistant in the group of Prof. Nenad Trinajstić, Ruđer Bošković Institute. Her PhD work was done with Prof. Ning Wang, Harvard School of Public Health, Boston, USA. She achieved the academic degree Doctor of biology at University of Zagreb in 2002. After this, she worked as a postdoctoral fellow with Prof. Kirstine Berg-Sørensen, Niels Bohr Institute, Copenhagen, Denmark and later with Prof. Francesco Pavone, LENS – European Laboratory for Non-Linear Spectroscopy, Florence, Italy. From 2005 until 2014 she worked as a Research Group Leader at Max Planck Institute of Molecular Cell Biology and Genetics in Dresden, Germany. Her research areas are mitosis, mitotic spindle mechanics, microtubules, motor proteins and other processes in the cell that rely on cytoskeletal components and motor proteins. Professor Tolić has received 15 research grants including the prestigious projects funded by the European Research Council (ERC), Consolidator and Synergy grants. She has published more than 90 papers in peer-reviewed journals including Science, Cell, and Nature Cell Biology, cited more than 4400 times, and served as reviewer for these and various other journals. She has been elected to EMBO and Academia Europaea membership and received numerous awards such as the Ignaz Lieben Award of the Austrian Academy of Sciences and European Biophysical Societies Association (EBSA) Young Investigators' Medal and Prize. To this date she has mentored 12 PhD and 23 Master theses. As an invited speaker, she has participated in more than 100 conferences and research seminars worldwide. She organized several scientific meetings including the EMBO Conference on Meiosis in 2017 and Mitotic spindle: From living and synthetic systems to theory in 2019, 2021 and 2023. Currently, professor Tolić is a Senior Research Group Leader with tenure at Ruđer Bošković Institute in Zagreb.

Acknowledgements

I would like to express my deepest gratitude to my PhD mentor Iva Tolić for opportunity to work on exciting scientific projects with amazing people. Thank you for your patience, guidance and all of the constructive criticism that helped me in my scientific development. Your passion and positive attitude towards everything that you do is empowering and inspirational.

Special thanks to Kruno Vukušić, who was my second mentor from the moment I came to the lab for everything that I learned from you troughout all these years and for being a true friend.

The biggest thanks go to Monika and Mateja for laughing till out stomach hurts even on the hardest days in the lab. Our friendship is the most important thing for me that I got from working in the lab.

Huge thanks to all of the great lab partners that I've met during the years here, specially to Snješka, Jurica and Martina.

Thanks to Ivana Šarić for being my lab mom and comfort person from the first day I got here and also Juraj Simunić for showing me that a great scientist could also be a relaxed and fun person.

Thanks to Nenad Pavin group for all of the helpful discussions and insights.

Big thanks go to all the professors at Faculty of Science in Zagreb who took part in developing my approach and mindset for the knowledge, research and passion towards science.

Thanks to my committee members Andreja Ambriović Ristov, Inga Urlić and Marin Barišić who took the time to read my thesis and for all the valuable comments.

I want to thank my love and my best friend in the world, Roko, for the past 10 years and I can't wait to see what we will acomplish together next.

Thanks to my amazing best friends for always being there for me and for so many beautiful memories.

Thanks to my sister Nikolina for being my best friend, my favourite person in the world and the person that I will always look up to even though you are younger.

Thanks to my grandma M. being my biggest inspiration in life.

Finally, I am thankful for my mom and dad, I am truly blessed with you as my parents. Thank you for making my life beautiful and always pushing me to chase my dreams.

University of Zagreb
Faculty of Science
Department of Biology

Doctoral thesis

Regulation of microtubule sliding and its effect on mitotic spindle length in human retinal cells RPE-1

Ivana Ponjavić

Ruđer Bošković Institute

Poleward flux of the microtubules in the mitotic spindle is a complex process driven by multiple motor proteins driving sliding of overlapping microtubules (MTs). However, coordination of the sliding in the midzone with the MT depolymerization at the pole remains unknown. Here I show, by using speckle microscopy to measure flux of individual MTs, that after kinesin-5 (EG5) inhibition while the spindle is collapsing, kinetochore fiber (k-fiber) movement away from the midplane is not impaired, however, bridging fiber movement from the midplaine is 30% slower when compared to the untreated metaphase spindles suggesting that sliding of overlapping MTs is impaired. At the same time poleward flux is similar as in untreated metaphase spindles. After dynein inhibition with Ciliobrevin D, the spindle retains its length but the bridging fiber overlap length is reduced and its connection with k-fibers is perturbed. Furthermore, k-fiber flux is significantly reduced, suggesting that dynein acts as a crosslinker of bridging and k-fibers. When EG5 is inhibited together with kinesin family member 4A (KIF4A), bridging fiber and k-fiber movement away from the midplane is significantly reduced, indicating that these two motors act together to slide overlapping MTs. Taken together, our results demonstrate that EG5 alone has a role in the sliding of antiparallel MTs and that in metaphase EG5 and KIF4A in the overlaps of the bridging fibers generate sliding forces which are transmitted to the associated k-fibers through dynein. We propose that the spindle consists of two mechanically distinct parts, the midzone part which remains functional during collapse, and the pole-proximal part of the spindle which is shortened during spindle collapse.

(126 pages, 59 figures, 2 tables, 162 references, original in English)

Key words: microscopy, mitosis, poleward flux, motor proteins, bridging fibers

Supervisor: Iva M. Tolić, PhD, Senior Research Group Leader

Reviewers:
1. Andreja Ambriović Ristov, PhD, Senior Research Group Leader
2. Inga Urlić, PhD, Associate Professor
3. Marin Barišić, PhD, Associate Professor

Sveučilište u Zagrebu
Prirodoslovno-matematički fakultet
Biološki odsjek

Doktorski rad

Regulacija klizanja mikrotubula te utjecaj na duljinu diobenog vretena u stanicama retina čovjeka RPE-1

Ivana Ponjavić

Institut Ruđer Bošković

Tok mikrotubula prema polu u mitotskom diobenom vretenu složen je proces kojeg pokreću višestruki motorni proteini koji pokreću klizanje preklapajućih mikrotubula. Međutim, koordinacija klizanja u središnjoj zoni vretena s depolimerizacijom mikrotubula na polu ostaje nepoznata. Ovdje pokazujem, korištenjem speckle mikroskopije za mjerenje toka pojedinačnih mikrotubula, da nakon inhibicije kinezina-5 (EG5) motornog proteina dok vreteno kolabira, kretanje kinetohornih vlakana (k-vlakana) od središnje ravnine nije poremećeno, međutim, kretanje premoščujućih vlakana je 30% sporije u usporedbi s netretiranim metafaznim vretenima što sugerira da je klizanje preklapajućih mikrotubula usporeno. U isto vrijeme tok mikrotubula prema polu sličan je kao i u netretiranim metafaznim vretenima. Nakon inhibicije dineina Ciliobrevinom D, vreteno zadržava svoju duljinu, ali se duljina preklapanja premosnog vlakna smanjuje i njegova veza s k-vlaknima je poremećena. Nadalje, protok k-vlakana značajno je smanjen, što sugerira da dinein djeluje kao poprečni povezivač premošćujućih i k-vlakana. Kada je EG5 inhibiran zajedno s kinezinom-4A (KIF4A), kretanje premosnih vlakana i k-vlakana od središnje ravnine je značajno smanjeno, što ukazuje da ova dva motora djeluju zajedno kako bi klizali mikrotubule koji se preklapaju. Zajedno, moji rezultati pokazuju da EG5 sam ima ulogu u klizanju antiparalelnih mikrotubula te da u metafazi EG5 i KIF4A u preklapanjima premosnih vlakana stvaraju sile klizanja koje se prenose na pridružena k-vlakna preko dineina. Predlažem da se vreteno sastoji od dva mehanički različita dijela, dijela srednje zone koji ostaje funkcionalan tijekom kolapsa i polu-proksimalnog dijela vretena koji se skraćuje tijekom kolapsa vretena.

(126 stranica, 59 slika, 2 tablice, 162 literaturna navoda, jezik izvornika engleski)

Ključne riječi: mikroskopija, mitoza, motorni proteini, diobeno vreteno, tok mikrotubula

Mentor: dr. sc. Iva M. Tolić, znanstvena savjetnica u trajnom izboru

Ocjenjivači:
1. Dr. sc. Andreja Ambriović Ristov, znanstvena savjetnica u trajnom izboru
2. Dr. sc. Inga Urlić, Izvanredni profesor
3. Dr. sc. Marin Barišić, Izvanredni profesor

Table of Contents

1 INTRODUCTION

There is only one possible way to make a new cell and that is to duplicate a cell that is already there. Every living organism is a product of cell duplication and growth. Essential mechanism by which all living organisms reproduce is a complex cycle called cell cycle. The cell cycle of most eukaryotic cells is composed of four phases. The main events of cell cycle appear during S phase (for synthesis), in which DNA replication occurs, and also during M phase when duplicated chromosomes divide into two daughter cells. In most cells, there are two G (for gap) phases, which separate the S phase and M phase events. G1, S and G2 phase belong to the interphase while the M phase consists of mitosis (nuclei division) and cytokinesis (cytoplasm division) (Alberts et al., 2014). In most eukaryotic cells, the nuclear envelope breakdown at the end of the first mitotic stage, prophase, marks the start of prometaphase, during which mitotic spindle assembly takes place, microtubules (MTs) reconstruct, and chromosomes begin to congregate in the metaphase plate. Sister chromatids must be appropriately attached to the opposing spindle poles because during metaphase, chromosomes are aligned at the spindle's central plane. Sister chromatids can split during anaphase following correct chromosomal congression thanks to securin ubiquitination that leads to separase activation and consequent cleavage of cohesin that keeps sister chromatids together. Chromosome decondensation, nuclear envelope reemergence, and cytoskeleton reorganization all take place during telophase. In the end, cytokinesis results in cytoplasmic division of the cell (Alberts et al., 2014).

The mitotic spindle, a structure made of MTs and related proteins, controls nearly all mitotic events. Its function is to precisely divide chromosomes between two daughter cells (Pavin & Tolić, 2016). Tubulin subunits are polymerized to form hollow cylindrical proteins called MTs. The tubulin subunit is made up of two noncovalently bound globular proteins named α-tubulin and β-tubulin that are closely related to one another. 13 parallel protofilaments form one MT, which is thereafter made up of a hollow cylindrical structure (Akhmanova & Steinmetz, 2008). MT ends with the β-subunits exposed are referred to as plus (+) ends, while those with the α-subunits exposed are referred to as minus (-) ends (Alberts et al., 2014). We can distinguish between parallel and antiparallel fibers based on the MT orientation. Kinetochore fibers (k-fibers), which attach with their (+) ends to the kinetochores, the protein complexes on the chromosome, are the most stable and essential fibers (Musacchio & Desai,

2017). The mitotic spindle can connect with chromosomes thanks to these k-fiber attachments. According to electron microscopy, human HeLa cells' k-fibers have 12–22 parallel MTs connected together (Wendell et al., 1993). A mitotic spindle also comprises interpolar and astral MTs in addition to k-fibers. Astral MTs extend from the spindle poles into the cytoplasm where they interact with the cell cortex and play a role in spindle placement inside the cell. Interpolar MTs are arranged into antiparallel bundles as they overlap at the spindle's center (Alberts et al., 2014).

Mitotic spindle MTs undergo continuous poleward flux, whose driving force and function in humans still remains unclear. MT poleward flux is an evolutionarily conserved process in metazoan spindles and is defined as a continuous poleward motion of MTs, whereby the whole k-fiber is shifted toward the pole. It is typically coordinated with addition of new tubulin subunits at the MT plus-ends and their removal at the MT minus-ends at spindle poles. This complex process is driven and regulated by multiple motor proteins (Ganem et al., 2005; Miyamoto et al., 2004a; Rogers et al., 2003; Steblyanko et al., 2020a). MT-flux was suggested to be involved in a number of mitotic processes, albeit its precise function is still unknown. As an illustration, MT-flux has been connected to the control of spindle length (Fu et al., 2015; Gaetz & Kapoor, 2004; Renda et al., 2017; Rogers et al., 2003). Its function, however, is still debatable because reducing MT-flux in human cells either had no effect on spindle length (Ganem et al., 2005; K. Jiang et al., 2017) or resulted in shorter spindles (J. Fu et al., 2015; Maffini et al., 2009) while attenuation of MT-flux led to spindle elongation in Drosophila embryos (Rogers et al., 2003) and Xenopus egg extracts (Gaetz & Kapoor, 2004). According to a theory based on electron microscope images of Xenopus extract spindles (Ohi et al., 2003), poleward flux of k-fibers is produced by motor-driven sliding of k-fibers with respect to interpolar MTs (T. J. Mitchison, 2005). Laser cutting of these fibers in human cells has shown the mechanical interaction between k-fibers and the related interpolar bundles known as bridge fibers (Kajtez et al., 2016a).

One of the primary regulators of the formation of the bipolar spindle is the MT motor protein EG5 (kinesin-5) (Tanenbaum & Medema, 2010b). EG5 has the ability to pull MTs apart and crosslink them into an antiparallel arrangement to push centrosomes outward (Kapitein et al., 2005; Kashina et al., 1996). When EG5 activity is inhibited, bipolar spindle formation is prevented and cells are arrested in mitosis with unseparated centrosomes. EG5’s outward-directed pushing force on spindle poles can be antagonized by minus-end-directed motors. In

human cells, as well as in Xenopus egg extracts, inhibition of the minus-end-directed motor dynein efficiently rescues bipolar spindle assembly in the absence of EG5 activity, indicating that dynein antagonizes EG5 activity (T. J. Mitchison, 2005). Previous studies also showed that the sliding velocity was significantly reduced after simultaneous depletion of KIF4A and EG5 inhibition, which suggests that the origin of blocked spindle elongation seen after perturbations of KIF4A and EG5 is a result of a defective MT sliding (Vukušić et al., 2021).

Despite intense research on poleward flux in human cells, coordination of the sliding in the midzone with the MT depolymerization at the pole remains unknown. To answer some of the questions, the motivation of this research is to examine how moving of the spindle poles, caused by inhibitions of motor proteins, is connected with poleward flux. Recently developed speckle microscopy assay on spindles of human cells (Risteski et al., 2022), now allows us to measure the flux of individual bridging MTs (bMTs) and kinetochore MTs (kMTs) and further explore regulation of MT sliding and its effect on mitotic spindle length.

The model that will be used is a non-transformed human cell line RPE-1 (retinal pigmented epithelium, female) stably expressing CENP-A-GFP and centrin1-GFP (protein of a centrosome complex). The first step in this study will be imaging of control human non-transformed RPE-1 cells without modifications of protein function or concentration to determine the referent measurement of MT dynamics and to exclude the negative nonspecific effects of used inhibitors and siRNAs. I will image MT poleward flux in control cells using speckle microscopy assay on spindles of human cells which is based on a very low concentration (1 nM) of tubulin dye called SiR-tubulin. Next, the depletion or inhibition of proteins of interest will be performed using techniques of RNA interference and available small molecule inhibitors of motor proteins. Main technique of protein perturbation will be by using small molecule inhibitors of mitotic kinesins which specifically interfere with protein function mainly by binding to important protein domains responsible for normal function of mitotic protein within the spindle. It is preferred to use inhibitors if they are available because of the immediate effect on target protein as opposed to RNA interference (RNAi) which depletes protein levels in a cell using small interfering RNAs (siRNAs) which interfere with translation of protein by specifically binding to mRNA, where the effect can be seen in 48 or 72 hours after the depletion. To determine the efficiency of protein depletion and inhibition I will use an immunostaining of cells to determine that protein is not localizing to the mitotic spindle as in control cells, where applicable. The obtained results will be compared with control cells to

determine if any of the candidate proteins have a significant effect on parameters of poleward flux. For proteins that are affecting poleward flux velocities, the inhibition and the depletion will be performed again but this time using RPE-1 cell line with stable expression of Protein Regulator of Cytokinesis 1 (PRC1) which stabilizes antiparallel interdigitating MTs within the overlap bundles to investigate bridging fibers in these treatments. Also, to check if candidates are affecting global structure of antiparallel bridging MTs as well as kinetochore MTs, MT fixation combined with STED microscopy of mitotic spindle will be used enabling superresolution imaging of mitotic spindle MTs. Furthermore, for proteins that are showing similar and significant effects on poleward flux of the bridging or kinetochore fibers, the combined inhibition will be performed to examine if these proteins work by the same or similar mechanism in the mitotic spindle thereby defining redundant pathways. After each experimental approach, the velocities for poleward flux of the bridging fibers and poleward flux of the kinetochore fibers will be calculated and compared with controls. The experimental data from modified cells is going to be obtained on a large number of cells, showed both, graphically and statistically, and compared to control cells. Finally, the goal is to determine which proteins are responsible for coordination of the sliding in the midzone with the MT depolymerization at the pole.

The main conceptual advance of this work is the finding of novel mechanisms which contribute to poleward flux in human cells and were not previously included in existing models. Future work should reveal what aberrations in this mechanism lead to errors in chromosome segregation in cells with unstable karyotypes in which misaligned chromosomes appear.

2 OVERVIEWS OF RESEARCH

2.1 Short history of cells as the basic units of life

A living system is one that has the capacity to both transfer genetic information to its offspring and catalyze metabolic activities. Such a system is designed to include the structures necessary for growth, development, and evolution. A cell, the smallest component of a multicellular organism or a fully functioning organism, is the basic unit of life. A membrane encloses the elements that give a system its life, and it also serves as a channel for communication between a cell's inside and exterior. There are hundreds of signaling pathways that coordinate the intricate life of a cell, from its membrane through its cytoskeleton and organelles, nucleus, and the genetic material contained within. The person first responsible for describing the cell as the basic unit of life was an architect, natural philosopher and scientist Robert Hooke. He first used the term in 1665, while looking at thin slices of cork (Figure 1a). His observations were soon extended to wood and plant tissue, as well as to fly's eye. About 10 years later, Leeuwenhoek's 1677 paper, the famous 'letter on the protozoa', gives the first detailed description of protists and bacteria living in a range of environments (Figure 1b).

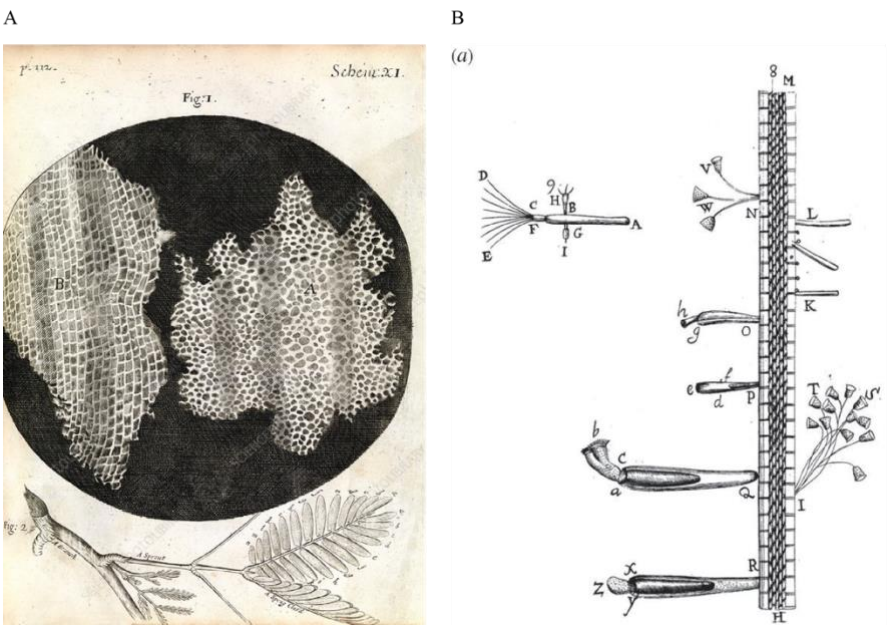

Figure 1. First view of the cells. A. Drawings of Hooke's sample of thin cork slice shows first insight into cellular organization (Hook, 1665). **B.** Drawings of rotifers, hydra and vorticellids

associated with a duckweed root, from a Delft canal by Leeuwenhoek, first live organisms observed under the microscope (Lane, 2015).

2.2 Visualising cells

Cells are small and complex systems and because of that it is hard to investigate their structure, discover molecular composition and even harder to find out how their different components function. Tools that we have determine what can we learn about cells and learning new super-resolution techniques recently resulted in major advantages in cell biology. Understanding of the structural organization of the cell is essential to learn how the cell works.

In order to understand modern cell biology, it is necessary to know something about its methods. Optical microscopy is the starting point because the development of cell biology began with the development of light microscopy, which is still an indispensable tool today. In recent years, optical microscopy has become even more important, owing to the development of methods for specific labeling and visualization of individual cellular components and the reconstruction of their three-dimensional architecture. An important advantage of optical microscopy is the fact that light is relatively indestructible. By labeling certain cell parts with fluorescent labels, such as intrinsically fluorescent proteins, we can observe their movement, dynamics and interaction in living cells.

Optical microscopy is limited in resolution by the wavelength of visible light. By using a beam of electrons instead of light, electron microscopy can visualize macromolecular complexes within cells at near-atomic resolution and in three dimensions. Although optical and electron microscopy are important methods, what makes them interesting is that they have allowed scientists to reveal a wealth of information about the structural architecture of the cell (Alberts et al., 2007). The scale between living cells and atoms, where the limit of visibility of the electron microscope is visible, is shown in Figure 2.

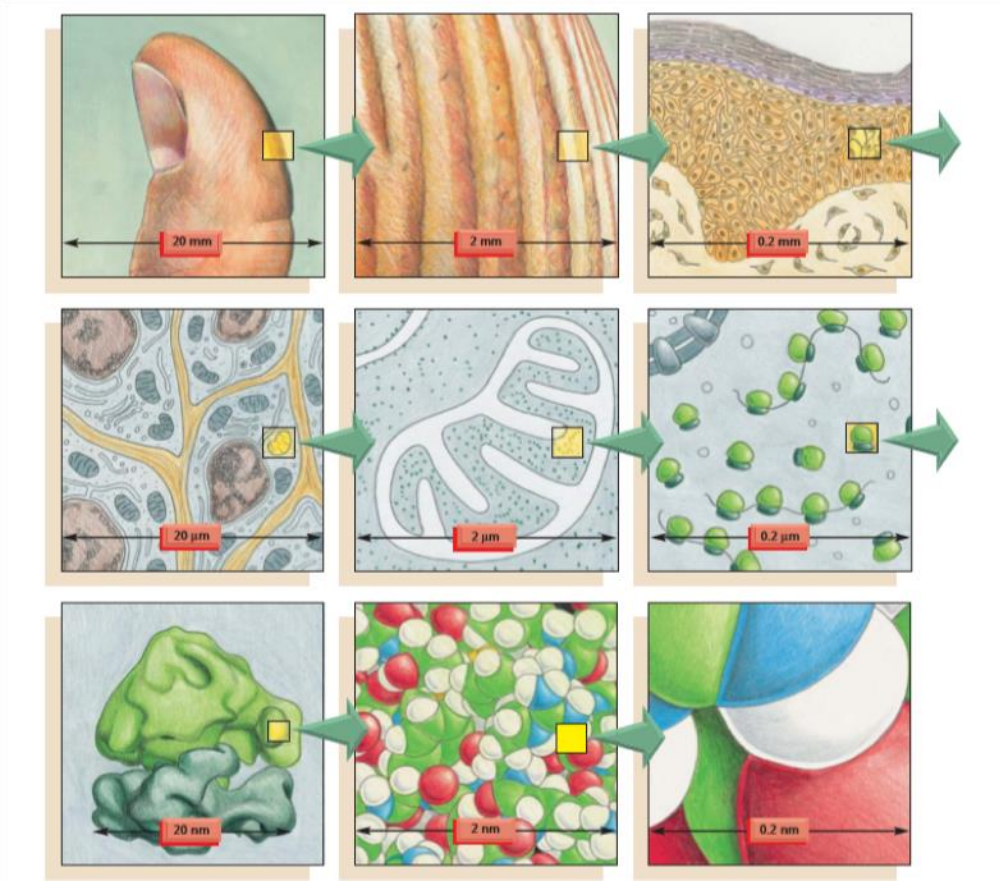

Figure 2. A scale between living cells and atoms. Each diagram shows an image magnified by a factor of 10 in an imaginary progression from the thumb, through skin cells, to ribosomes, clusters of atoms that form part of one of the many protein molecules in our body. The atomic details of macromolecules, which are shown in the last two panels, are mostly not visible even with an electron microscope (Alberts et al., 2007).

2.2.1 Fluorescent microscopy

Fluorescence microscopy is a sensitive method of studying the intracellular distribution of molecules. The use of fluorescence microscopes has an important role in the study of the dividing spindle (Balchand et al., 2016). When labeling molecules inside fixed and living cells, fluorescent dyes are used. Fluorescent dye absorbs light of one wavelength and emits light of another wavelength. Filters are used for visualization. The first filter allows the illumination of the sample with light of a wavelength that excites the fluorescent dye, while the second filter

allows the passage of a specific wavelength of light emitted by the fluorescent dye. Fluorescent dyes emit light of a longer wavelength after being excited by light of a shorter wavelength. Some of the fluorescent labels used are: FITC, rhodamine, Texas red, AMCA, Cy3 and Cy5, GFP. The GFP molecule is suitable for monitoring the position and movement of proteins in living cells (Figure 3). Today's recombinant DNA methods enable binding of the GFP molecule to any selected protein (Alberts et al., 2007). If the entrance aperture of the detector is located in the optical plane that is conjugate to the focal plane of the objective, the fluorescence microscope will still be called a confocal microscope. Confocal microscopy uses the features of fluorescence microscopy. Together with electronic analysis and image processing, obtaining images with more details and stronger contrast is achieved. A narrow beam of laser light of a specific wavelength is focused on a specific depth of the sample. The emitted light is collected by a detector (video camera). Before the emitted light reaches the detector, the fluorescent light emitted from the sample must pass through the confocal aperture. The confocal aperture is precisely located at the point where the light emitted from the selected sample depth is in focus. In this way, only the focused light emitted from the selected depth of the sample is detected, which achieves a sharper image than the image obtained with a standard fluorescence microscope. A series of images obtained from different depths can be used to reconstruct the three-dimensional structure of the sample being examined (Alberts et al., 2007).

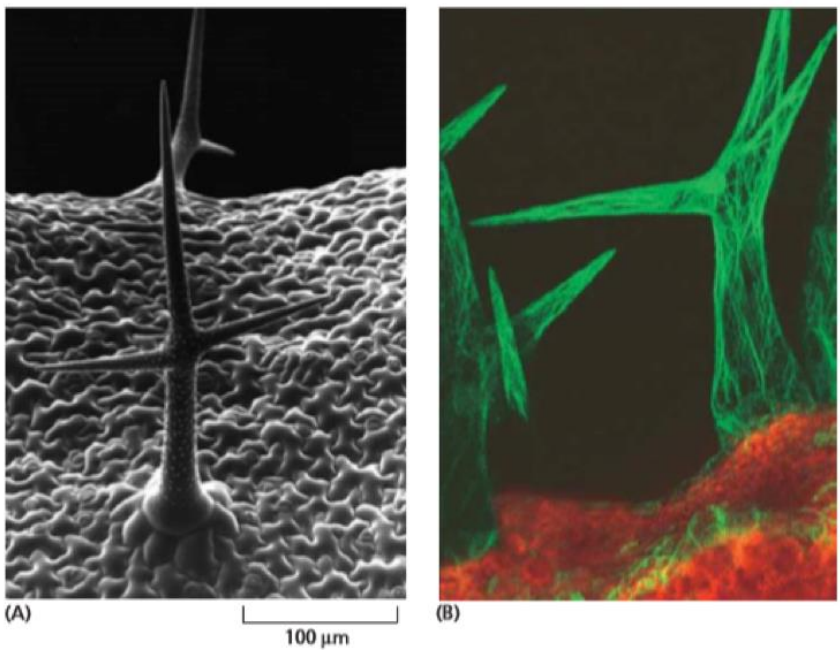

Figure 3. Proteins labeled with the GFP molecule. A. The upper leaf surface of Arabidopsis plants is covered with large branched unicellular hairs that rise from the surface of the

epidermis. These hairs, or trichomes, can be seen with a scanning electron microscope. **B.** If an Arabidopsis plant is transformed with a DNA sequence encoding talin (an actin-binding protein) fused to a DNA sequence encoding GFP, fluorescent talin binds to actin filaments in all living cells of the transgenic plant. Confocal microscopy can reveal the dynamics of the entire trichome actin cytoskeleton (A, property of Paul Linstead; B, property of Jaideep Mathur, adapted from: Alberts et al., 2007).

2.3 Cell cycle

The majority of eukaryotic cells go through a 24-hour cell cycle that can be loosely divided into two phases: interphase and the mitotic phase (M phase). A cell rearranges its interior during interphase, which occurs between two mitotic divisions. It also expands and gets ready for the following mitosis. During the S phase of interphase, when deoxyribonucleic acid (DNA) replication takes place, the majority of the cell cycle's changes manifest. The interphase also includes the G1 and G2 phases, during which the mass of the cell's proteins and organelles doubles (Alberts et al., 2014). Moreover, a cell can exit G1 phase and enter G0 phase, which is a resting phase that can last even longer until the cell cycle starts up again. The majority of cells transition from the G0 phase to the G1 phase, however others, known as post-mitotic cells, such as neurons, are metabolically active but do not divide (Uzman et al., 2000). As they offer the cell time to feed, expand, and regulate the accuracy of ongoing activities, G phases serve as a transitional phase between the S and M phases. Cells split to create two identical daughter cells during the M phase, which includes mitosis and cytokinesis. It's interesting to note that the cell spends more than 95% of its time in the interphase during the brief M phase (Figure 6) (Alberts et al., 2014). Although many eukaryotic species share conserved proteins and the fundamentals of the cell cycle, the process can vary greatly in some specifics, leading to the existence of numerous comparable principles that can exert the same function by various ways (J. Richard McIntosh et al., 2012).

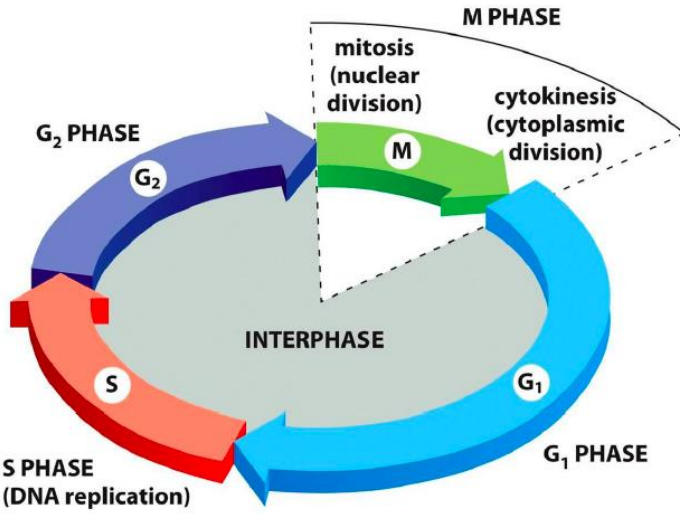

Figure 6. Overview of main phases of the cell cycle. Interphase can be defined as the time between two mitoses and it consists of three phases: S phase which includes DNA replication, G1 phase as the gap between M phase and S phase and G2 phase as the gap between S phase and M phase. The M phase consists of mitosis and cytokinesis (Alberts et al., 2014).

Cell cycle is regulated by surveillance systems that check the chronology, reliability, and correctness of key cell cycle events. If the cell experiences unfavorable conditions or it cannot complete a specific cell cycle phase, a regulation system is going to prevent the cell cycle to enter the next phase. Checkpoints are regulatory systems that prevent the cell cycle from moving on to the subsequent phase until the preceding phase's events are effectively completed (Figure 7). The aforementioned restriction point (or START) in late G1 is the first checkpoint; it keeps track of the cell's external environment as well as DNA integrity before committing it to cell cycle entrance and DNA replication. If DNA is not fully duplicated or has damage that has not been repaired, the second checkpoint at the G2/M transition prohibits entry into mitosis. The final checkpoint, also known as the spindle assembly checkpoint (or SAC), occurs at the metaphase-to-anaphase transition and ensures that the distribution of chromosomes to daughter cells is accurate by preventing sister chromatide separation unless all chromosomes are correctly attached to the mitotic spindle and aligned at the spindle equator (Alberts et al., 2017).

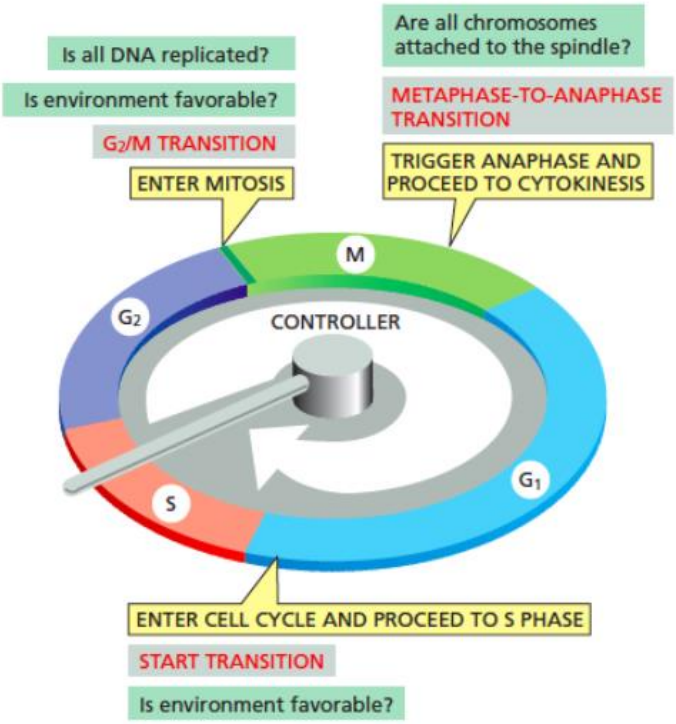

Figure 7. Control points or checkpoints in the cell cycle. G1 checkpoint makes sure that the conditions are appropriate for DNA duplication. G2 checkpoint checks whether DNA was duplicated without errors. Mitotic spindle checkpoint (checkpoint in mitosis) ensures that all chromosomes are properly attached to k-fibers and oriented in a way that they could be pulled to centers of new daughter cells at the end of mitosis (Alberts et al., 2017).

Cyclin dependent kinases (CDKs) are important players in the system that controls the cell cycle. They control important cell cycle activities such DNA replication, mitosis, and cytokinesis by phosphorylating specific intracellular proteins (Alberts et al., 2014; Galderisi et al., 2003). CDKs are constantly present in a cell but only become active during certain cycles. Although being in molar excess, the catalytic subunits remain inactive until they are associated with the appropriate cyclin subunits to form the cyclin-CDK complex (Alberts et al., 2014; (Barnum & O'Connell, 2014). Cyclin binding, CDK activating kinase (CAK) phosphorylation, regulatory inhibitory phosphorylation, and CDK inhibitor (CKI) binding are the four main mechanisms of CDK regulation (Alberts et al., 2014). Proteins called cyclins fluctuate in number during the cell cycle. They are created during a certain stage of the cell cycle and degraded once their function has been achieved. The serine and threonine residues of a target

protein are phosphorylated when the cyclins and CDKs that are produced specifically combine and become activated. The phosphorylated target protein carries out the activities that take place throughout the corresponding phases of the cell cycle (Asashima et al., 2010).

2.4 Mitosis

Condensed chromosomes move to the center of the cell during mitosis, when they separate into two daughter nuclei before cytokinesis (cell division), with the help of a dynamic mitotic spindle (Yanagida, 2014; Lodish, 2014) (Figure 8).

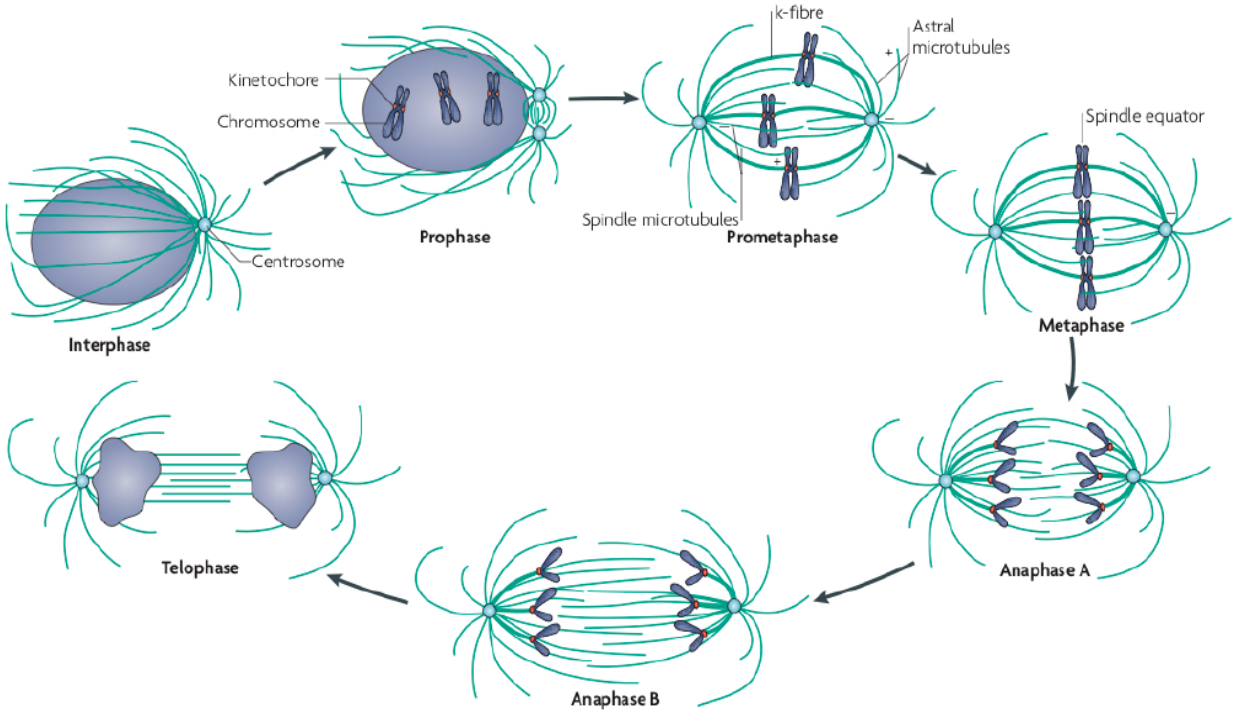

Figure 8. Phases of mitosis. Mitosis is divided into five stages: prophase, prometaphase, metaphase, anaphase and telophase followed by cytoplasmic division – cytokinesis (Walczak et al., 2010).

Prophase, the initial stage of mitosis, is characterized by the condensation of chromatin into distinct chromosomes, each of which has centromere regions where kinetochores assemble. As

prophase develops, each chromosome's length and thickness change, separating the DNA strands into discernible pieces. The nucleolus disperses as the chromatin condenses (Richard Mcintosh, 2016). Moreover, the nuclear envelope is intact during prophase, and the centrosome-like microtubule organizing centers (MTOCs) start to create the mitotic spindle outside the nuclear envelope (Wayne, 2010). When the MTs expand, centrosomes start to move to the cell's opposite poles, which causes the bipolar spindle to form (Wayne, 2010). Taken together, in prophase chromosomes consist of two sister chromatides, ready to be attached to MTs of the spindle, while outside of the nucleus centrosomes begin to separate and extensively nucleate radial network of MTs, thus starting the assembly of the mitotic spindle. The spindle experiences contractions and oscillations just before the next stage of mitosis, prometaphase (Figure 9), which is signaled by the collapse of the nuclear envelope or nuclear envelope breakdown (NEBD). Many proteins bind to the kinetochore within the centromeres during this phase, and chromosomes are starting to travel to the center of the cell by kinetochore MTs (Goodman, 2008). When all of the chromosome pairs are completely condensed, bound to the MTs of the mitotic spindle, and arranged at the central metaphase plate, metaphase has occurred. In order to draw the kinetochores toward the opposing spindle poles and create the tension that signifies that the sister chromatids have attained proper biorientation, the kinetochore fibers apply forces on them through the cohesin, a protein complex associated with chromosomes (Figure 9). In order to ensure that the sister chromatids are correctly positioned at the metaphase plate, the cell continuously monitors the attachments of MTs to the chromosomes (Malumbres, 2020; Musacchio & Salmon, 2007; Sacristan & Kops, 2015). The synchronized segregation of the sister chromatids during anaphase, the most beautiful stage of the cell cycle, is what makes it so spectacular (Figure 9). It is divided into two phases: anaphase A where chromosomes move poleward as a consequence of the k-fiber depolymerization at the plus and at the minus end (Mitchison et al., 1986), and anaphase B where the spindle elongates to additionally increase the distance between chromosomes (Asbury, 2017; Scholey et al., 2016). Telophase is the final phase of mitotic nuclear division. Sister chromatids reach their opposite poles during telophase, and the nuclear envelope enclosing the opposing chromosomal groups begins to take shape. The chromosomes start to decondense as the nuclear envelopes reform (McMillan, 2018). The cleavage furrow, an invagination of the cell membrane, draws

the plasma membrane toward the cell center to finish the cell cycle by compressing the cytoplasm into two lobes that are later divided into two cells during cytokinesis (Glotzer, 2004).

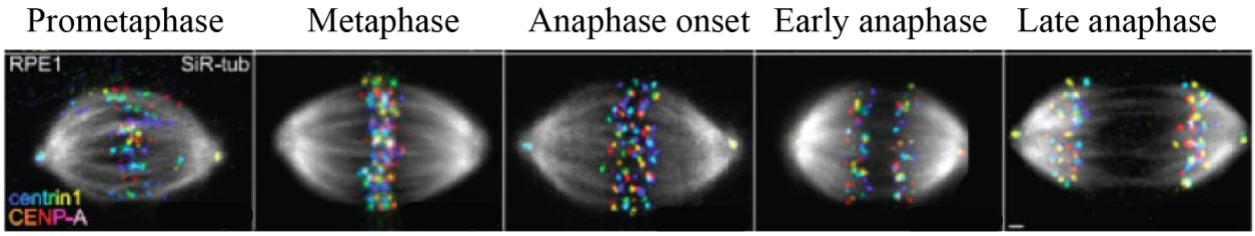

Figure 9. Various phases of mitosis. Spindles in hTERT-RPE1 cells expressing CENP-A-GFP and centrin1-GFP in different phases of mitosis. MTs are shown in gray (SiR-tubulin), and kinetochores/centrosomes are color-coded for depth (color bar) and filtered with a Gaussian blur (radius 0.7) (image was adapted from Trupinić et al., 2022).

2.5 Microtubules – structure, properties and dynamics

All eukaryotic cells depend on the ubiquitous cytoskeletal polymers known as MTs for survival. Here, I will focus on their involvement in the mitotic spindle because they are its core components determining both its organization and dynamics, despite the fact that they are an integral part of many biological processes and structures. Each MT is a dynamic, polar polymer with an outside diameter of 25 nm and is made up of 13 parallel, lateraly connected protofilaments (Downing & Nogales, 1999) (Figure 10). Each protofilament consists of a head-to-tail arrangement of αβ-tubulin heterodimers, each of which repeats every 8 nm, joined by non-covalent connections. All of the protofilaments within a MT have the same polarity because the subunits are orientated in the same direction throughout the whole protofilament, giving the MT as a whole an overall polarity (Akhmanova & Steinmetz, 2008). According to convention, the end with an exposed β-subunit is referred to as the plus-end and the end with an exposed α-subunit as the minus-end (Lodish et al., 2014). In addition to polarity, another crucial characteristic of MTs is their dynamics, which is affected by the guanosine triphosphate (GTP) nucleotide's binding and hydrolysis. In a heterodimer, both tubulins bind GTP, but only the α -tubulin subunit can hydrolyze it. The end of the MT will include GTP-containing subunits forming a GTP cap that stabilizes the end and enables ongoing development if the rate of addition of new subunits is rapid, in the way that new subunits are added before the GTP in the

previous ones hydrolysed. On the other hand, if the rate of addition of new subunits is low, GTP can hydrolyse before addition of new subunits, which causes conformational change in the tubulin subunits that forces protofilaments to aquire unstable curved shape subsequently leading to MT shortening (Desai & Mitchison, 1997). Dynamic instability is the ability of MTs to stochastically change between these states. The rapid interconversion from growth to shrinkage is known as catastrophe, while the opposite event is known as the rescue. The plus ends of MTs are where all these alterations tend to take place (Mitchison & Kirschner, 1984) (Figure 10).

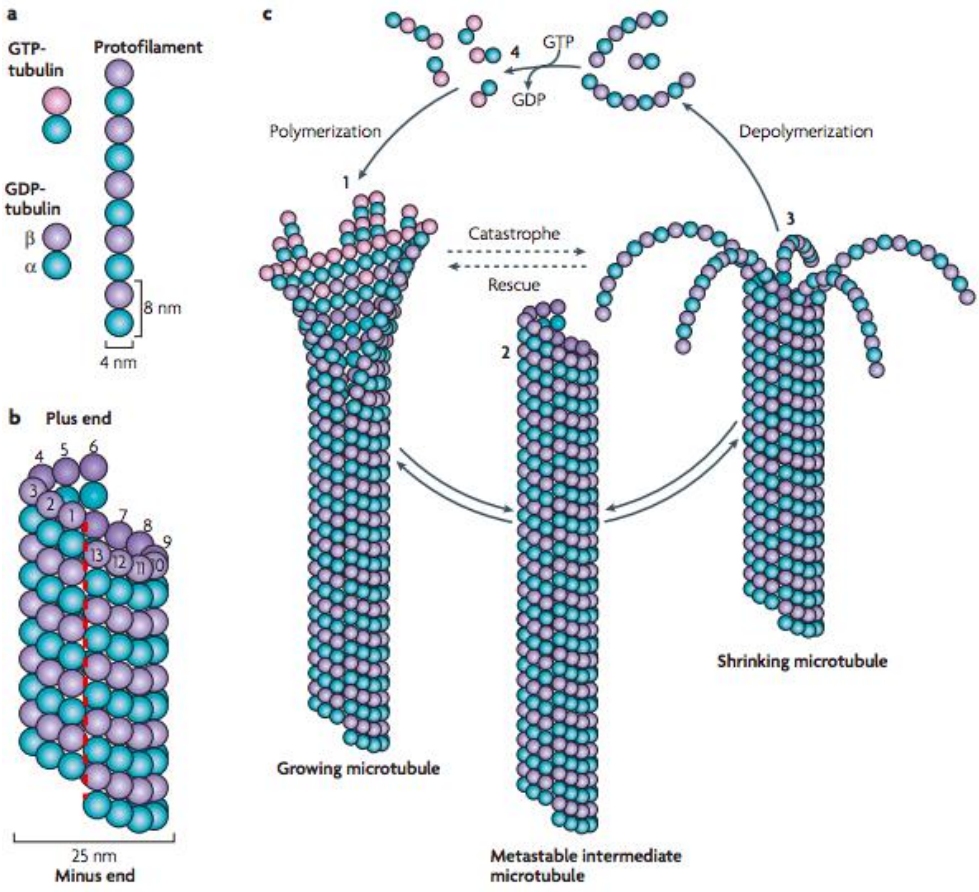

Figure 10. Structural and dynamic properties of microtubules. **A.** MTs are composed of stable α/β-tubulin heterodimers that are aligned in a polar head-to-tail fashion to form protofilaments. **B.** The cylindrical and helical MT wall typically comprises 13 parallelprotofilaments in vivo. **C.** Assembly–polymerization and disassembly–

depolymerization of MTs is driven by the binding, hydrolysis and exchange of a guanine nucleotide on the β-tubulin monomer (GTP bound to α-tubulin is nonexchangeable and is never hydrolysed) (Akhmanova & Steinmetz, 2008).

All MTs originate from structures known as microtubule-organizing centers (MTOCs), and spontaneous nucleation has no impact on the assembly of MTs in living organisms (Wiese & Zheng, 2006). Although there may be some exceptions, the major MTOC of an animal cell is known as the centrosome, and in most cases, the MT's minus end is situated close to the centrosome and its plus end radiates from it (McIntosh et al., 2012). The interphase radial array of MTs is produced when the centrosome is close to the nucleus (Lodish, 2014).

2.6 Different microtubule populations in the mitotic spindle

Kinetochore, nonkinetochore, and astral MTs are three distinct populations of MTs inside the mitotic spindle that are described by current models that accompany animal spindle topology (Figure 11) (Lodish, 2014). While coming from the same pool of tubulin subunits, they all have different architectures, dynamics, and mitotic spindle functions (S. Dumont & Mitchison, 2009).

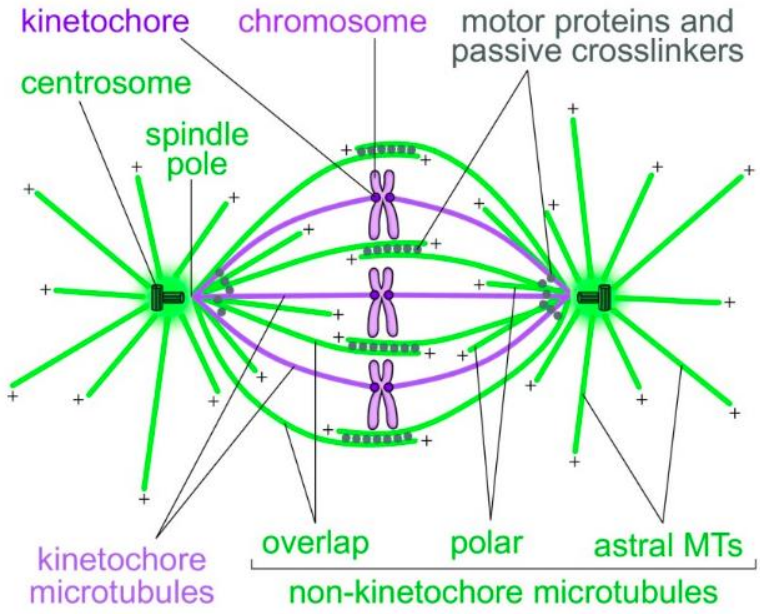

Figure 11. Textbook picture of the spindle. Kinetochore, nonkinetochore, and astral MTs are three distinct populations of MTs inside the mitotic spindle (Tolić, 2018).

Minus-ends of kinetochore MTs (kMTs) are located at or close to centrosomes, while plus-ends are embedded in the outer kinetochore layer (Figure 11). They appear to be essential for normal spindle operation because their primary purpose is to exert pulling pressures on chromosomes at their kinetochores, while some aspects of mitosis, such as the congression of chromosomes to the spindle's equatorial plane, can still occur without these MTs (Cai et al., 2009). As previously mentioned, they perform their tasks by applying pulling forces to sister chromatids during metaphase, and during anaphase, when cohesin between chromatids is destroyed, they pull split sister chromatids to different poles of the spindle. Also, they turn off the SAC, a unique signaling mechanism that is active on sister kinetochores when those kinetochores are not connected to MTs and when the kinetochores are not under enough strain (Dumont & Desai, 2012). According to the cell type being studied, the typical number of kMTs that bind to one kinetochore in mammalian cells ranges from 10 to 30 (McEwen et al., 1997; O'Toole et al., 2020). The majority of the MTs within one fiber are continuous from the kinetochore to the pole and run in parallel orientation. KMTs that are attached to the same kinetochore tend to group together to form a bundle known as a k-fiber. The interactions between the MTs within the fiber are weak along the k-fiber, with the exception of the vicinity of the spindle poles, where they are strong and evenly distributed at 50–100 nm apart (McDonald et al., 1992). These kMTs are not stationary, as was once believed, yet they have a dynamical property named poleward flux. At the plus ends of MTs, where they are attached to the kinetochore, polymerization takes place during poleward flux, while during stationary states like metaphase, depolymerization takes place at the minus ends of MTs, which are close to the spindle poles. As a result of this mechanism, kMT subunits are constantly moving poleward at a rate of 0.5 μm min-1 (Rogers et al., 2005). When steady state balancing at the kMT polymerizing plus-end is suppressed, flux is thought to be able to create force that can perform work (Waters & Salmon, 1997).

Astral MTs are another population of MTs that have been described in recent models of the mitotic spindle (aMTs). They are usually defined as MTs nucleated at centrosomes whose plus-ends go all the way to the cell cortex (S. Dumont & Mitchison, 2009) Figure 11). When compared to other populations of MTs, astral MTs grow and contract at very high rates - roughly 10-15 μm min^{-1} due to the dynamic instability of their plus-ends, but they do not emit flux because their minus-ends do not depolymerize (Waterman-Storer & Salmon, 1998). Last

MT population within spindle are nonkinetochore or interpolar MTs which are defined as all MTs within the body of mitotic spindle that are not kMTs (S. Dumont & Mitchison, 2009). The basic 'textbook' structure of the mitotic spindle so far was mainly visualized as in Figure 11, where k-fibers and interpolar MTs are completely separate and independent populations of MTs. However, recent electron microscopy studies gave us a more detailed insight into the structure of the spindle regarding MT spatial organisation and interactions between different MT populations. The connection between k-fibers and interpolar MTs was explored recently. Observations that confirmed relationship between k-fibers and interpolar MTs were made by fluorescence microscopy where bundles of interpolar MTs were seen connecting k-fibers of sister kinetochores in metaphase spindles acting as a bridge between them and therefore they were named the bridging fibers (Figure 12) (Kajtez et al., 2016b). Laser ablation experiments in HeLa (cervical cancer cells taken from Henrietta Lacks), PtK1 (female rat kangaroo kidney epithelial cells) and U2OS (human osteosarcoma cells) cells demonstrated tight physical coupling of k-fibers and bridging fibers, as they moved outward together as a single mechanical unit after k-fiber cutting (Buđa et al., 2017; Kajtez et al., 2016b).

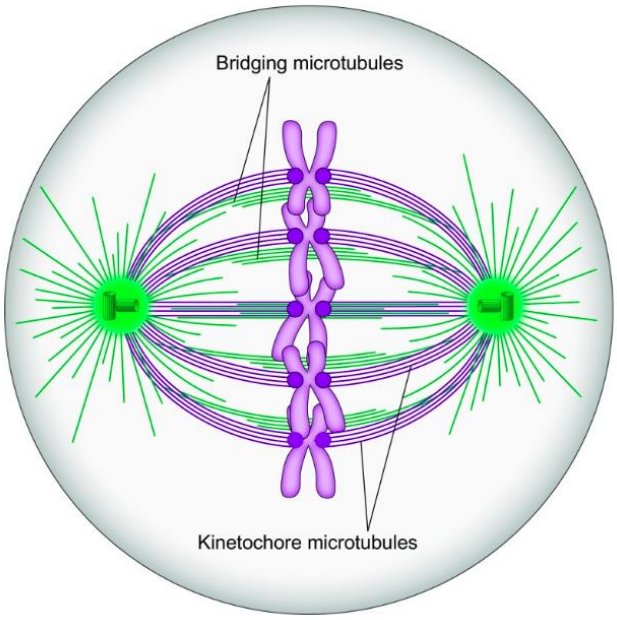

Figure 12. Updated scheme of the spindle. The spindle in a human somatic cell is made of modules consisting of a pair of sister kinetochore fibers and a bridging fiber that connects them (Tolić, 2017).

According to physical modeling, bridging fibers are essential structural components that balance forces on kinetochores and at the poles, allowing the spindle to assume its rounded shape and maintaining the tension between sister kinetochores, which has physiological significance for the cell as tension is monitored by the SAC (Kajtez et al., 2016b; Musacchio & Salmon, 2007). The kinetochore fiber is thus under tension in the region between the kinetochore and the junction points, and under compression along rest of its length, between the junction and the spindle pole, where lateral interaction between bridging fibers and k-fibers takes place (Tolić, 2018). The role of bridging fibers in driving spindle elongation in anaphase through MT sliding, which is driven by plus-end directed motors localized within the bridge, was revealed by laser ablation experiments of outer k-fibers in early anaphase, which showed kinetochores can separate without connection to one pole but cannot if the bridging fiber between them was also ablated (Vukušić et al., 2017).

2.7 Microtubule associated proteins

Microtubule associated proteins (MAPs) are proteins that interact with MTs and can function as their stabilizers, destabilizers, capping proteins and bundling/crosslinkers (Alberts et al., 2017). We can divide MAPs into four groups. The first group consists of crosslinking side-binding proteins that stabilize and align MTs in specific structures. The second group of plus-end tracking proteins (+TIPs) either regulate MT growth at plus-end or link plus-ends to the other cellular structures. The third group consists of enzymes that regulate MT destabilisation and the fourth of motor proteins that move along MTs powered by chemical energy (Lodish, 2014). MAPs are essential for controling the MT dynamics and also for generating the forces for proper function of the mitotic spindle. While some MAPs work to maintain the finished polymer, others mediate interactions between individual MTs inside bundles as well as between MT bundles that have previously formed. They serve as cross-linkers that keep MTs close together in this fashion. They support the basic composition of distinct bundle populations in the spindle by precisely controlling the time and location for MT affinity. Additionally, they facilitate interactions between MTs and other cytoskeleton and spindle elements.

2.8 Protein regulator of cytokinesis 1

Protein regulator of cytokinesis 1 (PRC1) is a conserved non-motor cross-linking protein that is positioned in the spindle midzone (Jiang et al., 1998; Kurasawa et al., 2004; Mollinari et al., 2002; Pellman et al., 1995; Zhu et al., 2006) and the antiparallel overlaps of MTs *in vitro* (Bieling et al., 2010; Kapitein et al., 2008; Subramanian et al., 2013), where it is crucial for controlling the spindle's development and cytokinesis (Zhu et al., 2006). *In vitro* phosphorylation screening was used to find this human CDK substrate protein in 1998. With the help of that research, it was demonstrated that its expression is delicately regulated throughout the cell cycle, peaking in mitosis. MTs are specifically crosslinked and bundled in an antiparallel orientation *in vitro* by PRC1, a conserved non-motor MAP from the Ase1/PRC1/MAP65 family (Bieling et al., 2010; Janson et al., 2007; Mollinari et al., 2002; Subramanian et al., 2010). The motor-driven MT sliding can be controlled by these diffusible MT cross-linkers using methods like mechanical friction (Braun et al., 2011; Forth et al., 2014; Janson et al., 2007; Subramanian et al., 2010). Structure of PRC1 protein consists of four domains: a dimerization domain, rod domain, spectrin domain and an unstructured C-terminal domain (Kellogg et al., 2016; Subramanian et al., 2010). PRC1 specifically marks the anti-parallel areas of the bridging fibers in the overlap bundles of the metaphase spindle (Kajtez et al., 2016b; Polak et al., 2017) (Figure 13). PRC1 creates bundles of MTs that are in alignment, and the inter-microtubule linking is accomplished by filamentous projections that are positioned at a fixed angle of 38° with regard to the longitudinal axis of the MTs (C. Fu et al., 2007; W. Jiang et al., 1998; Zhu et al., 2006). In addition to having a preference for interacting with MTs, PRC1 also has other binding partners. According to chromatin *in vivo* immunoprecipitation experiments, widely used technique for determining the in vivo location of binding sites of transcription factors, KIF4, a chromokinesin, is its binding partner. KIF4 is a member of the class of MT-based motors that provide directional movement along MTs, as will be discussed in more detail in the following section. PRC1 is transported to the plus ends of interdigitating MTs by the motor protein KIF4. The stalk and tail domains of KIF4 are necessary for contact with PRC1, and association with KIF4 is made possible by PRC1 dephosphorylation during the metaphase-to-anaphase transition. PRC1's amino-terminal half interacts with KIF4's carboxyl-terminal half as well as PRC1. PRC1 can localize to the midzone and bundle antiparallel MTs in late mitosis thanks to this interaction. According to KIF4

depletion studies, this protein is necessary for the construction and stability of the ordered central spindle midzone and midbody (Kurasawa et al., 2004; Subramanian et al., 2013; Zhu & Jiang, 2005).

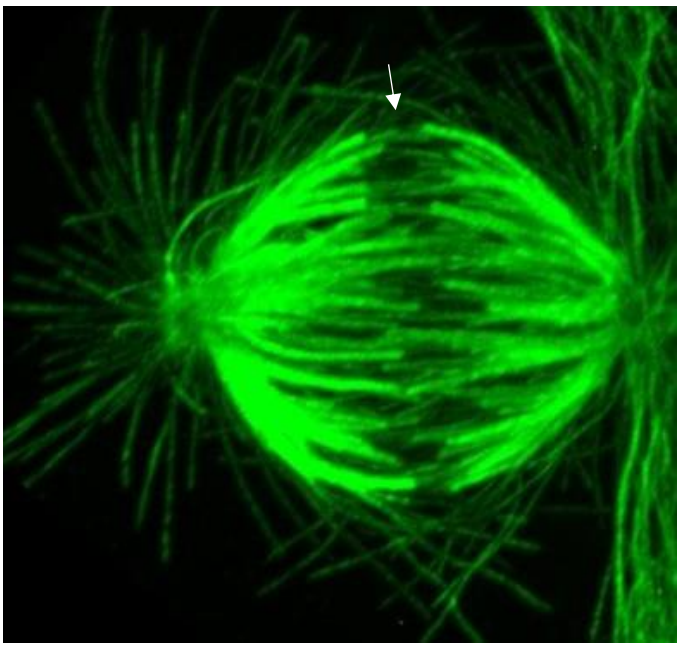

Figure 13. Bridging MTs in metaphase spindle. Expansion microscopy images RPE-1 cell stained with AlexaFluor594 conjugated with α-tubulin antibody. Expansion factor is estimated from spindle length to be 2.3x. White arrow indicate bridging fiber (my own unpublished image).

2.9 Molecular motors

Force production in mitotic spindle can be active and passive. Active force production is defined by processes that convert chemical energy from ATP or GTP hydrolysis into mechanical work. Passive forces are defined by energy consumption that was put into system by one of the active processes (Dumont & Mitchison, 2009). A class of proteins known as molecular motors bind to and catalyze the hydrolysis of ATP into ADP and a free phosphate ion. These enzymes are generally referred to as ATPases (Barton and Goldstein, 1996). To do mechanical labor, they tie the chemical energy released by ATP hydrolysis to reversible conformational changes in one or more of their motor domains. Motor proteins cycle between

their bound and unbound states as a result of this mechanochemically induced cycling, which enables them to "walk" along MTs (Lodish et al., 2014). Almost all of them have a motor domain conserved within one family or more motor domains at opposite sides that bind and hydrolyse ATP to walk along more than one track (Figure 14). They always move in a single direction along the MT under the given conditions, which is due to the intrinsic polarity of the MTs mentioned above. Thus, it is believed that some of these proteins travel toward the plus- and some toward the minus-end of MTs (Lodish et al., 2014). The role of each motor protein in spindle construction and maintenance is determined by the direction of movement (Figure 15). Every "walking" motor has a distinct step size, distinct rate of movement along the MT, and distinct processivity, which may be summed up as the number of steps the motor can take without detaching from the MT (Rath & Kozielski, 2012).

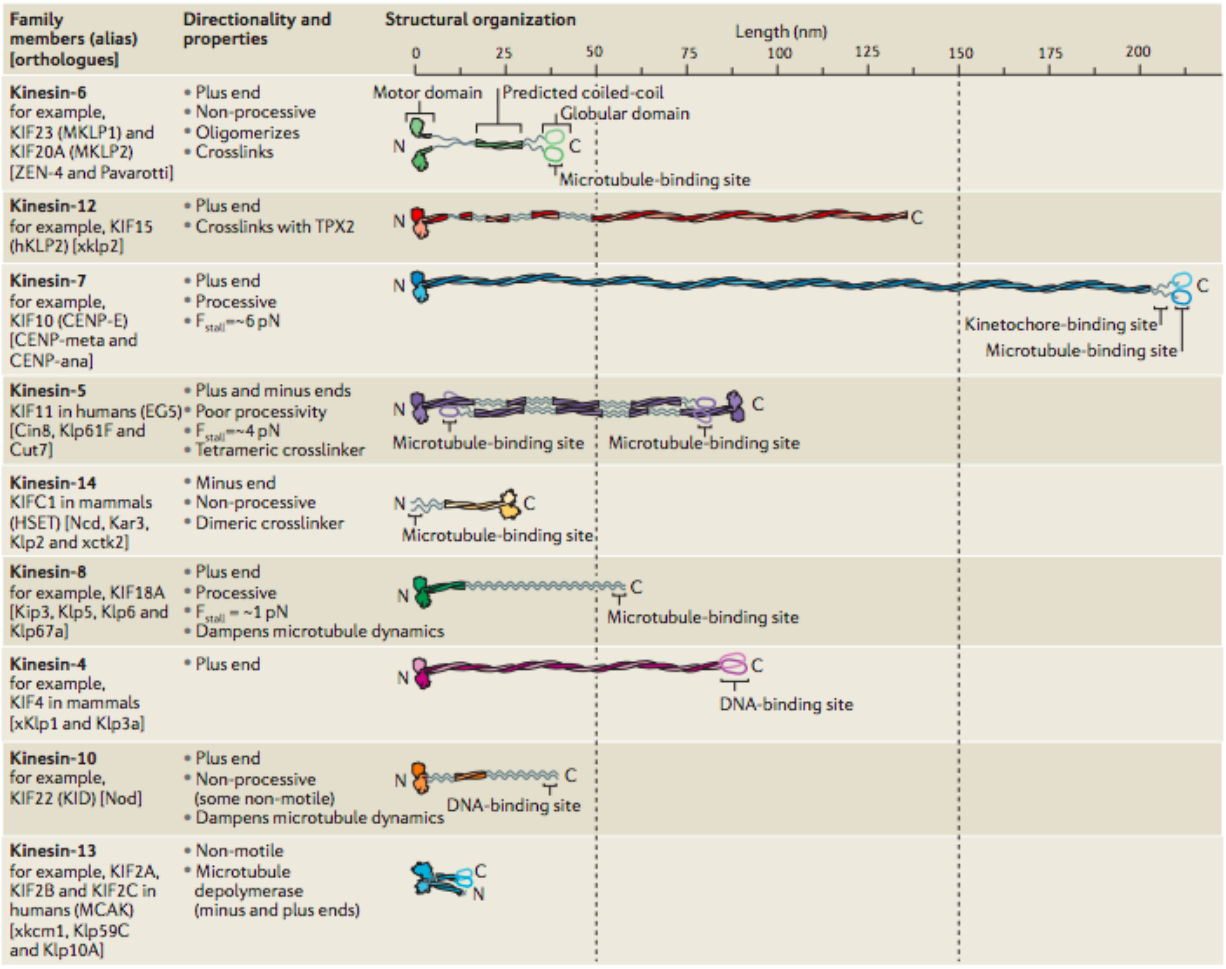

Figure 14. Mitotic kinesins. Homologous kinesin heads (also known as motor domains) are coupled to subfamily-specific tail (Cross & McAinsh, 2014).

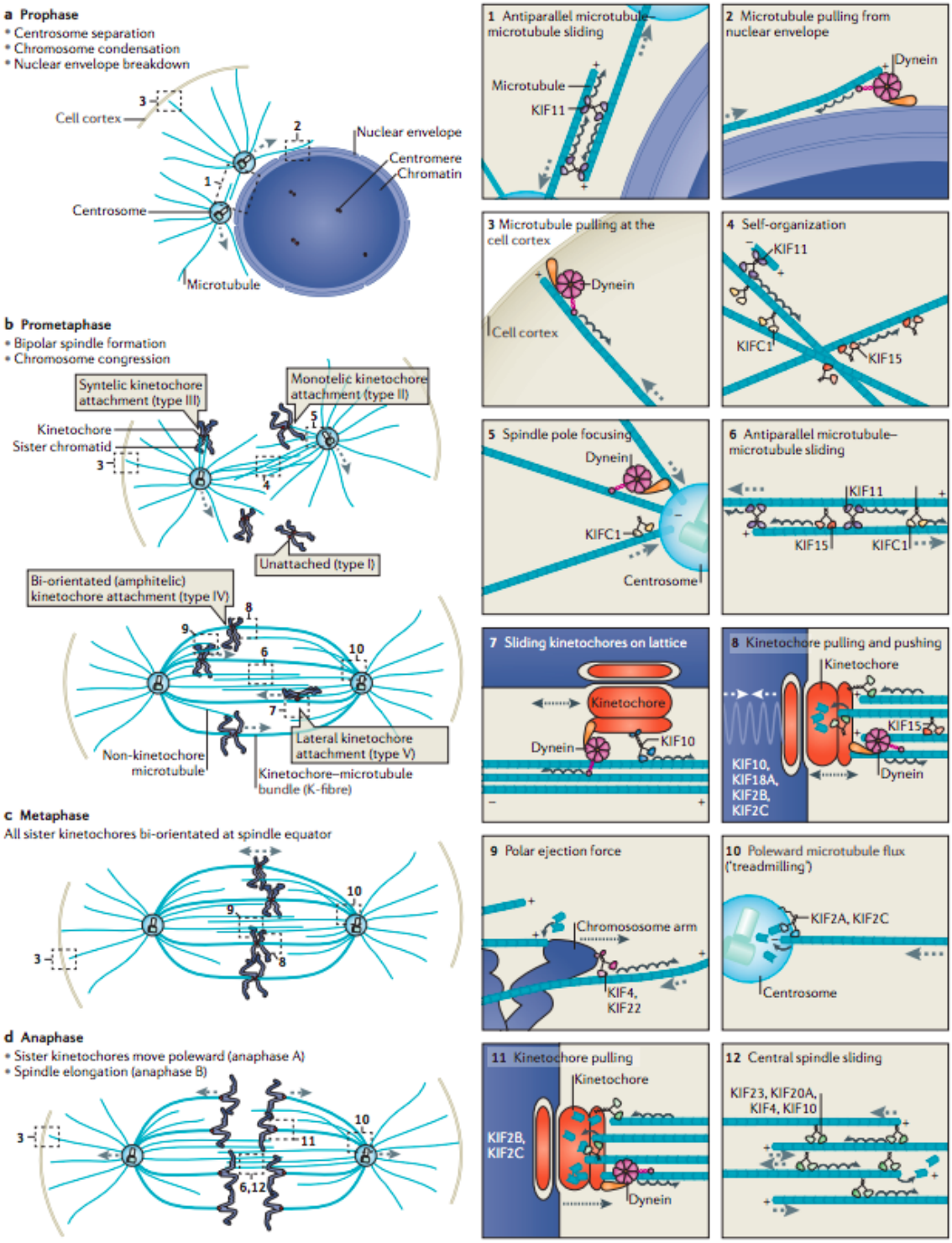

Figure 15. Motor proteins in phases of mitosis. Proposed roles of some key motor proteins troughout different phases during mitosis (Cross & McAinsh, 2014).

2.9.1 Kinesin-5 (EG5) plays a major role in the mitotic spindle

Motor protein that plays a critical role in the mitotic spindle is kinesin-5, the product of Kif11 gene, also known as EG5. EG5 is a bipolar homotetramer complex with four heavy chains forming two motor domains that are capable of binding and cross-linking two MTs (Waitzman & Rice, 2014). A motor domain, an internal stalk domain, and a tail domain are present in the majority of EG5 proteins. The stalk domains of the four EG5 proteins engage to form a bipolar homotetrameric complex, which positions two motor domains at either end of the tetramer (Fig (Figure 16a). Tetramers can simultaneously move in the direction of two anti-parallel microtubules' plus ends, which causes them to move in opposing directions (Zhou et al., 2018) (Figure 16b). EG5, due to orientation of its motor domains, preferentially binds to antiparallel MTs and then slides them by walking to their plus-ends. Result of such motion is aligning of plus-ends of antiparallel MTs and pushing apart of their minus-ends (anti-parallel sliding filament mechanism) (McIntosh et al., 1969). The fundamental roles of EG5 are conserved throughout a variety of eukaryotic organisms. Tetramers made of EG5 monomers serve a crucial part in the creation of spindle bipolarity in mammals, fungi, and plants. Moreover, it has been noted that persistent EG5 dimers encourage MT polymerization in a lab setting. Experimental research in cells of several species has shown that EG5 is necessary for mitosis. A monopolar spindle is created as a result of EG5 deletion (Figure 17), downregulation of its expression, or suppression of its activity, which activates the spindle checkpoint and prevents cell division. The creation of a monopolar spindle in response to EG5 impairment confirms the widely held belief that EG5's primary role in mitosis is to slide apart anti-parallel MTs (Zhou et al., 2018).

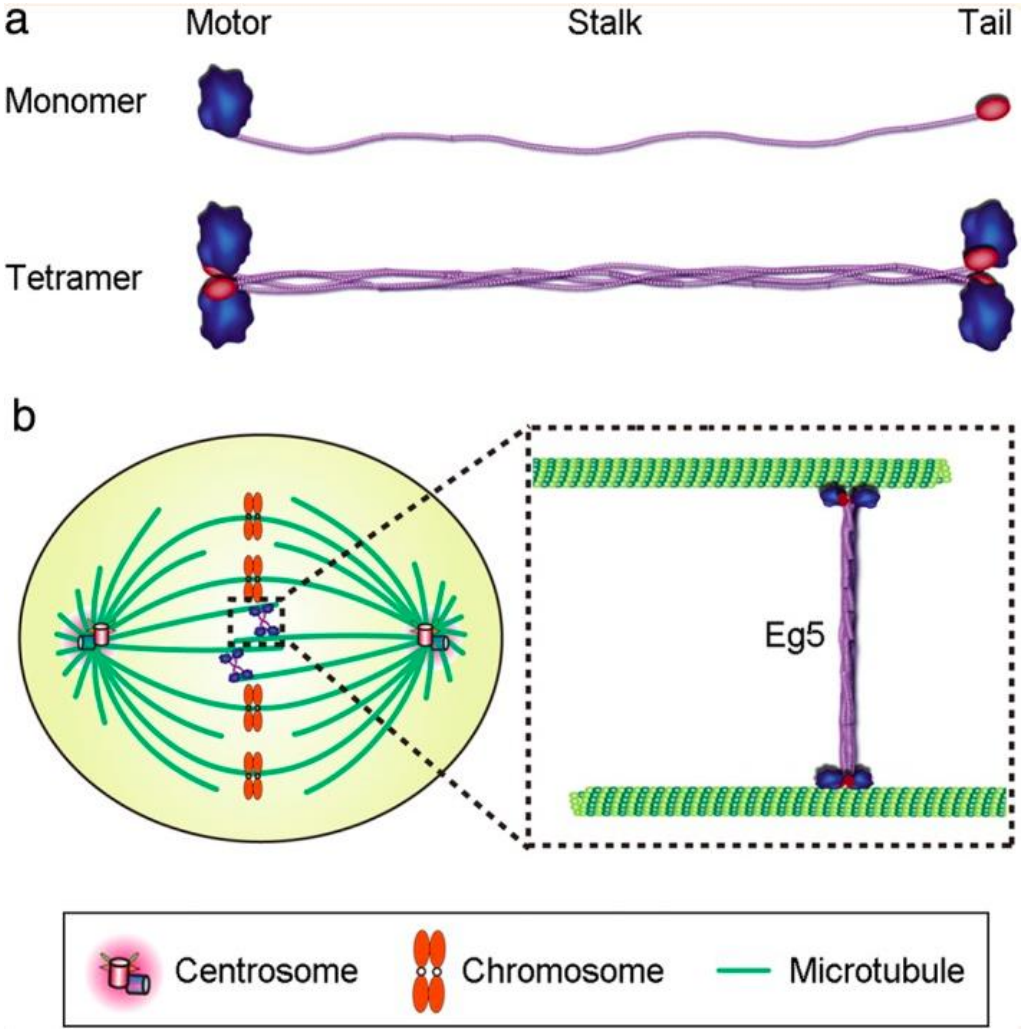

Figure 16. EG5 structure. A. A motor domain, a stalk domain, and a tail domain are present in an EG5 monomer (top). The stalk domains of four EG5 monomers interact to form a homotetramer (bottom). **B.** Diagram illustrating how the EG5 tetramer interacts with and dissociates anti-parallel MTs to aid in the creation and maintenance of the bipolar spindle (Liu et al., 2018).

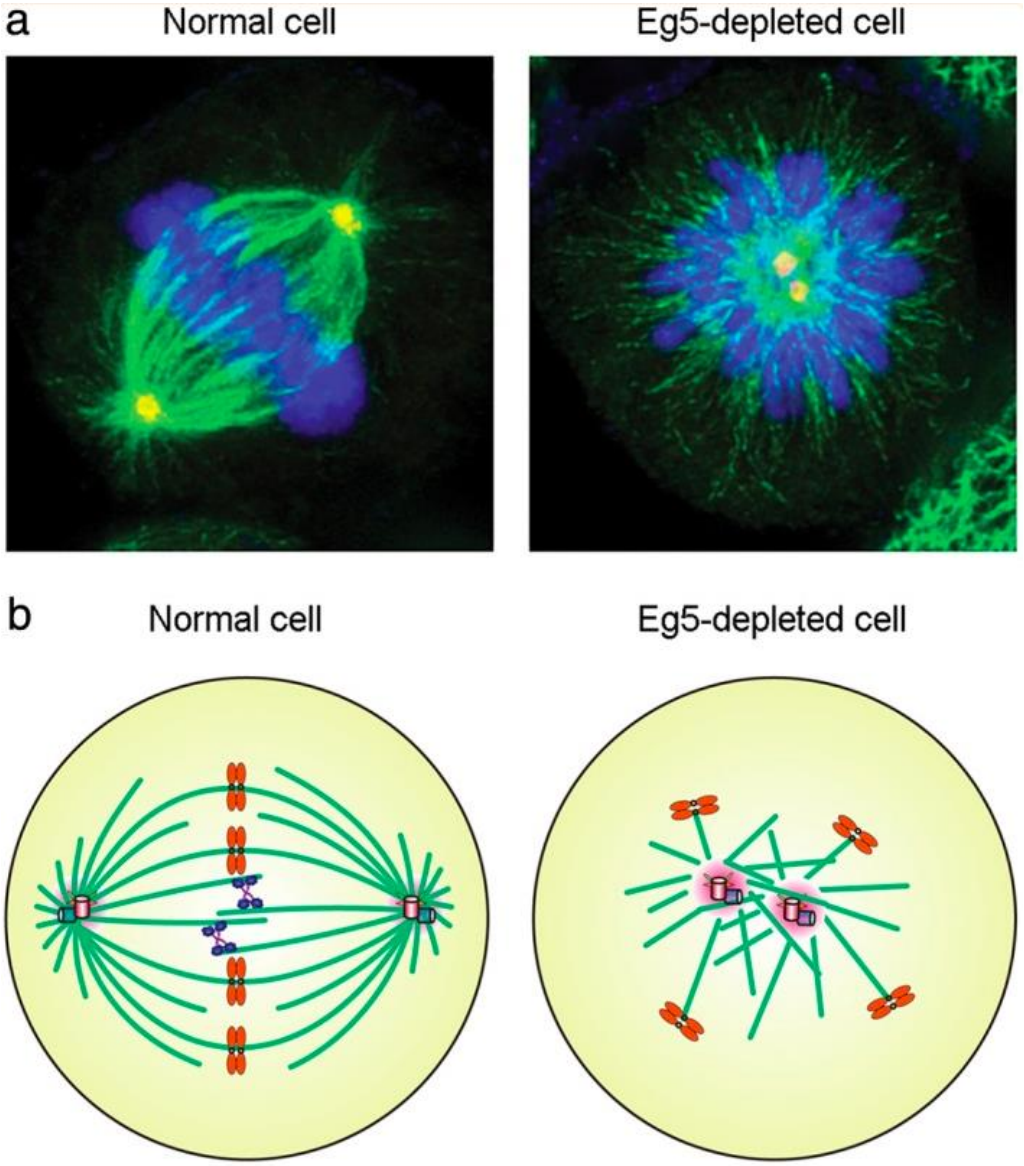

Figure 17. Depletion of EG5 impairs mitotic spindle formation. A. Immunofluorescence microscopy showing MTs (green), γ-tubulin (red), and chromosomes (blue) in normal metaphase or EG5-depleted HeLa cells where the effects of EG5 depletion can be seen. **B.** Diagram showing a monopolar spindle in the EG5-depleted cell and a bipolar spindle in the typical metaphase cell (Liu et al., 2018).

Although EG5 is critical for maintaining of mitotic spindle bipolarity in non-cancerous human cells like RPE-1, it is not required to maintain this bipolarity in all systems. It has been shown that kinesin-12 plus-end directed protein, Kif15 in humans, can have a redundant role with EG5

in maintaining this bipolarity, probably by sliding parallel MTs apart (Drechsler et al., 2014). It's interesting to note that a recent study found that appropriate spindle assembly is controlled by coordination between the plus-end directed EG5, Kif15, and minus-end directed dynein motor, highlighting the significance of a proper force balance in mitotic spindle. Hence, monopolar spindles form when excessive inward forces are present, while spindle poles splay when excessive outward forces are present (vanHeesbeen et al., 2014). Motors that are minus-end-directed can counteract EG5's pushing force that is directed outward toward the spindle poles. Inhibition of the minus-end-directed motor dynein effectively restores bipolar spindle formation in the absence of EG5 activity in human cells and Xenopus egg extracts, demonstrating that dynein inhibits EG5 function (Florian & Mayer, 2012; T. J. Mitchison, 2005; Tanenbaum et al., 2008, 2013). Except dynein, the minus-end-directed kinesin-14 can also antagonize the activity of the kinesin-5 homolog Klp61F in Drosophila (Sharp et al., 1999).

2.9.2 Dynein as the oposing force to EG5

The dominant minus-end directed motor in the mitotic spindle is the cytoplasmic dynein. A homodimer of two heavy chains, dynein has an N-terminal "tail," a stalk needed for MT attachment, and a ring of six AAA domains that binds and hydrolyzes ATP. The dynein heavy chain's tail plays a crucial role in homodimerization and serves as a scaffold for a number of dynein subunits that are not catalytic. The two dynein intermediate chains (DICs), four light intermediate chains (LICs), and three distinct light chain dimers (LL1/2, Roadblock-1/2, and TCTex1/1L) (Kardon & Vale, 2009; Pfister et al., 2006; Raaijmakers et al., 2013) interact with the cytoplasmic dynein 1 heavy chains (DHCs). By transporting minus end cargoes to the minus ends of nearby MTs, dynein produces contractile tension after being attracted to the minus ends of MTs by its targeting factor NuMA (Foster et al., 2015; Gaglio et al., 1996; Hueschen et al., 2017). According to several studies (Howell et al., 2001; Sharp et al., 2000; Varma et al., 2008), dynein is involved in chromosomal motions, spindle organization, spindle location, and checkpoint silencing during mitosis. Dynein localizes to a wide range of subcellular structures during G2 and mitosis, including the nuclear envelope (NE), centrosomes, kinetochores (KTs), spindle MTs, and the cell cortex (Dujardin & Vallee, 2002; Kiyomitsu & Cheeseman, 2012; Pfarr et al., 1990; Steuer et al., 1990; Tanenbaum & Medema, 2010a). Interestingly, dynein clusters the minus-ends of MTs together. This process constitutes the basis of slide-and-cluster

mechanism of spindle length maintenance (Figure 10). Dynein therefore has a main role in focusing MTs into a united pole, function obviously very important to maintain bipolar shape of the spindle (Civelekoglu-Scholey & Scholey, 2010). As opposed to EG5 inhibition, NuMA or dynein loss results in spindles with turbulent, disorganized activity and MT bundles protruding against the cell cortex (Hueschen et al., 2017). Dynein can also bind various cargo and deliver them to minus-ends of MTs, which are primarily found at spindle poles, in addition to its function in arranging MTs in the spindle. In addition to NuMa, which stabilizes the pole structure, these cargoes can also include various motor proteins, primarily kinesins, which are transported from the plus ends of MTs to the minus ends (Goshima & Scholey, 2010). Human spindles form as usual bipoles when dynein and EG5 are depleted together, despite their significance to spindle design (Florian & Mayer, 2012; Neahring et al., 2021; Tanenbaum et al., 2008; vanHeesbeen et al., 2014). When the homologous EG5 and the dominant end-clustering motor (dynein or a kinesin-14) are suppressed, bipolar spindle forms and similar effects have been observed in yeast, Drosophila, Xenopus laevis extract, and pig spindles (T. J. Mitchison, 2005; Saunders & Hoyt, 1992; Sharp et al., 1999). If the identical structure can be created without opposing, energy-intensive motor actions in the spindle, what purpose do they serve? Furthermore, it is still unknown what effect does the double depletion has on MT dynamics.

2.9.3 Kinesin-4 (KIF4A)

Last but not least, several motor proteins have been discovered that bind to both chromosomal arms and MTs. One of the processes for producing force on chromosomes is called polar ejection force, and the most significant of them are known as chromokinesins (Rieder & Salmon, 1994) (Figure 10). Chromosome segregation, spindle organization, and cytokinesis are a few additional processes in which chromokinesins play a different role (Mazumdar & Misteli, 2005). Plus-end directed Kid/kinesin-10 and kinesin-4 family members KIF4A and KIF4B, who contain conserved motor domains but differ in the organization of other domains, are two members of these groupings. Especially interesting here is the chromokinesin KIf4A which was shown to drive sliding of the antiparallel overlaps together with Eg5 (Vukušić et al., 2021). The plus-end-directed motor kinesin-4 KIF4A, which is conserved in metazoans, is one of the proteins that PRC1 recruits in human cells (Kurasawa et

al., 2004; Powers et al., 2004; Vernos et al., 1995; Zhu & Jiang, 2005). KIF4A is a homodimer that has a 116 nm-long C-terminal tail domain and a lengthy coiled coil region after its N-terminal motor domain (Sekine et al., 1994). Kinesin-4 motors can prevent MT growth, hence KIF4A regulates the length of central antiparallel MT overlaps in the anaphase spindle (Hu et al., 2011; Kurasawa et al., 2004; Zhu & Jiang, 2005). KIF4A moves along the MTs towards their plus ends and upon its accumulation at the plus end, reduces MT polymerisation and depolymerisation dynamics (Bieling et al., 2010; Bringmann et al., 2004). A subpopulation of KIF4 builds up at the central spindle and then the midbody shortly after anaphase begins (Wang & Adler, 1995). Reflecting this localization pattern, KIF4 is involved in a number of processes of cell division, including the precise creation of the central spindle (Kurasawa et al., 2004; Mazumdar et al., 2004; Zhu & Jiang, 2005). According to Hu et al. (2011), KIF4 depletion results in aberrant central spindle elongation and misdirected MT overlaps. As I previously mentioned, depletion of KIF4A together with EG5 inhibition completely blocks spindle elongation, suggesting that both proteins exert forces during anaphase by sliding apart antiparallel MTs (Vukušić et al., 2021) (Figure 18). It has also been recently showed that MT-sliding motors EG5 and KIF15 collaboratively act on interpolar MTs, assisted by CENPE at kinetochores in prometaphase and KIF4A on chromosome arms in metaphase (Steblyanko et al., 2020a).

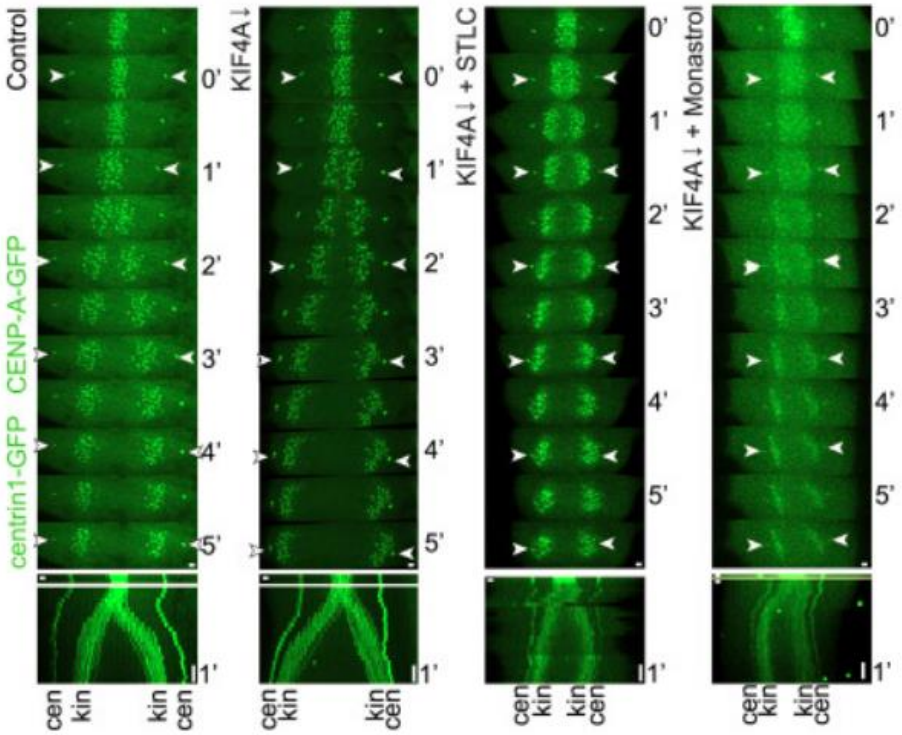

Figure 18. Depletion of KIF4A together with inhibition of EG5 block spindle elongation. Live-cell images of control, KIF4A siRNA-depleted, KIF4A-siRNA-depleted 40-μM STLC treated, and KIF4A-siRNA-depleted 100-μM monastrol-treated RPE-1 cells stably expressing CENP-A-GFP and centrin1-GFP. kin, kinetochore; cen, centrosome (Vukušić et al., 2021).

2.10 Bridging fibers are crucial for chromosome segregation

Sister kinetochores can separate independently of attachment to one spindle pole in human cells, as evidenced by the separation of a pair of them from the rest of the spindle right before the commencement of anaphase. This separation is caused by antiparallel MTs sliding apart between them (Vukušić et al., 2017). It is shown that the continual removal of the majority of interpolar MTs from the central spindle reduced spindle elongation rates and that bridging fibers were necessary for the separation of displaced kinetochores (Vukušić et al., 2017). Short-term laser ablation of all interpolar MTs in human cells immediately stopped anaphase chromosome mobility for a brief period of time, supporting the latter finding (Yu et al., 2019). Additionally, it was confirmed that ablation assays that were done close to the kinetochore, less than a micrometer away, renders kinetochores incapable of separating (Vukušić et al., 2017), possibly

due to disruption of the connection between the bridging and k-fiber given that they merge 1-2 μm away from the kinetochores (Kajtez et al., 2016a).

One of the most interesting questions related to the bridging and k-fiber dynamics in the mitotic spindle is how is the force that is produced in the spindle midzone transmitted to the spindle poles. Data from human cells collectively refute earlier theories that interpolar MTs can slide apart and generate forces that can travel down k-fibers, pushing the poles apart and lengthening the spindle (Belar, 1929; (McIntosh et al., 1969; Östergren, 1951). Likewise, interpolar MTs in human cells generally start distant from the pole (Yu et al., 2019), supporting pushing through k-fibers. As a result, the interpolar MT sliding velocity is higher than the spindle elongation velocity (2.1 μm/min and 1.3 μm/min, respectively) (Vukušić et al., 2017) which means that part of the sliding force dissipate somehow on its way to the spindle poles. These unbalanced velocities in the mitotic spindle were one of the main motivations to futher explore forces and poleward flux while spindle poles are moving in my disertation.

2.11 Poleward flux

In metazoan cells, a process known as "poleward flux" is characterized as a constant transfer of MTs towards the spindle poles (Forer, 1965; T. J. Mitchison, 1989). The molecular mechanisms behind this process are not yet completely understood. According to one scenario (Ganem et al., 2005; Maiato et al., 2005), flow is driven by CLASP-mediated polymerization at kinetochore MT plus-ends and Kif2a/kinesin-13-mediated depolymerization at spindle poles. Unfortunately, this hypothesis has been refuted by a number of lines of evidence. Fluorescence speckle imaging on newt lung cells, in particular, revealed no flux in astral MTs, which begin at the poles and extend toward the cell cortex (Waterman-Storer & Salmon, 1998). Kinetochore MTs, also known as k-fibers, were the subject of laser microsurgery research, which indicated normal MT-flux despite stable MT minus-ends removed from the spindle poles (Maiato et al., 2004; Matos et al., 2009). Last but not least, MTs remained to flow at the same rates even after controlled mechanical

compression was given to metaphase mitotic spindles to prevent MT-depolymerization at spindle poles (Dumont & Mitchison, 2009). Combined, these tests show that MT-flux and MT minus-end depolymerization may be separated. According to a different model, the origin of the poleward flux is a downstream reaction to the antiparallel interpolar microtubules' kinesin-

5-driven sliding. This response may then be transmitted to the kinetochore MTs due to their coupling, which is mediated by various crosslinking molecules (Brust-Mascher et al., 2009; Miyamoto et al., 2004a). However, inhibition of EG5 in mammalian cells led to only minor reduction of poleward flux rates, suggesting EG5 is not a predominant generator of flux-driving force in mammalian spindles (Cameron et al., 2006). Recently, in a paper from our group (Vukušić et al., 2021), we showed that joint action of EG5 together with KIF4A slides midzone MTs apart in RPE-1 cells. Furthermore, it was shown that combined action of EG5 and KIF15 support MT-flux driving activities of CENP-E and KIF4A in U2OS cells stably co-expressing PA-GFP-α-tubulin and mCherry-α-tubulin (Steblyanko et al., 2020b).

MT poleward flux has been linked to kinetochore activity regulation (Maddox et al., 2003), regulation of spindle length (Maiato et al., 2005; Rogers et al., 2004), correction of incorrect kinetochore-MT attachments (Ganem et al., 2005), and equalization of forces at kinetochores prior to segregation (Matos et al., 2009). Latest paper from out group (Risteski et al., 2022) shows that bridging MTs undergo poleward flux at a higher velocity than kinetochore MTs as well as that the kinetochore centering efficiency depends on the flux velocity of k-fibers.

2.12 Different approaches to measure poleward flux

Analyzing the motions of individual MTs is necessary in order to estimate the poleward flux of various kinds of MTs (kinetochore and bridging), which is necessary in order to test the predictions of the flux-driven centering model experimentally. Tubulin photoactivation is a common method for studying flux (Mitchison, 1989). With this method, all of the MTs in the lighted region are photoactivated, making it impossible to discern between the motions of kMTs and non-kMTs. In order to get around this problem, assay was created (Risteski et al., 2022) based on speckle microscopy (Waterman-Storer & Salmon, 1998) to investigate MTs within spindles of the human immortalized epithelial cell line hTERT-RPE1 (referred to as RPE-1). By using a very low concentration (1 nM) of SiRtubulin (Lukinavičius et al., 2014), speckled signal of SiR-tubulin was obtained in the spindle (Figure 19A), which comes from a few dye molecules within a resolution-limited region (Waterman-Storer & Salmon, 1998). To identify the speckles that are localized on kMTs or bMTs, one has to follow the position of their first appearance and their subsequent movement. The speckles that originate close to a kinetochore, at the pole-facing side, are defined as those on a kMT (Figure 19B). The speckles that appear

on one side of a pair of sister kinetochores, pass the region between them, and end up on the other side, are defined as those on a bMT (Figure 19C). To calculate velocity of poleward flux or the moving speckle, individual speckles need to be tracked together with the spindle poles marked by centrioles and then poleward flux can be calculated as the change of the speckle-to-pole distance over the whole duration of their movement. This assay is now allowing us to study the movement of kMTs and bMTs with respect to the poles and to each other (Risteski et al., 2022).

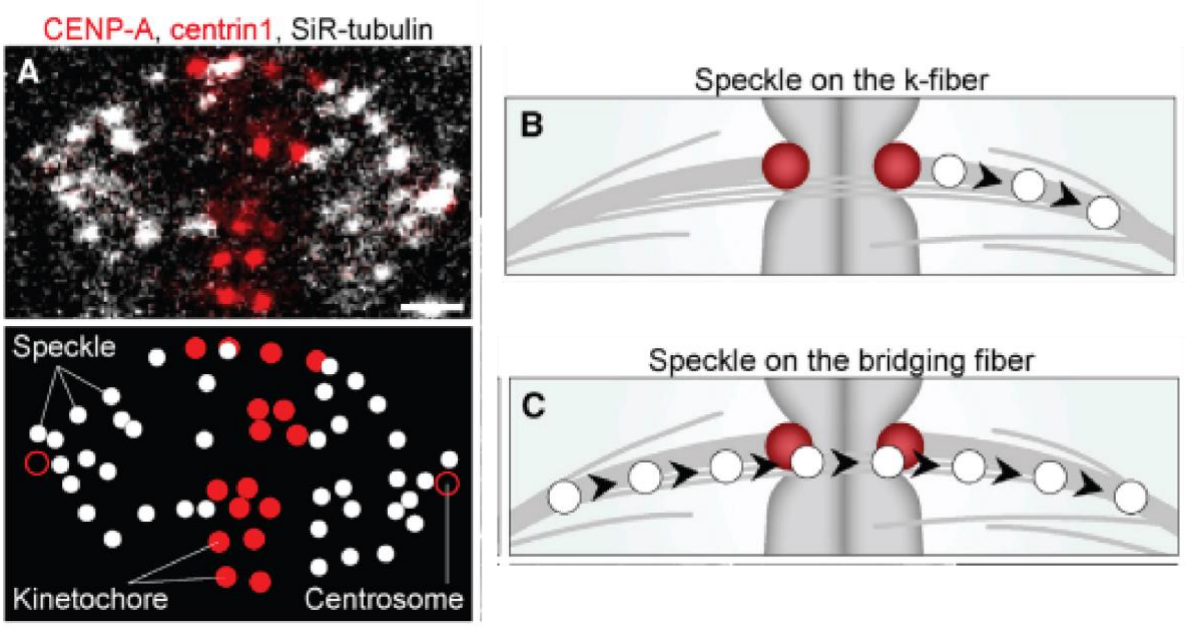

Figure 19. Speckle microscopy assay for measurement of poleward flux of individual MTs. **A.** Spindle in a RPE1 cell stably expressing CENP-A-GFP and centrin1-GFP (red) stained with 1 nM SiR-tubulin dye. **B.** The speckles that originate close to a kinetochore, at the pole-facing side, are defined as those on a kMT. **C.** The speckles that appear on one side of a pair of sister kinetochores, pass the region between them, and end up on the other side, are defined as those on a bMT. Image is adapted from (Risteski et al., 2022).

3 MATERIALS AND METHODS

3.1 Cell lines

The human cell lines used are: 1. human hTERT-RPE-1 (retinal pigmented epithelium, female) permanently transfected and stabilized using CENP-A-GFP (centromere-specific variant of histone H3) and centrin1-GFP (protein of a centrosome complex) (RPE-1-CC), which was a gift from Alexey Khodjakov (Wadsworth Center, New York State Department of Health, Albany, NY) (developed in (Magidson et al., 2011) and 2. human hTERT-RPE-1 (retinal pigmented epithelium, female) expressing mGFP-PRC1 (RPE-1-PRC1-GFP), which was a gift from Thomas Surrey (Center for Genomic Regulation, Barcelona, Spain) (developed in (Asthana et al., 2021). Cells were grown in cell culture flasks in DMEM-FBS composed of Dulbecco's Modified Eagle's medium (DMEM) with Ultraglutamine (1 g/l D-glucose, pyruvate) (Lonza, Basel, Switzerland) supplemented with 10% of heat-inactivated Fetal Bovine Serum (FBS) (Sigma-Aldrich, St Louis, MO, USA), and penicillin/streptomycin solution (Lonza) to a final concentration of 100 I.U./mL penicillin and 100 µg/mL streptomycin. Media was additionally supplemented for selection of some cell lines as follows: 50 µg/mL geneticin G418 (Life Technologies, Waltham, MA, USA) was added in media for cell lines described above and 500 µg/mL G418 was added in media for hTERT-RPE-1 PA-GFP-α-tubulin cell line. The cells were grown at 37°C and 5% CO2 in a Galaxy 170s humidified incubator (Eppendorf, Hamburg, Germany). When cells reached 80% confluence, DMEM medium was removed from the flask and the cells were washed with 5 mL of 1% PBS (Roth, Germany). Afterward, 1 mL of 1% Trypsin/EDTA (Biochrom AG, Berlin, Germany) was added and the cells were incubated at 37 °C and 5% CO2 in a humidified incubator (Eppendorf). After 5 min incubation, Trypsin was blocked by adding 2-5 mL of DMEM-FBS. Cells were counted using the Improved Neubauer chamber (BRAND GMBH + CO KG, Wertheim, Germany) and 4.5x105 cells were seeded and cultured in 2 mL DMEM medium with same supplements (as above) at 37°C and 5% CO2 on 14 or 20 mm glass microwell uncoated 35mm dishes with 0.16-0.19mm (#1.5 coverglass) glass thickness (MatTek Corporation, Ashland, MA, USA). All used cell lines were confirmed to be mycoplasma free by monthly checks using MycoAlert Mycoplasma Detection Kit (Lonza) and regular checks during imaging experiments with DNA labelling stains.

3.2 Constructs, transfections and RNAi

For siRNA treatments, 2×10^5 or 3×10^5 cells were seeded and cultured in 1 mL DMEM-FBS medium with same supplements (as above) at 37°C and 5% CO_2 in 12-well cell culture plates (Greiner). After one-day growth, at ~70% confluency cells were transfected with 200 nM raw targeting or non-targeting siRNA diluted in an Opti-MEM medium (Life Technologies, Waltham, MA, USA). Transfection was performed using Lipofectamine RNAiMAX Reagent (Life Technologies) using protocol provided by the manufacturer. After 5h of transfection the medium was changed to DMEM-FBS. The cells were imaged always 48 hours after transfection, unless otherwise indicated. The siRNAs used were as follows: human KIF4A siRNA (sc-60888, Santa Cruz Biotechnology), control siRNA (sc-37007, Santa Cruz Biotechnology). For inspection of the knockdown of all target proteins by transfection of specific siRNA I performed immunofluorescence for estimation of protein depletion levels before and after specific siRNA.

3.3 Drugs

The stock solution of S-trityl-L-cysteine (STLC, Sigma-Aldrich) was prepared in dimethyl sulfoxide (DMSO) to a final concentration of 25 mM. The working solution was prepared in DMEM at 80 μM (the half-maximal inhibitory concentration for STLC in HeLa cells is 700 nM) (Debonis et al., 2004). At the time of treatment, the working solution was added to cells at 1:1 volume ratio to obtain a final concentration of 40 μM. To inhibit EG5, STLC was added during metaphase. Quick response was observed as most metaphase spindles collapsed into monopolar spindles in RPE1 cells, minutes after STLC was added (Gayek & Ohi, 2014). Because of that quick collapse all experiments than included the STLC treatment were done in the "one metaphase cell per one well" regime. For immunofluorescence of alpha-Tubulin, in treatments with STLC, drug was added to the cell culture media 5 min before fixation. The stock solution of Ciliobrevin D (MedChemExpress) was prepared in DMSO to a final concentration of 10 mM immediately before use. At the time of treatment, the 5μL of the stock solution was added to the cells (1mL of DMEM-FBS) to obtain a final concentration of 50 μM. To inhibit dynein, Ciliobrevin D was added during metaphase. Most dynein inhibitors interact with FBS and are not effective when added to cells growing in DMEM supplemented with 10%

of heat-inactivated FBS. Thus, approximately 10 minutes before adding Ciliobrevin D we changed the medium in wells to OPTI-MEM medium without FBS. Quick response was observed as most metaphase spindles poles started splaying and k-fibers detaching from the bridging fibers. Immunofluorescence of dynein and tubulin after exposure to Ciliobrevin D was performed after 15 minutes. For experiments when dynein and EG5 were inhibited together, a final concentration of 10 μM STLC and 50 μM Ciliobrevin D were used.

3.4 Immunofluorescence

For visualization of EG5 RPE-1-CC were grown on glass-bottomed dishes (14 mm, No. 1.5, MatTek Corporation) and fixed by 1 mL of ice-cold methanol for 3 min at -20°C. To visualize alpha-tubulin ice-cold methanol protocol was avoided because it destroyed unstable fraction of MTs and cells were instead fixed by a MT-preserving mixture of 3.2% paraformaldehyde (PFA) and 0.25% glutaraldehyde (GA) in MT-stabilizing PEM buffer (0.1 M PIPES, 0.001 M MgCl2 x 6 H2O, 0.001 M EDTA, 0.5 % Triton-X-100) for 10 min at room temperature (Heuser and Kirschner, 1980). After fixation with PFA and GA, for quenching, cells were incubated in 1mL of freshly prepared 0.1% borohydride in PBS for 7 min and after that in 1 mL of 100 mM NH_4Cl and 100 mM glycine in PBS for 10 min at room temperature. Both methanol fixed cells and PFA and GA fixed cells were then washed with 1 mL of PBS, 3 times for 5 min. To block unspecific binding of antibodies, cells were incubated in 500 μL blocking/permeabilization buffer (2% normal goat serum (NGS) and 0.5% Triton-X-100 in water) for 45 min at room temperature. Cells were then incubated in 500 μL of primary antibody solution for 24h at 4°C. The following primary antibodies were used: mouse monoclonal EG5 (sc-365681, Santa Cruz Biotechnology), diluted 1:50; rat anti-alpha Tubulin YL1/2 (MA1-80017, Invitrogen, 1:500). After primary antibody, cells were washed in PBS and then incubated in 500 μL of secondary antibody solution for 45 min at room temperature. Following secondary antibodies were used: donkey anti-mouse IgG Alexa Fluor 594 (ab150112, Abcam); donkey anti-rat IgG Alexa Fluor 594 (ab150156, Abcam), both diluted 1:1000. Finally, cells were washed with 1 mL of PBS, 3 times for 5 min.

3.5 STED microscopy

STED microscopy of fixed cells and live-cell imaging of anaphase were performed using an Expert Line easy3D STED microscope system (Abberior Instruments, Göttingen, Germany) with the 100 x/1.4NA UPLSAPO100x oil objective (Olympus, Tokio, Japan) and an avalanche photodiode (APD) detector. The 488 nm line was used for excitation in both cases, with the addition of the 561 nm line for excitation and the 775 nm laser line for depletion during STED superresolution imaging. Images were acquired using the Imspector software. The xy pixel size for fixed cells was 20 nm and 6 focal planes were acquired with 300 nm distance between planes were acquired.

3.6 Speckle microscopy

Cells grown in glass coverslip dishes were stained with 1 nM SiR-tubulin dye (Spirochrome AG). After 15 min of staining, confocal live imaging was performed on a Dragonfly spinning disk confocal microscope system (Andor Technology) using 63x/1.47 HC PL APO glycerol objective (Leica) and Zyla 4.2P scientific complementary metal oxide semiconductor camera (Andor Technology), and Expert Line easy3D STED microscope system (Abberior Instruments) using 60x/1.2 UPLSAPO 60XW water objective (Olympus) and avalanche photodiode detector. Images were acquired using Fusion software and Imspector software. During imaging, cells were maintained at 37C and 5% CO2 within heating chamber (Okolab). For live imaging of RPE-1-CC, and stained with SiR-tubulin, 488-nm and 640-nm laser lines for Dragonfly microscope system, and 485-nm and 640-nm for Expert Line microscope system were used to excitate GFP, and SiR, respectively. In order to visualize SiR-tubulin speckles, images were acquired with 80% laser power and exposure of 1 s. Image acquisition was done on one focal plane every 7 or 10 s. Note that time-frame within which SiR-tubulin, at 1 nM concentration, can be visualized in patches on the mitotic spindle is between 15 and 75 min after SiR-tubulin staining.

3.7 Quantification and statistical analysis

No statistical methods were used to predetermine sample size. At least 3 independent experiments were done for every treatment. Quantification and statistical analysis were performed in MatLab. Data are given as mean ± sem (standard error of mean), unless otherwise stated. P values were obtained using unpaired two-sample Student's t-test (significance level

was 5%).$p < 0.05$ was considered statistically significant, very significant if $0.001 < p < 0.01$ and extremely significant if $p < 0.001$. The number of analysed cells and specific parameters are given in the text and in the tables.

3.8 Image analysis

Measurements were performed in Fiji/ImageJ (National Institutes of Health). Quantification and data analysis were performed in MATLAB (MathWorks). Figures and schemes were assembled in Adobe Illustrator CC (Adobe Systems). Statistical analysis was performed using Student's t-test, Mann-Whitney test and two-proportions z-test.

Upon inspection of tubulin speckle movement within the spindle, speckles which could be followed for at least 30 s were taken into account. For every tubulin speckle position, corresponding CENP-A and centrin positions, representing the location of sister kinetochores and spindle poles, respectively, were also tracked. Tracking was done by using the Multi-point tool. Speckles which started at the outside of the kinetochore and never passed through sister kinetochores were categorized as a part of k-fiber, whilst speckles which started between sister kinetochores or/and passed through sister kinetochores were categorized as a part of bridging fiber. Note that all kinetochore pairs within each spindle were exhaustively inspected for occurrence of k-fiber or bridging fiber speckles, thus the ratio of k-fiber speckles and bridging fiber speckles provides information on the relationship of the number of MTs in these categories. In some treatments, like EG5 inhibition with STLC and dynein inhibition with Ciliobrevin D, k-fiber speckles which started at kinetochore were hard to find so speckles that started maximally 1 micron from the kinetochore and were associated with one pole were also tracked and analyzed as k-fiber speckles. Speckle-equator velocity is a new measure that I used in order to quantify speckle movement that was independent of moving of the poles. The equator of the spindle was defined as the midline between two poles in every frame that was tracked. Speckle-pole, pole-pole and speckle-equator velocity were calculated by fitting linear regression on distances between the tubulin speckle and the associated spindle pole during its entire trajectory. For speckle-equator velocities, absolute values were used because I wanted to measure the sliding velocity of the MTs in the midzone and it was not important from which side of the equator the speckle started.

For kinetochore alignment measurements, the Multipoint tool was used to track positions of sister kinetochore pairs. The equatorial plane was defined with two points placed between outermost pairs of kinetochores on the opposite sides of the spindle. Kinetochore oscilations were analyzed as the distance between the midpoint of kinetochore pairs and the equatorial plane.

To determine the percentage of protein depletion, I measured mean spindle intensity by encompassing the area of the spindle with the Polygon selection tool. Mean background intensity in the cytoplasm, measured using a 1 3 1 mm rectangle, was subtracted from the mean spindle intensity.

4 RESULTS

4.1 Speckle microscopy assay while spindle poles are moving

To measure the poleward flux of different classes of MTs (kinetochore and bridging), which requires analysis of the movements of individual MTs, I used recenlty developed assay for speckle microscopy (Risteski et al., 2022). By using a very low concentration (1 nM) of SiR-tubulin (Lukinavičius et al., 2014), I managed to obtain speckled signal of SiR-tubulin in the spindle which comes from a few dye molecules within a resolution limited region. Speckles which started at the outside of the kinetochore and never passed through sister kinetochores were categorized as a part of k-fiber, whilst speckles which started between sister kinetochores or/and passed through sister kinetochores were categorized as a part of bridging fiber. Here, I wanted to investigate the connection between the force producing midzone of the spindle and the spindle poles so I was interested in analyzing MT sliding while poles are moving from or towards eachother, for example in anaphase or during EG5 inhibition where immediate effect can be seen on spindle length. Since poleward flux is a value which is measured as the velocity of the speckle towards the spindle pole, in cases of moving poles I needed a new measure to measure only sliding of the MTs in the midzone, independent of the moving of the poles.

Speckle-equator velocity (Figure 20) is a new measure that I used in order to quantify speckle movement that was independent of moving of the poles. The equator of the spindle was defined as the midline between two poles in every frame that was tracked. Thus, speckle-equator velocity is calculated by the distance that speckle crosses from or towards the equator of the spindle. For speckle-equator velocities, absolute values were used because I wanted to obtain the speckle velocity and it is not important from which side of the equator the speckle started. All the values in this thesis are given as mean ± sem.

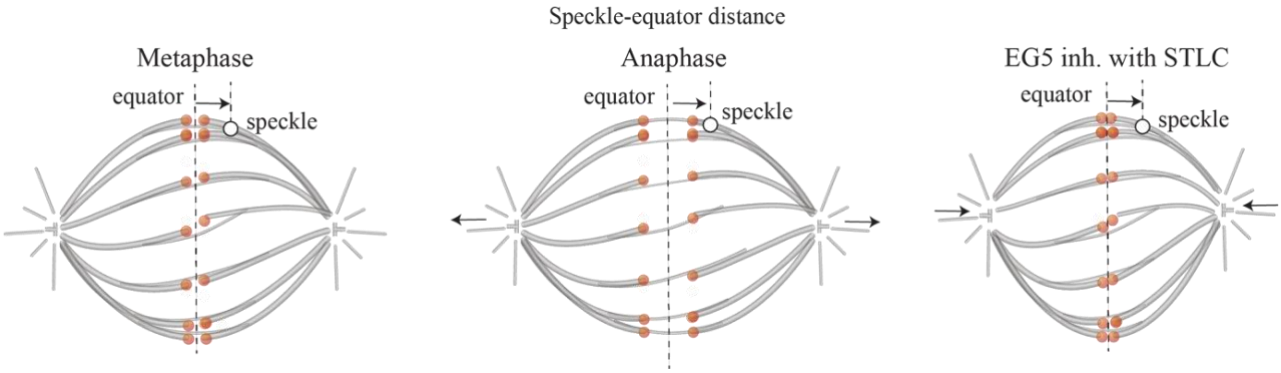

Figure 20. Sheme describing new measure for speckle movement using speckle microscopy. Speckle-equator velocity is a new measure that I used in order to quantify speckle movement that was independent of moving of the poles. The equator of the spindle was defined as the middle line between two poles in every frame that was tracked. In anaphase, the poles are moving away from eachother so poleward flux is dependent of the moving of the poles. In STLC treated spindles, EG5 motor is inhibited and spindle starts to rapidly decrease in length, but the speckle-equator velocity measure can still be compared to that in metaphase since it does not depend on spindle length.

4.2 Bridging fibers slide at a similar rate as k-fibers in anaphase

All of the results are summarized at the end of the Results section in Table 1. and Table 2. Since anaphase is a mitotic phase where the spindle poles are moving, poleward flux highly depends on the pole-pole velocity. Thus, speckle-equator velocity is the appropriate measure for calculating the MT sliding velocity in anaphase. Our previous work (Vukušić et al., 2021) measured sliding velocities during anaphase but here for the first time I had a chance to measure individual MT sliding and compare it with metaphase flux velocities. Interestingly, after measuring speckle-equator velocity in anaphase, difference in bridging and k-fiber sliding was not significant (Figure 21 and 22) and as previously reported (Risteski et al., 2022) bridging fibers slide at a higher rate than k-fibers in metaphase (Figure 22). Speckle-equator velocity for untreated anaphase cells for bridging fibers is 1.86 ± 0.18 μm/min (n = 13 speckles from 8 cells) and for k-fibers is 1.70 ± 0.20 μm/min (n = 14 speckles from 7 cells). On the other hand, speckle-pole velocity for untreated anaphase cells for bridging fibers is – 0.66 ± 0.13 μm/min (n = 13 speckles from 8 cells) and for k-fibers is – 0.77 ± 0.14 μm/min (n = 14 speckles from 7 cells), which nicely shows why I needed a new measure for describing the speckle movement since speckle-pole velocity is highly influenced by the moving of the poles, thus this value is much lower than speckle-equator velocity (Figure 21 and 22). Negative values for speckle-pole velocity mean that the speckle was moving towards the pole so distance was getting shorter between them. Pole-pole velocity for untreated anaphase cells measured for speckles tracked on bridging fibers is 1.99 ± 0.22 μm/min (n = 13 speckles from 8 cells) and for speckles that were tracked on k-fibers is 1.92 ± 0.34 μm/min (n = 14 speckles from 7 cells) which is in agreement with previous sliding velocities measured in anaphase with photoactivation assay

(Vukušić et al., 2021) (Figure 21 and 22). Limitation of this study is small number of speckles that could be tracked for at least 40 seconds and also speckles on bridging fiber and k-fiber could not be tracked for the same kinetochore pair, thus I have two pole-pole velocities, one for the bridging fibers and one for the k-fibers. This is a good control to see that these two populations of MTs were tracked approximately at the same phase of the anaphase if these velocities are similar as they are in this case. Since there is no difference in sliding of the bridging and k-fibers in anaphase this would suggest that after chromosomes separate from eachother in anaphase and there is less friction, k-fibers can slide at a similar velocity as the bridging fibers.

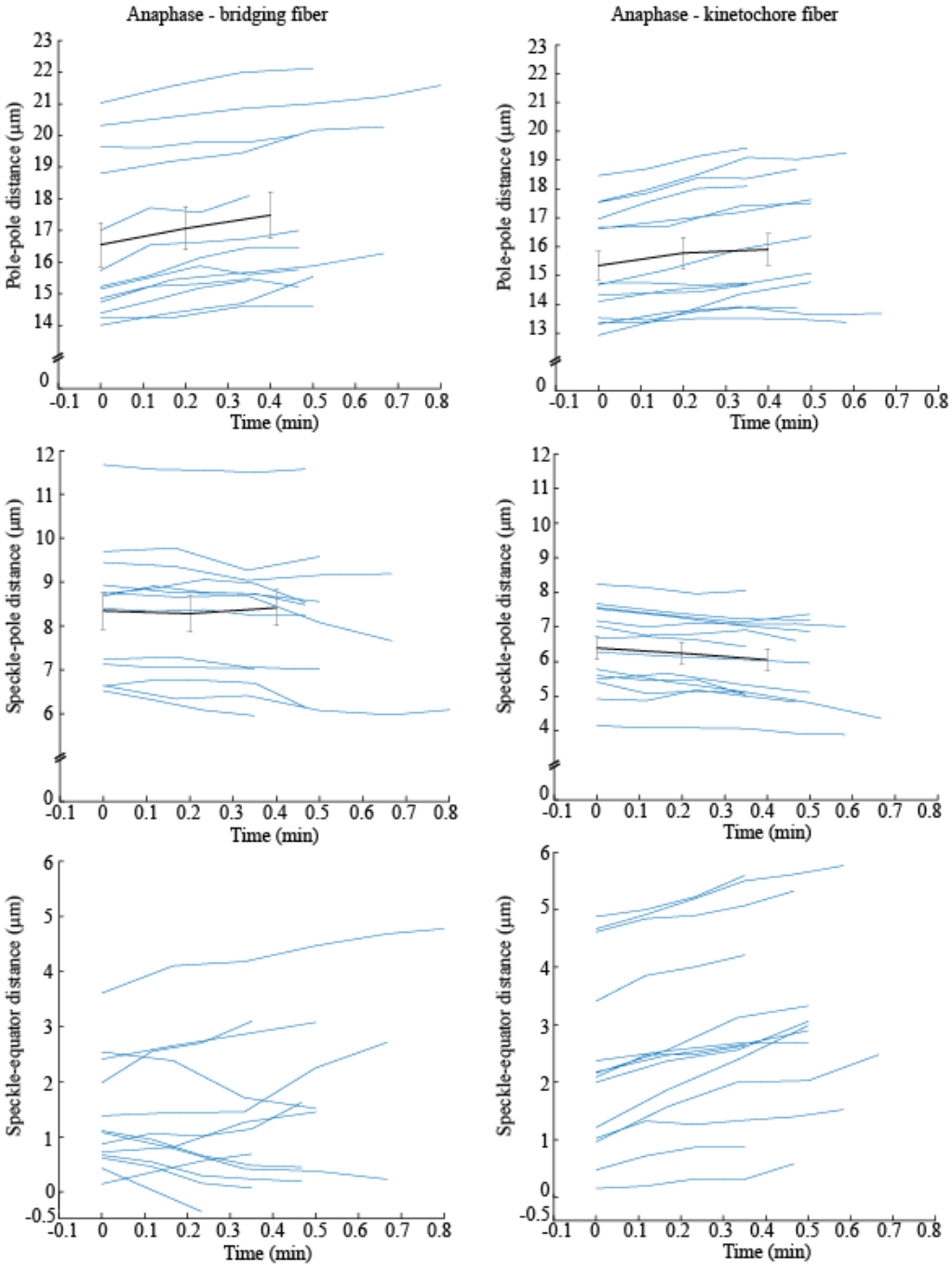

Figure 21. Raw data describing poleward flux in untreated anaphase cells. Here I show the data about pole-pole movement, speckle-pole movement and speckle-equator movement in untreated anaphase spindles. On te left side there is data related to measurements on the bridging fiber and on the right side to k-fiber.

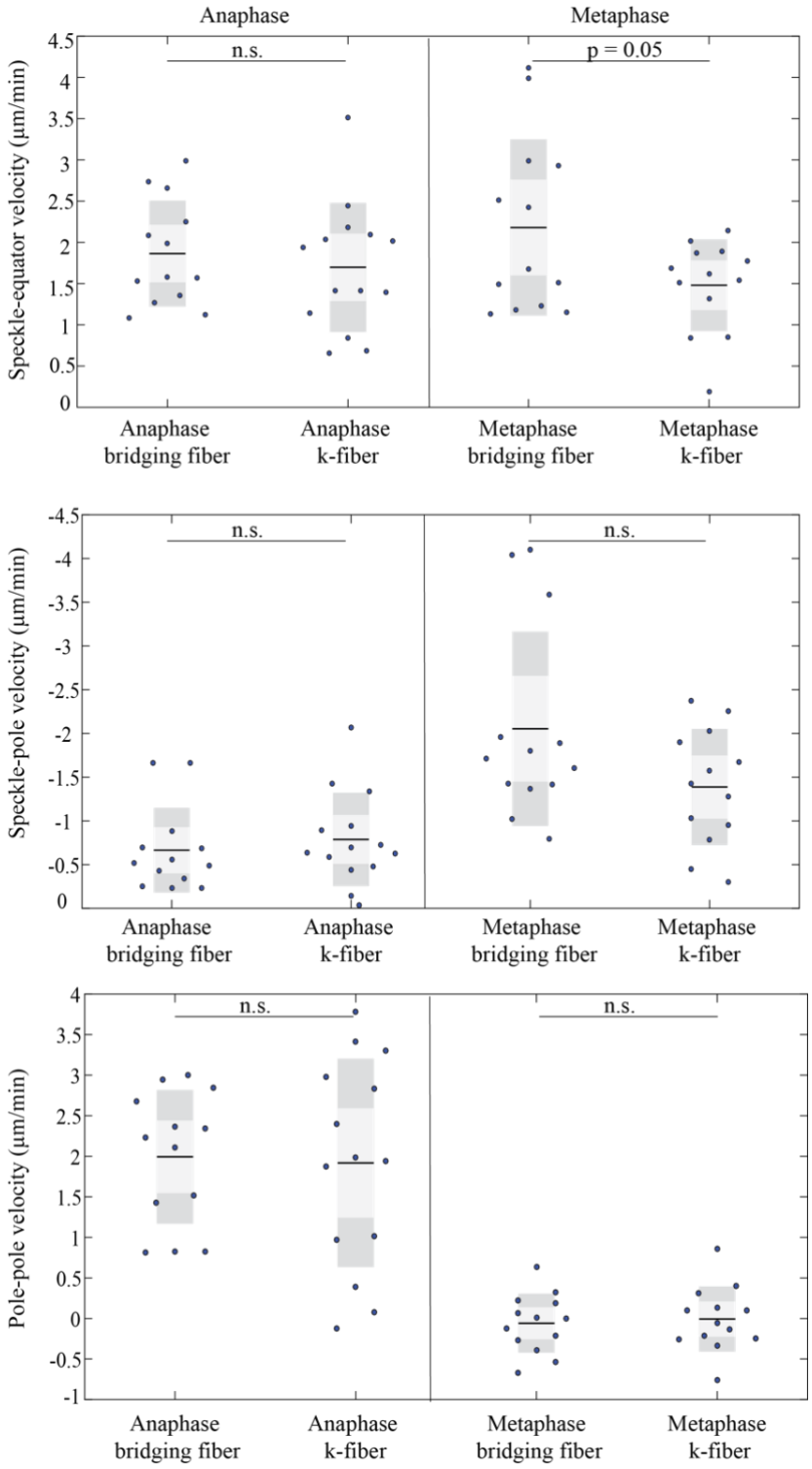

Figure 22. Speckle-equator, speckle-pole and pole-pole velocities in untreated anaphase and metaphase spindles. Speckle-equator velocity for the bridging fiber and for the k-fiber is not significantly different in anaphase. In metaphase bridging fibers slide at a higher rate than

k-fibers. Speckle-pole velocity for the bridging fiber and for the k-fiber is not significantly different in anaphase, but in metaphase bridging fibers flux at a higher rate than k-fibers. Pole-pole velocity is the same for the bridging and k-fiber in metaphase, and also it is the same for the bridging and k-fiber in anaphase. Each dot corresponds to an individual speckle. The light and dark area in the boxes mark 95% confidence interval on the mean and standard deviation, respectively; and the black line shows mean value. Statistical analysis, t-test.

4.3 EG5 inhibition results in a 30% slower sliding of antiparallel microtubules

The most well-known sliding motor, kinesin-5 family member EG5, was investigated as a first step in the research of molecular motors responsible for force generation in producing of the poleward flux. It was hypothesized by many that EG5 is the primary sliding motor in various circumstances during mitosis (Gayek & Ohi, 2014; Hoyt, 1994; Kapoor et al., 2000; Mann & Wadsworth, 2019; Saunders & Hoyt, 1992; Straight et al., 1998). To check if EG5 is crucial for poleward flux of the bridging and k-fibers, EG5 small molecule drug inhibitor STLC (Skoufias et al., 2006) was added to the metaphase cells. STLC was used because it quickly inhibits EG5-driven MT sliding velocity by targeting the catalytic domain of EG5 and
inhibiting EG5 basal and MT-activated ATPase activity as well as mant-ADP release of the motor. STLC is a tight binding inhibitor of EG5 (Skoufias et al., 2006) which removes EG5 signal from the spindle (Figure 23). It is known that adding the STLC earlier in mitosis leads to immediate spindle collapse into monopolar spindle (Gayek & Ohi, 2014). Our goal here was to investigate the phase of the spindle collapse and measure sliding during the active collapse of the spindle while the spindle is still bipolar. Thus, speckle movement tracking was done immediately after STLC was added to cells and measured during spindle collapse and not in monopolar spindles (Figure 24). It has been shown that in human osteosarcoma (U2OS) cell line, MT-sliding motors EG5 and KIF15 collaboratively act on interpolar MTs (Steblyanko et al., 2020b; Tanenbaum et al., 2009; vanHeesbeen et al., 2014; Vanneste et al., 2009), but in RPE-1 cells that were used here, only EG5 inhibition was sufficient for spindle collapse. When added in metaphase, addition of STLC in most cases led to significant spindle length decrease (Figure 24, 26 and 27) meaning that EG5-outward force generation is crucial during metaphase. Speckle-equator velocities for untreated metaphase cells for bridging fibers is 2.18 ± 0.30 μm/min (n = 13 speckles from 8 cells) and for k-fibers is 1.48 ± 0.15 μm/min (n = 13 speckles

from 7 cells) (Figure 25 and 27) which are very similar with speckle-pole velocities from Risteski et al. (2022). This confirms that speckle-equator measure can be used to describe poleward flux in conditions where the poles are moving. Also, same as previously reported, bridging fibers flux at a higher rate than k-fibers in metaphase ($p = 0.0467$). Speckle-equator velocity for EG5 inhibited metaphase cells for bridging fibers is 1.54 ± 0.30 μm/min ($n = 15$ speckles from 10 cells) and for k-fibers is 1.28 ± 0.11 μm/min ($n = 13$ speckles from 8 cells) (Figure 26 and 27) which is not significantly different from control metaphase cells ($p = 0.1288$). Interestingly, in cells upon EG5 inhibition there was not significant difference between bridging fiber and k-fiber sliding as in untreated metaphase cells, even though bridging fiber sliding is still slightly faster than k-fiber sliding. Speckle-pole velocity for untreated metaphase cells for bridging fibers is -2.05 ± 0.30 μm/min ($n = 13$ speckles from 8 cells) and for k-fibers is -1.38 ± 0.18 μm/min ($n = 13$ speckles from 7 cells), and for EG5 inhibited metaphase cells for bridging fibers is -1.76 ± 0.31 μm/min ($n = 15$ speckles from 10 cells) and for k-fibers is -1.29 ± 0.28 μm/min ($n = 13$ speckles from 8 cells) (Figure 24, 25 and 26). Pole-pole velocity for untreated metaphase cells measured for speckles tracked on bridging fibers is -0.06 ± 0.10 μm/min ($n = 13$ speckles from 8 cells) and for speckles tracked on k-fibers is -0.001 ± 0.111 μm/min ($n = 13$ speckles from 7 cells) which means that the poles in metaphase during the time that speckles were tracked were not moving. Pole-pole velocity for EG5 inhibited metaphase cells for speckles tracked on bridging fibers is -1.13 ± 0.26 μm/min ($n = 15$ speckles from 10 cells) and for speckles tracked on k-fibers is -1.13 ± 0.26 μm/min ($n = 13$ speckles from 8 cells) (Figure 25, 26 and 27). Negative values for pole-pole velocity mean that the poles were moving towards eachother so the distance between them was getting shorter. Speckle on bridging fibers and k-fibers could not be tracked for the same kinetochore pair because of the limitations of the method as previously mentioned, but values like pole-pole velocity are good control to see that the pole-pole velocities for speckles tracked on the bridging fibers and speckles tracked on the k-fibers are the same which means that the speckles were tracked at the same phase of the collapse after EG5 was inhibited.

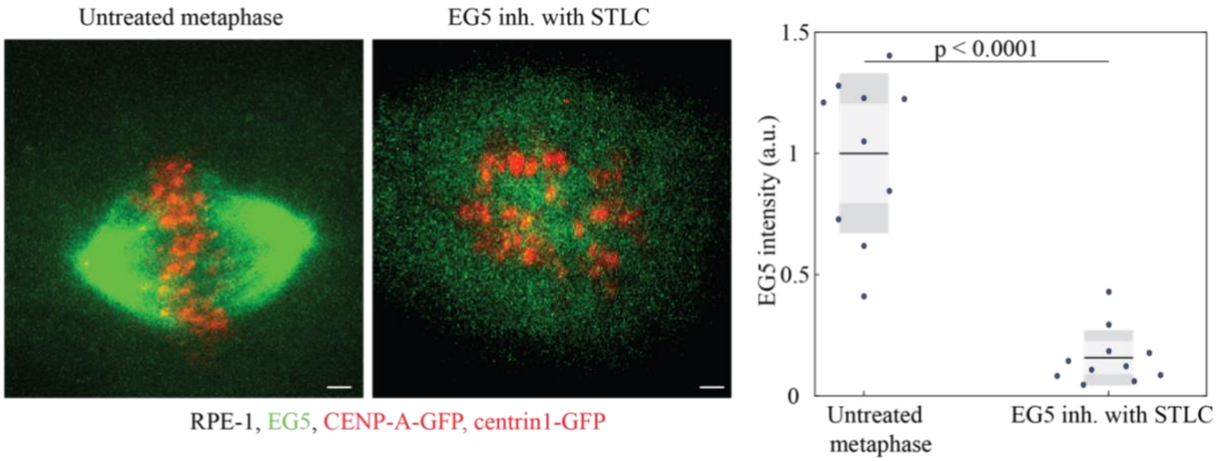

Figure 23. After inhibition of EG5 motor with STLC, mitotic spindle collapses into monopolar spindle. Immunofluorescence (IF) images of untreated (left) and STLC-treated (middle) metaphase mitotic spindle in a RPE-1 cells stably expressing CENP-A-GFP and centrin1-GFP (red) and stained with AlexaFluor488 conjugated with EG5 antibody (green). The graph on the right side of the image shows decrease in EG5 intensity after STLC treatment. Each dot corresponds to an individual cell. The light and dark area in the boxes mark 95% confidence interval on the mean and standard deviation, respectively; and the black line shows mean value. Statistical analysis, t-test. p-value: < 0.0001. Scale bar is 1µm.

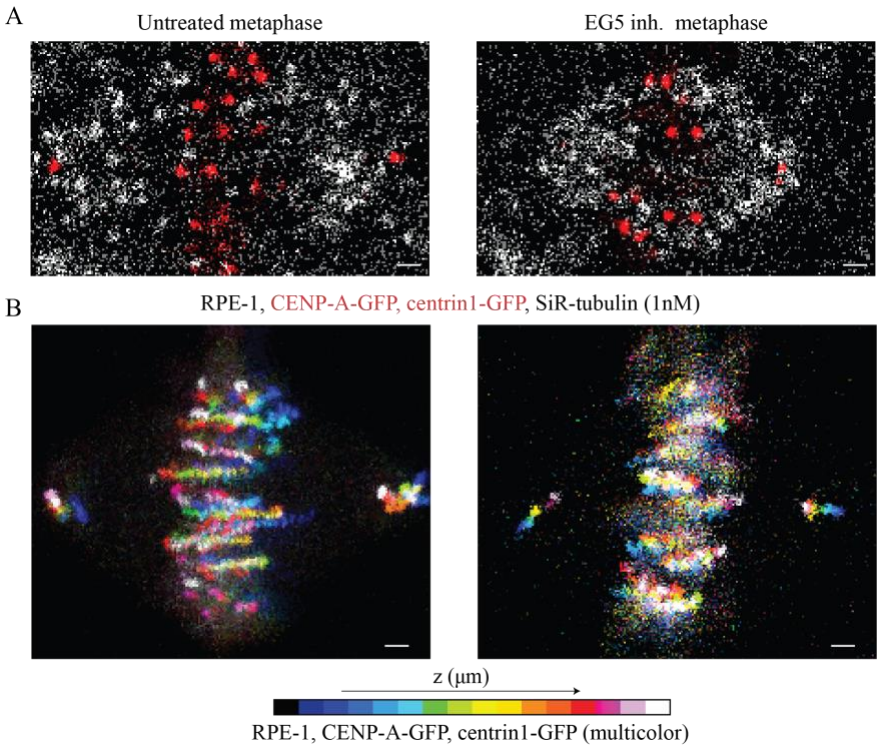

Figure 24. Speckle microscopy assay for measurement of poleward flux of individual MTs. **(A)** Live images of untreated metaphse spindle (left) and EG5 inhibited metaphase spindle (right) in a RPE-1-CC (red) stained with 1 nM SiR-tubulin dye, which appears as distinct speckles marking individual MTs (white). **(B)** Depth color coded (see color bar) live images filmed for 2 minutes of untreated metaphse spindle (left) and EG5 inhibited metaphase spindle (right) in a RPE-1 cells stably expressing CENP-A-GFP and centrin1-GFP. After STLC treatment the spindle rapidly shortens until it becomes a monopolar spindle. Scale bar is 1µm.

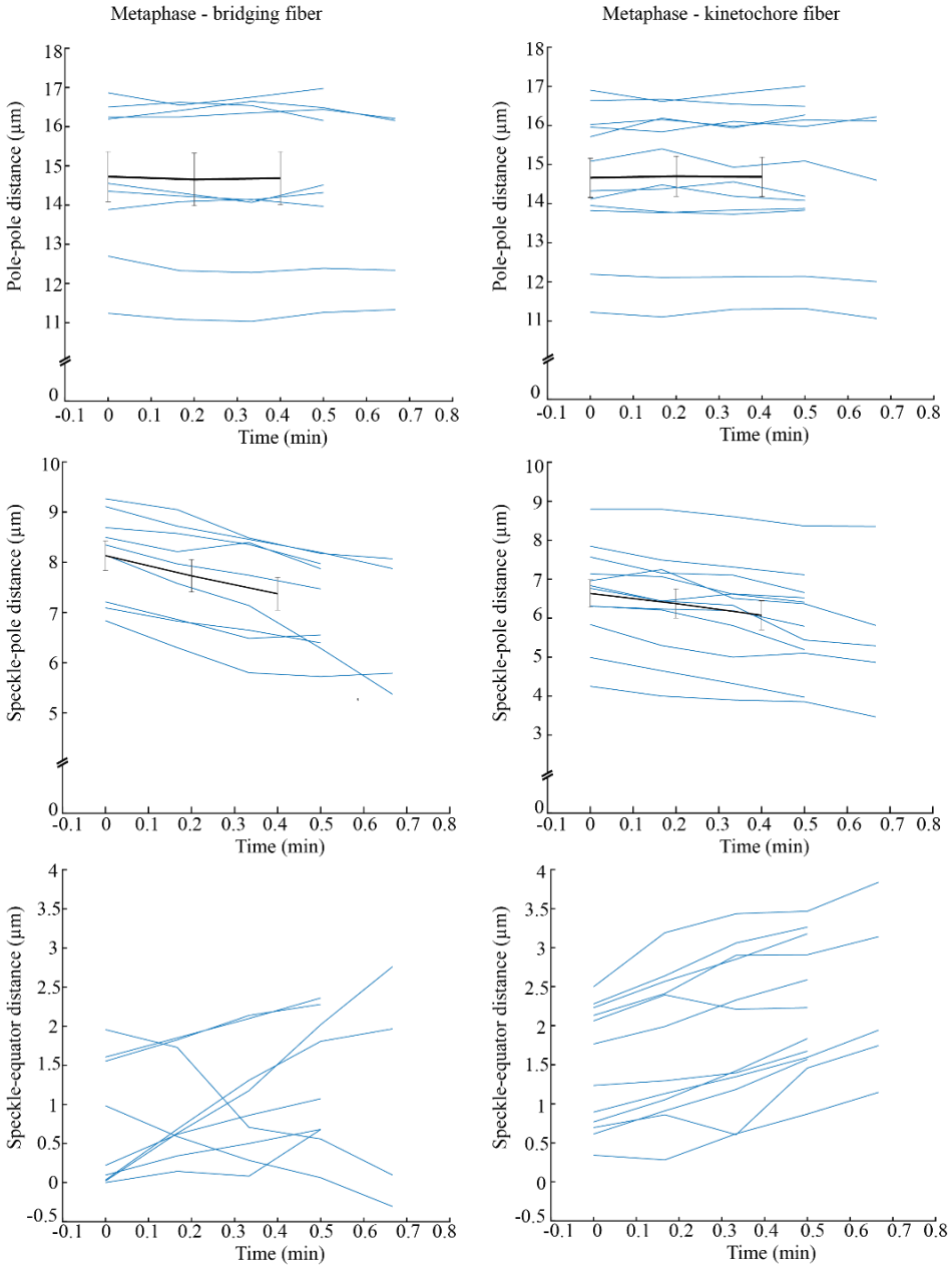

Figure 25. Raw data describing poleward flux in untreated metaphase cells. Here I show the data about pole-pole movement, speckle-pole movement and speckle-equator movement in

untreated metaphase spindles. On the left side there is data related to measurements on the bridging fiber and on the right side to k-fiber.

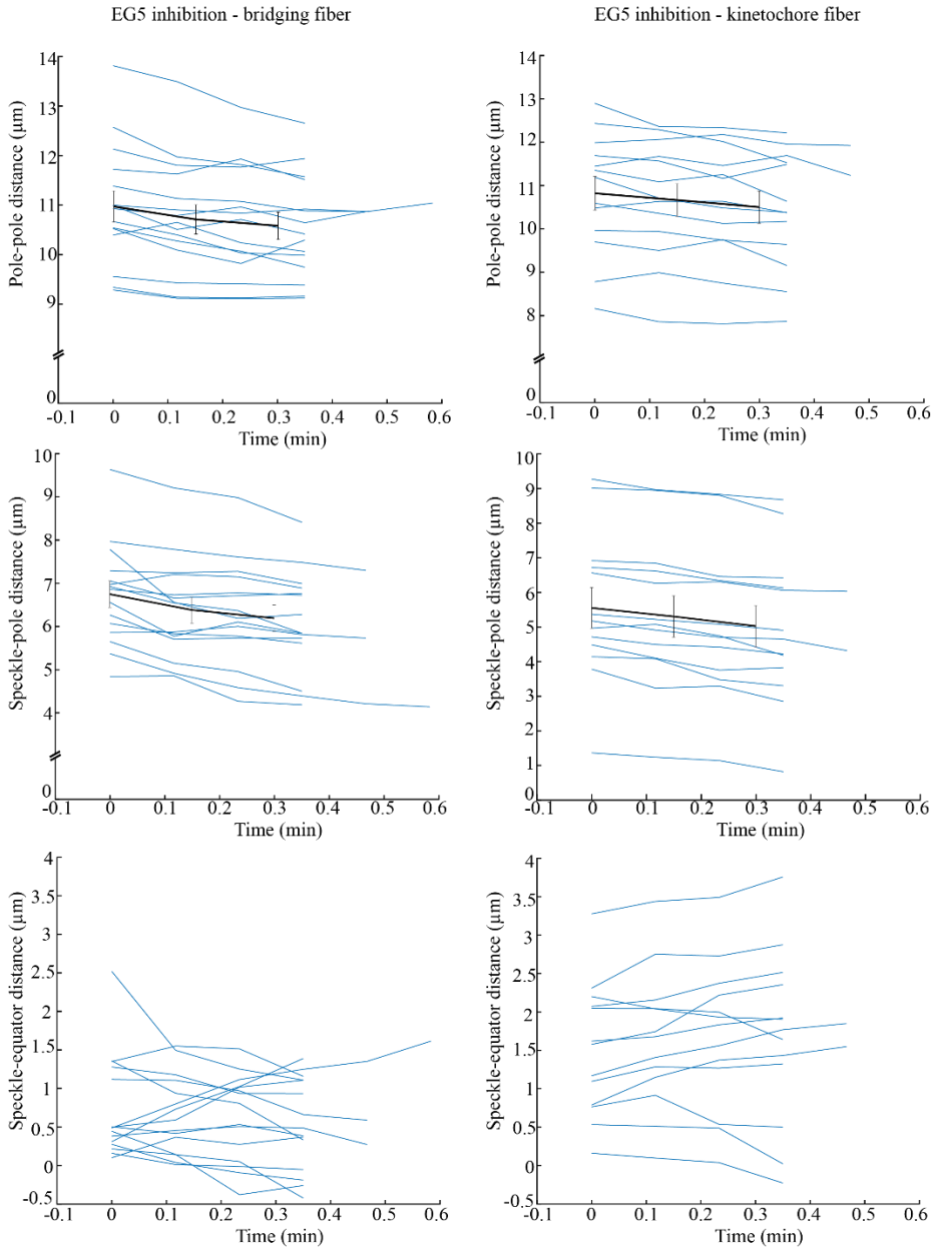

Figure 26. Raw data describing poleward flux in EG5 inhibited metaphase cells. Here I show the data about pole-pole movement, speckle-pole movement and speckle-equator

movement in EG5 inhibited metaphase spindles. On the left side there is data related to measurements on the bridging fiber and on the right side to k-fibers.

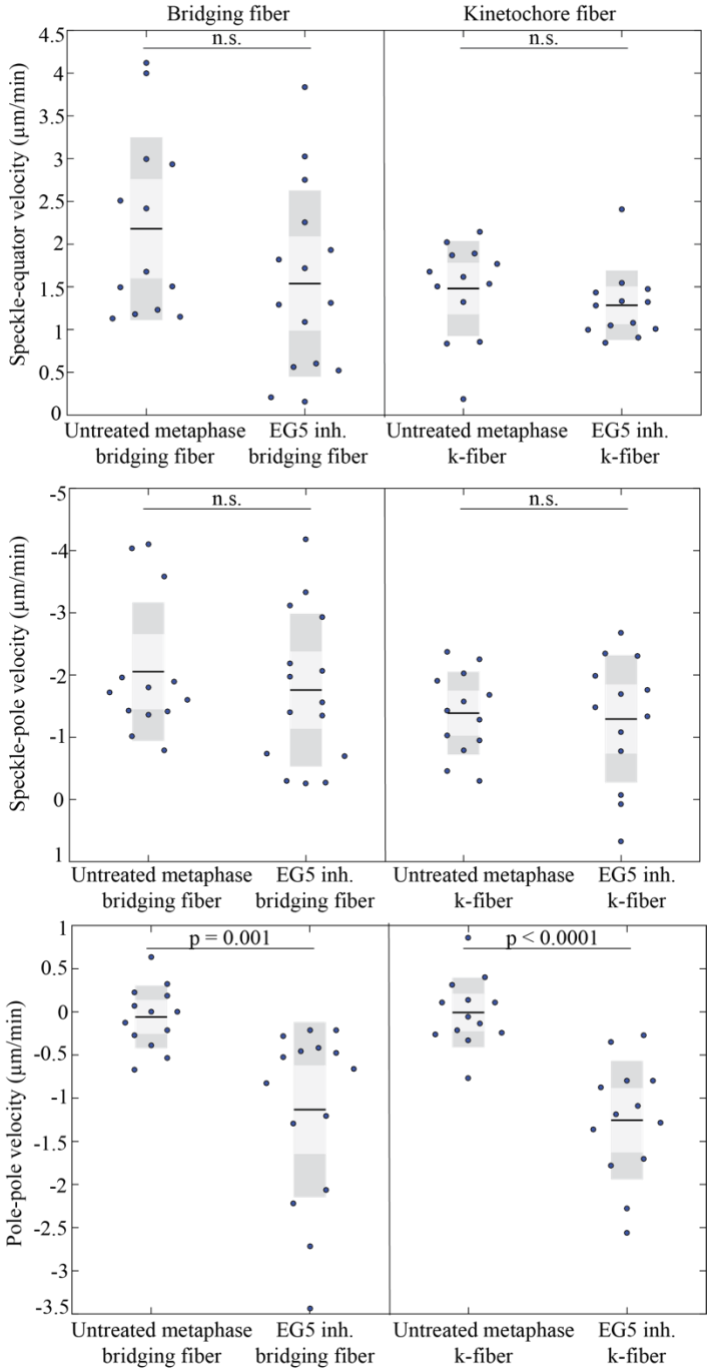

Figure 27. Speckle-equator, speckle-pole and pole-pole velocities in untreated metaphase and EG5 inhibited metaphase spindles. Speckle-equator velocity for the bridging fiber and for the k-fiber is not significantly different after EG5 inhibition in the metaphase spindles when

compared to the untreated metaphase spindles. Pole-pole velocity plots nicely show decrease of spindle length after EG5 inhibition with STLC. Each dot corresponds to an individual speckle. The light and dark area in the boxes mark 95% confidence interval on the mean and standard deviation, respectively; and the black line shows mean value. Statistical analysis, t-test.

Since speckle-equator velocity remains similar after EG5 inhibition with STLC, I speculate that the spindle midzone after EG5 inhibition remains the same as in untreated spindles and that other motor proteins in the midzone slide without EG5 activity. To test this hypothesis I decided to image RPE-1 cells with stable expression of PRC1 protein and investigate localization and intensity of PRC1 after EG5 inhibition in metaphase. PRC1 protein is known as the main bundler of antiparallel MTs (W. Jiang et al., 1998; Lee et al., 2012; She et al., 2019; Subramanian et al., 2010). In untreated metaphase spindles, PRC1 bundles extent mostly troughout the middle part of the spindle where the antiparallel overlaps are located (Kajtez et al., 2016b; Polak et al., 2017). RPE-1 cells with stable expression of PRC1 protein which I used here, have a slightly overexpressed PRC1 protein when compared to the endogenous PRC1 signal in the spindle, so PRC1 signal can be seen extending troughout the most part of the spindle and also concetrated on the spindle poles (Figure 28) whereas endogenous PRC1 signal can be seen only in the middle part of the spindle. Interestingly, after EG5 inhibition with STLC, PRC1 signal is localized similarly to the untreated metaphase during the whole spindle collapse (Figure 28). After analyzing PRC1 signal intensities in control metaphase and 2 minutes after EG5 was inhibited I can notice the spindle shortening after EG5 inhibition and correspondingly with the spindle length, the PRC1 signal is also shortened after EG5 inhibition (Figure 28). The length of the PRC1 signal in individual bundles in untreated metaphase RPE-1 cells with stable expression of PRC1 protein is 6.75 ± 0.19 μm (n of bundles = 33 from 10 cells), and in EG5 inhibited metaphase spindle the length of the PRC1 signal is 4.85 ± 0.13 μm (n of bundles = 53 from 12 cells) which is significant ($p < 0.0001$) but spindle length shortening also needs to be considered. Spindle length of untreated metaphase RPE-1 cells with stable expression of PRC1 protein is 12.34 ± 0.40 μm (n = 10 cells) and after EG5 inhibition the spindle length is 7.81 ± 0.24 μm (n = 12 cells) which is again significant ($p < 0.0001$) (Figure 28). When PRC1 signal length is divided with spindle length I get the percentage of the mitotic spindle length that the PRC1 takes. In untreated metaphase cells PRC1 signal takes 58% of the entire spindle length,

and in EG5 inhibited cell the PRC1 signal length is 61% of the spindle length which is the same ($p = 0.2$). Thus, even though the PRC1 signal is significantly shortened after EG5 inhibition their localization in the spindle remains similar as in untreated metaphase spindles. Taken together, these results suggest that even though PRC1 bundles are shortened, their structure is still functional and other motor proteins like KIF4A can slide the antiparallel bundles and keep the speckle-equator velocities at the similar rates as in untreated spindles.

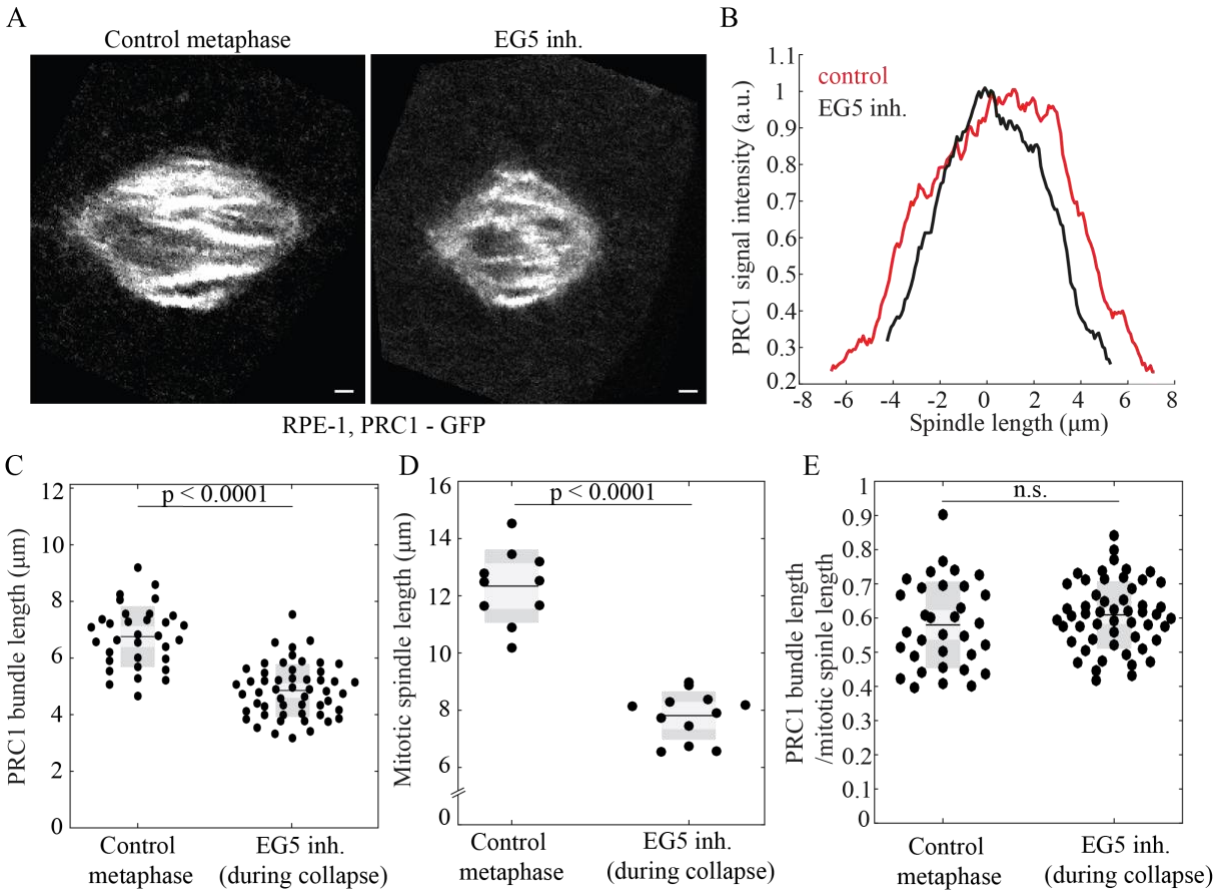

Figure 28. PRC1 signal in RPE-1 cells with stable expression of PRC1-GFP protein is significantly shortened after EG5 inhibition with STLC. (A) Live images of RPE-1 cells with stable expression of PRC1-GFP protein (gray) before and after EG5 inhibition. **(B)** After EG5 inhibition with STLC, spindles begin to collapse but as the spindle length gets shorter, PRC1 signal has similar localization to the control metaphase. **(C)** PRC1 signal length is significantly shorter 2 minutes after EG5 inhibition when compared to untreated metaphase spindles, **(D)** as well as the spindle length. **(E)** PRC1 length to spindle length ratio is the same for untreated and EG5 inhibited cells. Each dot corresponds to an individual PRC1 bundle or

cell. The light and dark area in the boxes mark 95% confidence interval on the mean and standard deviation, respectively; and the black line shows mean value. Statistical analysis, t-test. Scale bar is 1µm.

I speculate that the bridging fibers in EG5 inhibited RPE-1 cells are functional and appear the same as in untreated RPE-1 cell. To investigate this hypothesis I decided to study and compare the structure of the midzone MTs using MT preservation fixation protocol and STED microscopy. Using this super-resolution approach to visualise MTs in the spindle, I showed that midzone MT organization is similar in control cells and in EG5 inhibited cells (Figure 29). Thus, I suggest that the spindle midzone remains functional after EG5 inhibition with STLC and that the structure of the antiparallel MTs is similar in untreated metaphase spindles and in EG5 inhibited spindles.

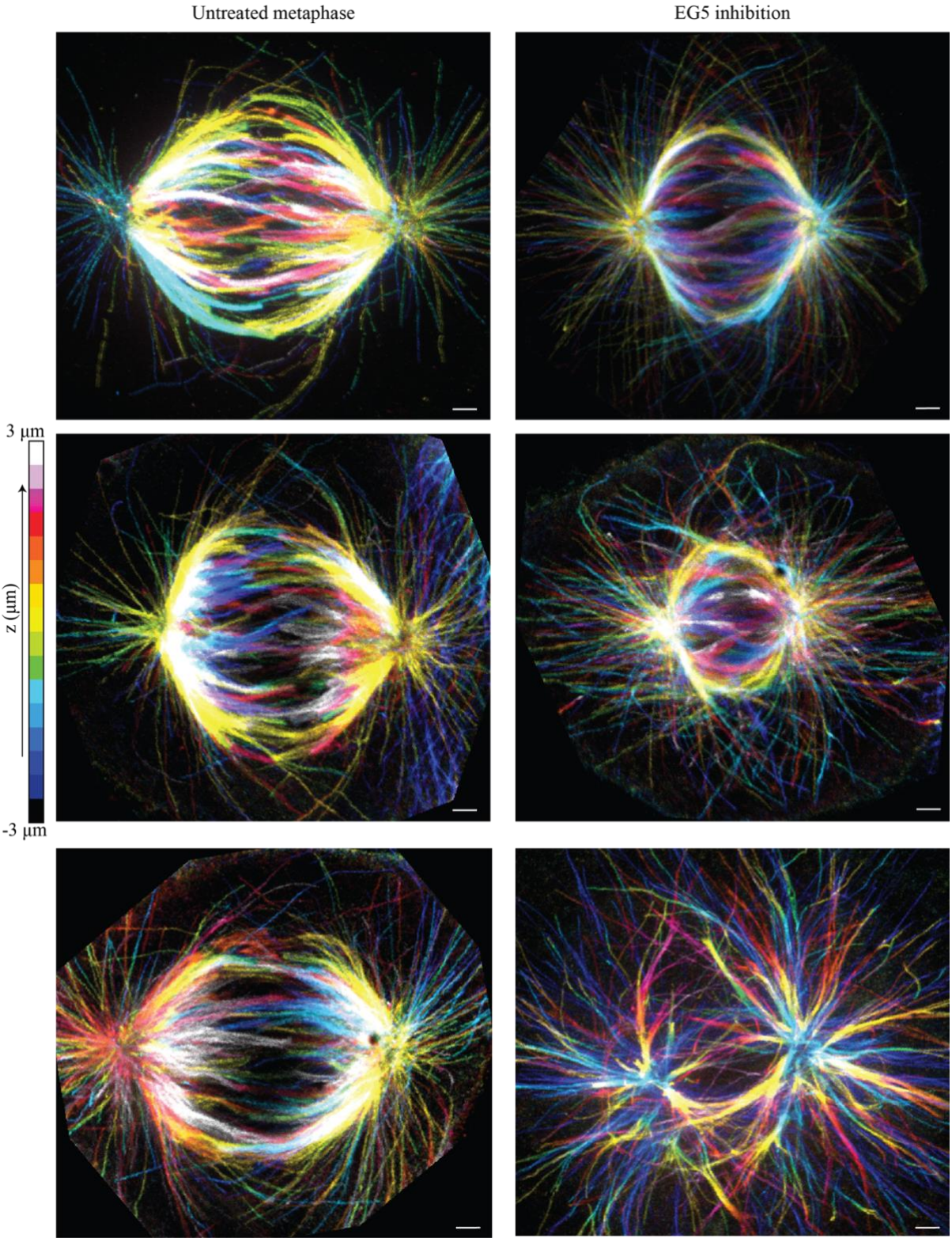

Figure 29. After EG5 inhibition spindles are shortened before they collapse to monopolar spindles. Immunofluorescence images of fixed control and STLC-treated RPE-1 cells stably

expressing CENP-A-GFP and centrin1-GFP (not showed here) and stained with AlexaFluor594 conjugated with α-tubulin antibody (multicolor). Scale bar is 1μm.

Afterwards, I decided to study kinetochore oscilations to see if there were some abnormal behaviors in EG5 inhibited cells when compared to the untreated metaphase spindles. I tracked kinetochore oscilations of 10 pairs of kinetochores from control cells and also 10 pairs of kinetochores from EG5 inhibited cells. Kinetochore oscilations were tracked by measuring the distance of both kinetochores from one pair from the equator of the spindle. Equator of the spindle is the midline between both poles in every frame that was imaged. When compared to control cells, oscilations in EG5 inhibited cells are higher (Figure 30) which is in agreement with the phenotype that could be seen during imaging. Also, I measured interkinetochore distance in control and EG5 inhibited cells and confirmed what can also be seen in the movies, that EG5 inhibited cells have shorter interkinetochore distance when compared to control ($p<0.0026$) (Figure 30). Taken together, these results show that the speckle-equator velocity of the bridging MTs after EG5 inhibition decreased around 30% when compared to the untreated metaphase spindles. Even though this is not statistically significant, speckle-equator velocity changed more than speckle-pole velocity after EG5 inhibition when compared to the untreated metaphase spindles thus I can speculate that inhibition of EG5 motor had more effect on the sliding of the bridging MTs than on the depolymerization at the poles.

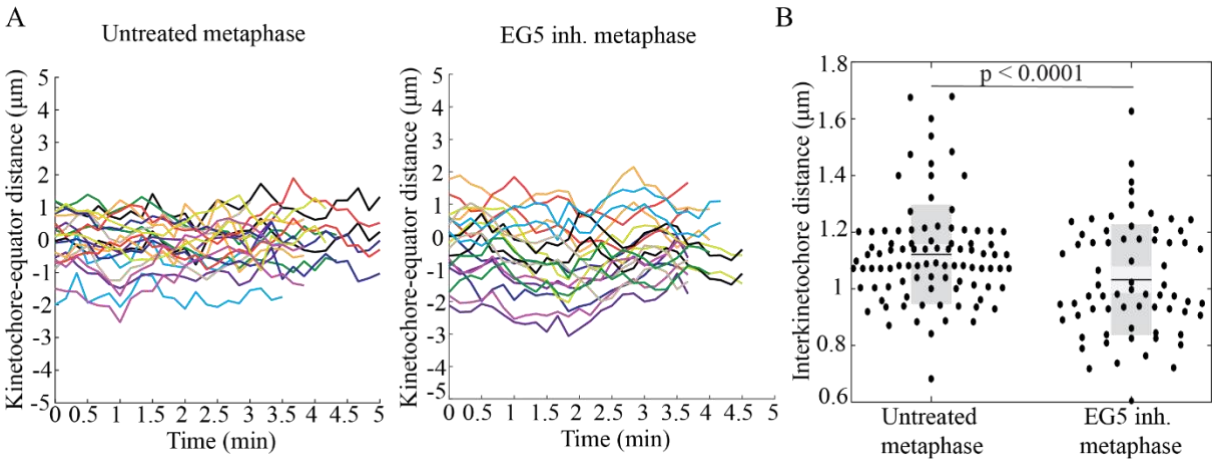

Figure 30. Kinetochore-equator distance tracked in time for control and EG5 inhibited cells is similar but interkinetochore distance for EG5 inhibited cells is significantly shorter than in untreated spindles. (A) Kinetochore oscilations are higher EG5 inhibited cells. **(B)**

Graph on the right side of the figure is showing interkinetochore distances for control and EG5 inhibited cells. I can notice that EG5 inhibited cells have significantly shorter interkinetochore distances. Each dot corresponds to an individual kinetochore pair. The light and dark area in the boxes mark 95% confidence interval on the mean and standard deviation, respectively; and the black line shows mean value. Statistical analysis, t-test.

4.4 EG5 and KIF4A in metaphase slide together as the key motors in the midzone

Recent work from our lab (Vukušić et al., 2021) showed that kinesins KIF4A and EG5 together drive elongation of the anaphase spindle. Furthermore, recently it was showed by Steblyanko et al. (2020) that MT-sliding motors EG5 and KIF15 collaboratively act on interpolar MTs, assisted by CENPE at kinetochores in prometaphase and KIF4A on chromosome arms in metaphase. Since I observed that MT sliding is perturbed after combined depletion of KIF4A and inhibition of EG5 by STLC during anaphase, I was interested in investigating sliding of individual MTs in the metaphase spindle. After EG5 inhibiton in KIF4A depleted cells I can observe two scenarios. One is that spindles start to shorten immediately after addition of STLC, then start anaphase A and after that I observed blocked spindle elongation. This is the case that I observed and described previously (Vukušić et al., 2021). Second scenario is when after addition of STLC spindles start to shorten and collapse into monopolar spindles which is the same response observed when STLC is added to control RPE-1 cells (Figure 31). This is the case I was interested to explore further. KIF4A is depleted by siRNA and addition of STLC and imaging is done after 48 hours (Figure 32). In these collapsing spindles I measured pole-pole velocity, speckle–pole velocity and speckle-equator velocity. Distance that poles go trough time of the tracked speckles is similar to that of only EG5 inhibited spindles (Figure 33) which is suggesting that the collapse of the spindle is similar between the two cases and also it is the same for bridging and for the kinetochore fibers. Distance of the speckle and the poles trough time of the tracked speckles is affected by the moving of the poles towards eachother but compared to the control cells and only EG5 inhibited cells is shorter for the bridging as well as for the k-fiber (Figure 33). Distance of the speckle from the equator of the spindle trough time of the tracked speckles is shorter when compared to control and only EG5 inhibited cells for the bridging and for the k-fibers. Pole-pole velocity for EG5 inhibited and KIF4A depleted cells during collapse for bridging fibers is -0.81 ± 0.15

μm/min (n = 10 speckles from 5 cells) and for k-fibers is – 0.95 ± 0.20 μm/min (n = 10 speckles from 7 cells) (Figure 34). Speckle-pole velocity for EG5 inhibited and KIF4A depleted cells for bridging fibers is – 1.17 ± 0.21 μm/min (n = 10 speckles from 5 cells) and for k-fibers is – 0.81 ± 0.22 μm/min (n = 10 speckles from 7 cells) (Figure 34). Speckle-equator velocity for EG5 inhibited and KIF4A depleted cells for bridging fibers is 0.80 ± 0.17 μm/min (n = 10 speckles from 5 cells) and for k-fibers is 0.46 ± 0.13 μm/min (n = 10 speckles from 7 cells) (Figure 34). Both values are significantly different from control metaphase cells ($p = 0.0013$ for bridging fiber velocity in control and EG5 inhibited and KIF4A depleted cells, $p < 0.0001$ for k-fiber velocity in control and EG5 inhibited and KIF4A depleted cells). Furthermore, similar as in only EG5 inhibited cells, in EG5 inhibited and KIF4A depleted cells there was not significant difference between bridging fiber and k-fiber flux even though bridging fiber flux is still slightly higher than k-fiber flux. As a whole, this result suggests that in metaphase, as in anaphase, EG5 and KIF4A are the main sliding forces in the midzone and that without these two motors bridging fiber sliding is severly slowed and as a consequence so is k-fiber sliding.

Figure 31. Speckle microscopy assay for measurement of poleward flux of individual MTs.

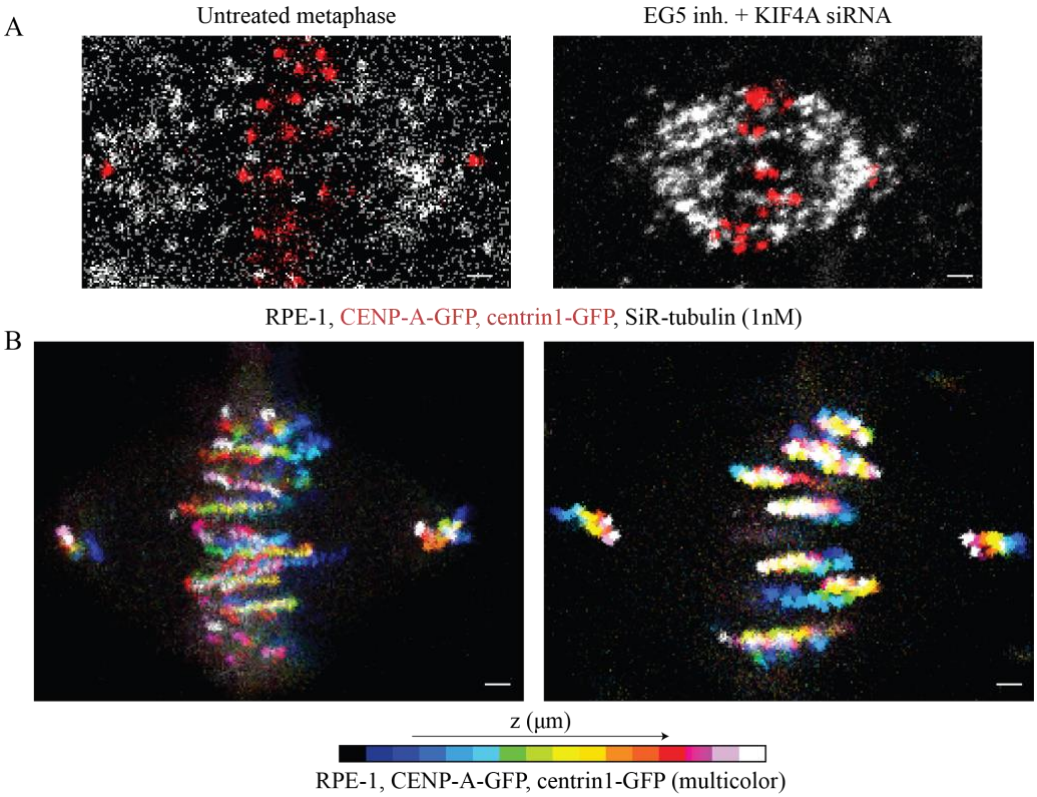

(A) Live images of untreated metaphase spindle (left) and EG5 inhibited and KIF4A depleted metaphase spindle (right) in a RPE-1 cells stably expressing CENP-A-GFP and centrin1-GFP

(red) stained with 1 nM SiR-tubulin dye, which appears as distinct speckles marking individual MTs (white). **(B)** Depth color coded (see color bar) live images filmed for 2 minutes of untreated metaphase spindle (left) and EG5 inhibited and KIF4A depleted metaphase spindle (right) in a RPE-1 cells stably expressing CENP-A-GFP and centrin1-GFP. After EG5 inhibition in KIF4A depleted cells one of the scenarios that I observe is collapse into monopolar spindles. The first phase of this collapse is shown as spindle length is actively decreasing. Scale bar is 1µm.

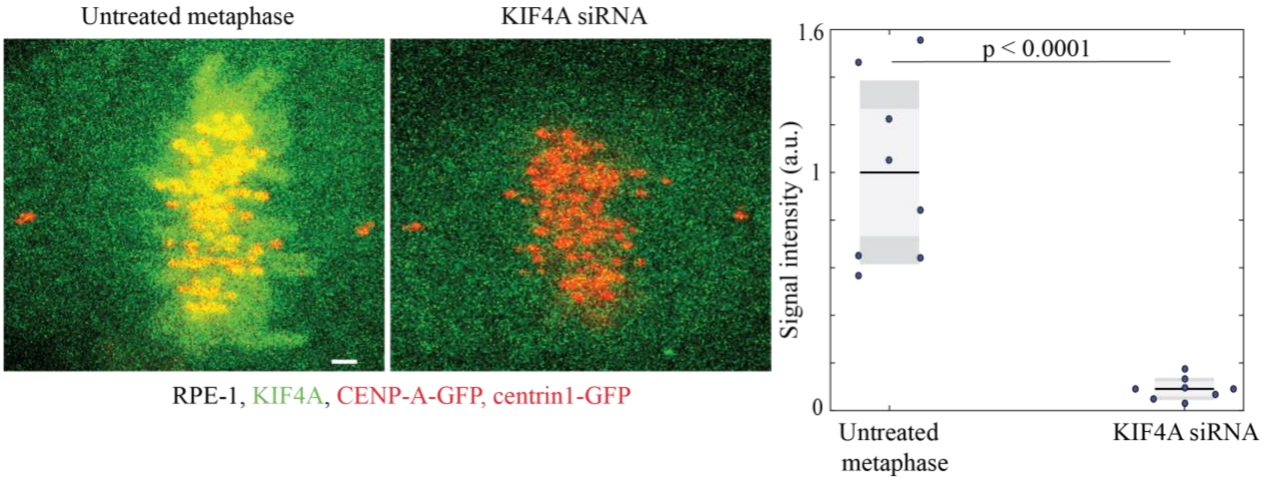

Figure 32. After KIF4A depletion with siRNA there is no KIF4A signal on the spindle. Immunofluorescence images of fixed untreated (left) and KIF4A depleted spindles (right) of RPE-1 cells stably expressing CENP-A-GFP and centrin1-GFP (red) and stained with AlexaFluor594 conjugated with KIF4A antibody (green). Scale bar is 1µm. On the right side of the image the graph shows signal intensity of KIF4A protein decreased after depletion with siRNA.

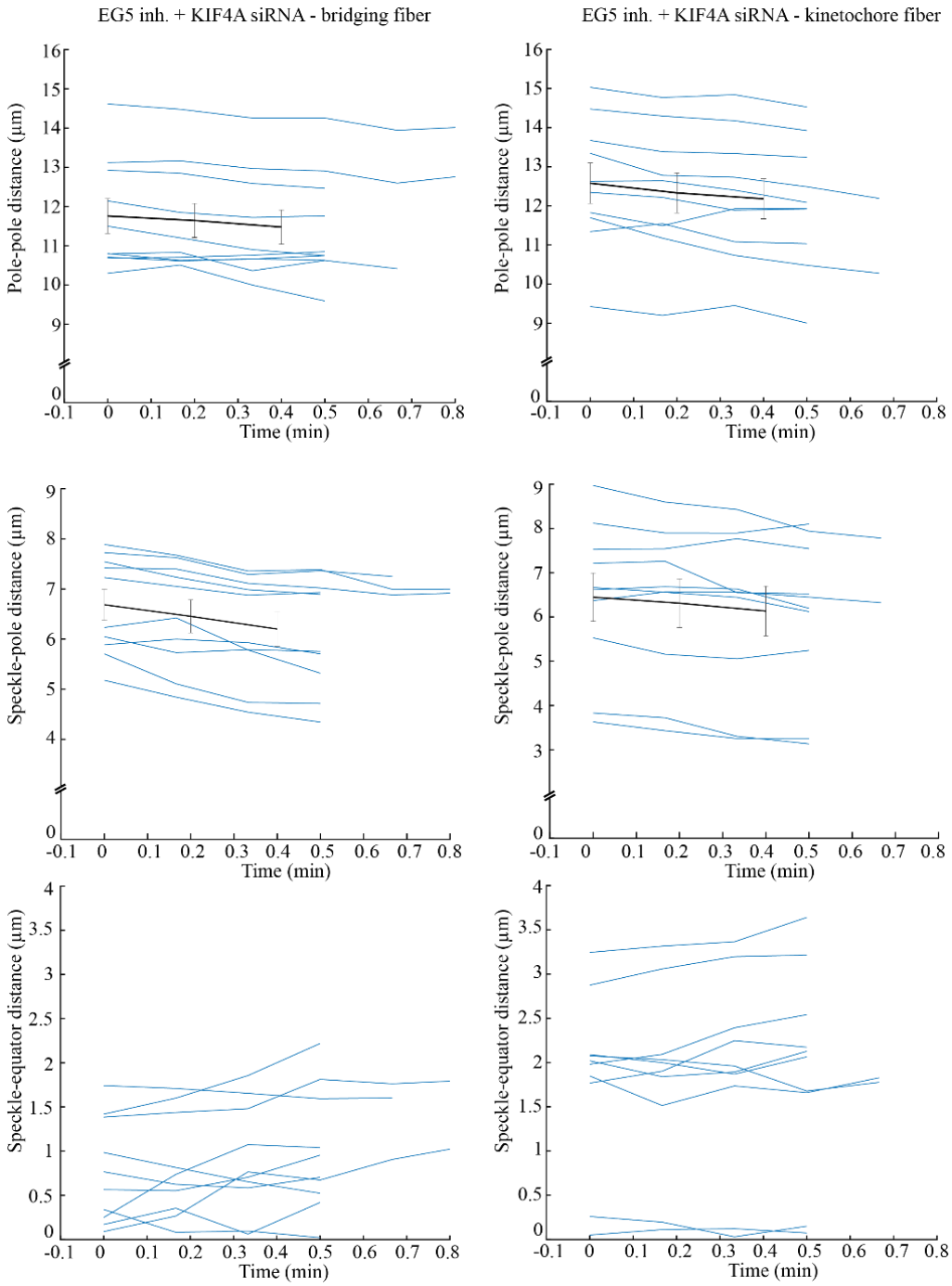

Figure 33. Raw data describing poleward flux in EG5 inhibited and KIF4A depleted cells. Here I show the data about pole-pole movement, speckle-pole movement and speckle-equator movement in EG5 inhibited and KIF4A depleted spindles. On te left side there is data related to measurments on the bridging fiber and on the right side to k-fibers.

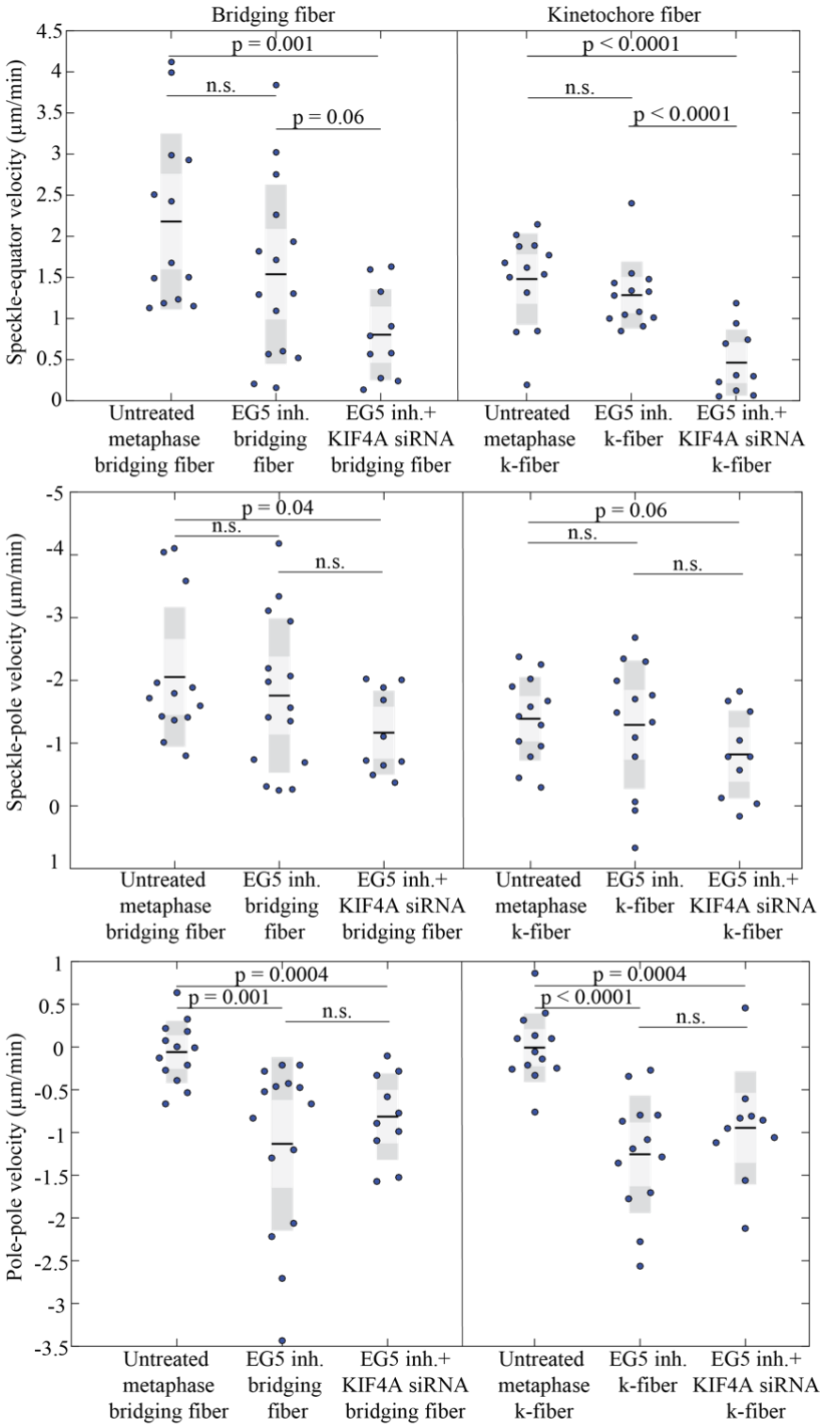

Figure 34. Speckle-equator, speckle-pole and pole-pole velocities in untreated metaphase, EG5 inhibited and EG5 inhibited and KIF4A depleted spindles. Speckle-equator velocity of the bridging fiber and the k-fiber is singificantly slower after KIF4A depletion and EG5 inhibition suggesting that they are the main drivers of sliding in metaphase spindles. Each dot corresponds to an individual speckle. The light and dark area in the boxes mark 95% confidence

interval on the mean and standard deviation, respectively; and the black line shows mean value. Statistical analysis, t-test.

Since speckle-equator velocity significantly decreased after EG5 inhibition together with KIF4A depletion, I again decided to image RPE-1 cells with stable expression of PRC1 protein this time after EG5 inhibition together with KIF4A depletion and compare the PRC1 signal with control spindles. Interestingly, after EG5 inhibition with STLC together with KIF4A siRNA, PRC1 signal is taking similar amount of spindle length as in only EG5 inhibited spindles (Figure 35). When PRC1 signal is measured in control spindles and 2 minutes after EG5 was inhibited in KIF4A depleted spindles and their signal intensities are compared it is visible that in the EG5 inhibited and KIF4A depleted spindles spindles shortened similar to the only EG5 inhibited mitotic spindles and that the PRC1 signal length is also very similar to the EG5 only inhibition (Figure 35). For the PRC1 measurments in this experiment, I decided to take KIF4A depleted spindles as the control since KIF4A depleted RPE-1 metaphase spindles have very similar phenotype and velocities as untreated metaphase spindles (Risteski et al., 2022). The length of the PRC1 signal in individual bundle in KIF4A depleted metaphase RPE-1 cells with stable expression of PRC1 protein is 7.56 ± 0.20 µm (n of bundles = 46 from 10 cells), and in EG5 inhibited and KIF4A depleted metaphase spindle the length of the PRC1 bundle is 5.23 ± 0.15 µm (n of bundles = 18 from 8 cells) which is statistically significant ($p < 0.0001$). Spindle length of KIF4A depleted metaphase RPE-1 cells with stable expression of PRC1 protein is 13.52 ± 0.40 µm (n = 10 cells) and after EG5 inhibition the spindle length is 8.51 ± 0.26 µm (n = 8 cells) which is again statistically significant ($p < 0.0001$). In KIF4A depleted metaphase cells PRC1 signal takes 56% of the entire spindle length which is not different than in untreated metaphase ($p = 0.6$), and in EG5 inhibited and KIF4A depleted cell the PRC1 signal length is 62% of the spindle length which is the same as in untreated metaphase ($p = 0.2$). Thus, even though the PRC1 signal is significantly shortened after EG5 inhibition and KIF4A depletion, their localization in the spindle remains similar as in KIF4A depleted metaphase spindles (Figure 36). Taken together, these results suggest that even though PRC1 bundles are shortened, their structure is perserved same as in only EG5 inhibited spindles. One difference in this treatment is that the two main motors that slide together in the midzone of the spindle are removed which would explain significant decrease in the speckle-equator velocities for the bridging and k-fibers when compared to the untreated metaphase RPE-1 cells.

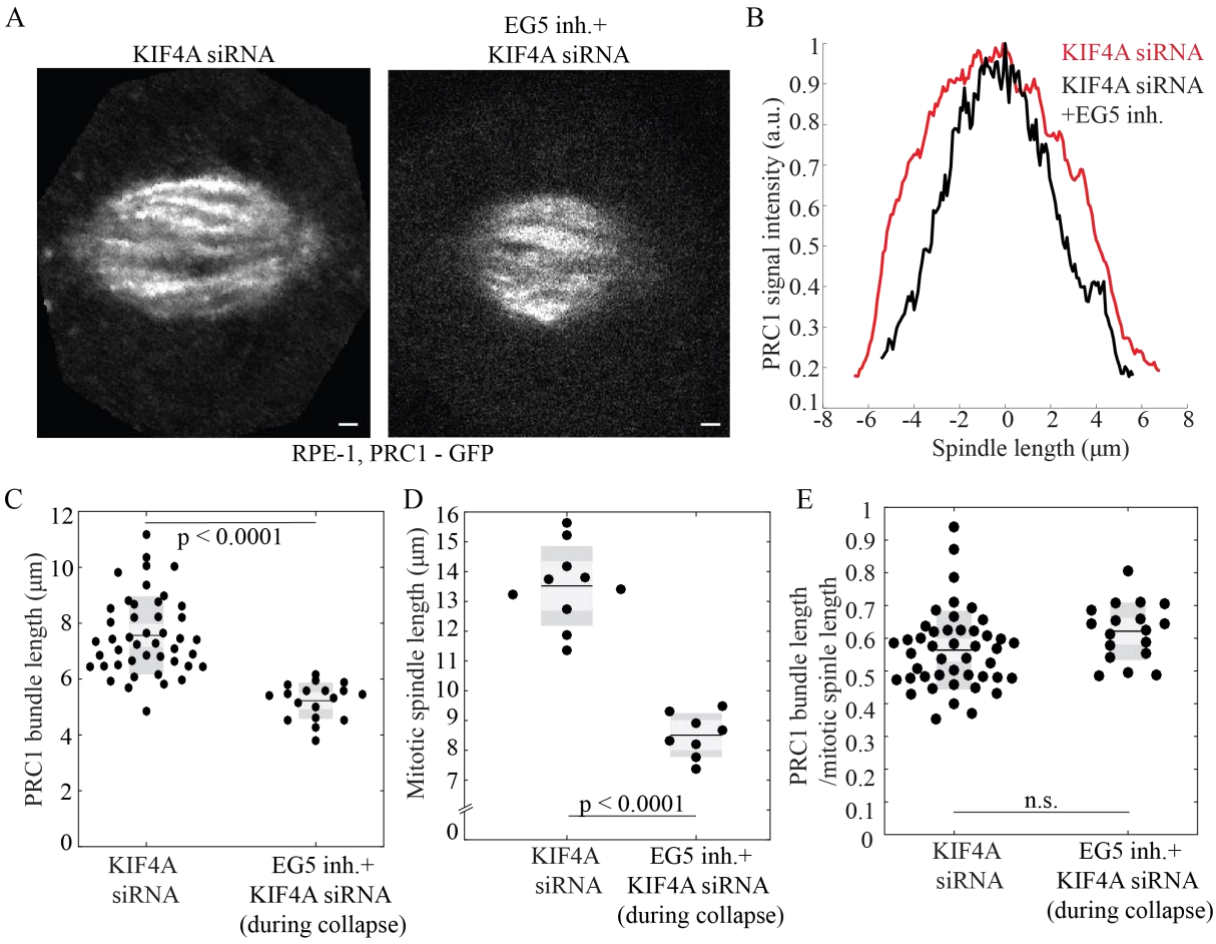

Figure 35. PRC1 signal in RPE-1 cells with stable expression of PRC1-GFP protein is significantly shortened after EG5 inhibition and KIF4A depletion. (A) Live images of KIF4A depleted RPE-1 cells with stable expression of PRC1-GFP protein (gray) before and after EG5 inhibition. **(B)** After EG5 inhibition with STLC in KIF4A depleted cells, spindles begin to collapse but as the spindle length gets shorter, PRC1 signal localization is similar to the KIF4A depleted metaphase. **(C)** PRC1 bundle length is significantly shorter 2 minutes after EG5 inhibition in KIF4A depleted spindles when compared to only KIF4A depleted metaphase spindles, **(D)** as well as the spindle length. **(E)** PRC1 length to spindle length ratio is the same for untreated and EG5 inhibited and KIF4A depleted cells.. Each dot corresponds to an individual PRC1 bundle or cell. The light and dark area in the boxes mark 95% confidence interval on the mean and standard deviation, respectively; and the black line shows mean value. Statistical analysis, t-test. Scale bar is 1µm.

Furthermore, to investigate the structure of bridging MTs in EG5 inhibited and KIF4A depleted cells I turned to study and compare the structure of the midzone MTs using MT preservation fixation protocol and STED microscopy. As a control, MT preservation fixation protocol and STED microscopy were done on the KIF4A depleted spindles which have a very similar phenotype as the untreated control metaphase spindles. Using this approach, it was showed that MTs in the spindle midzone after KIF4A depletion and EG5 inhibition have similar structure to only KIF4A depleted metaphase spindles (Vukušić et al., 2021) (Figure 36). After EG5 inhibition together with KIF4A depletion, the spindle length is shorter than in untreated metaphase spindles and in KIF4A depleted spindles which is similar to the only EG5 inhibited spindles. In one example of EG5 inhibited and KIF4A depleted spindle (Figure 36 – bottom right image), I imaged completely impaired MT structure which could suggest that significantly slow speckle-equator velocities after this treatment could possibly be due to some structural damage. Since structural changes in the spindle midzone mostly could not be detected, these results suggests that the impaired sliding of the bridging and k-fibers in EG5 inhibited and KIF4A depleted metaphase RPE-1 spindles is mainly a result of non-existent motor protein activity.

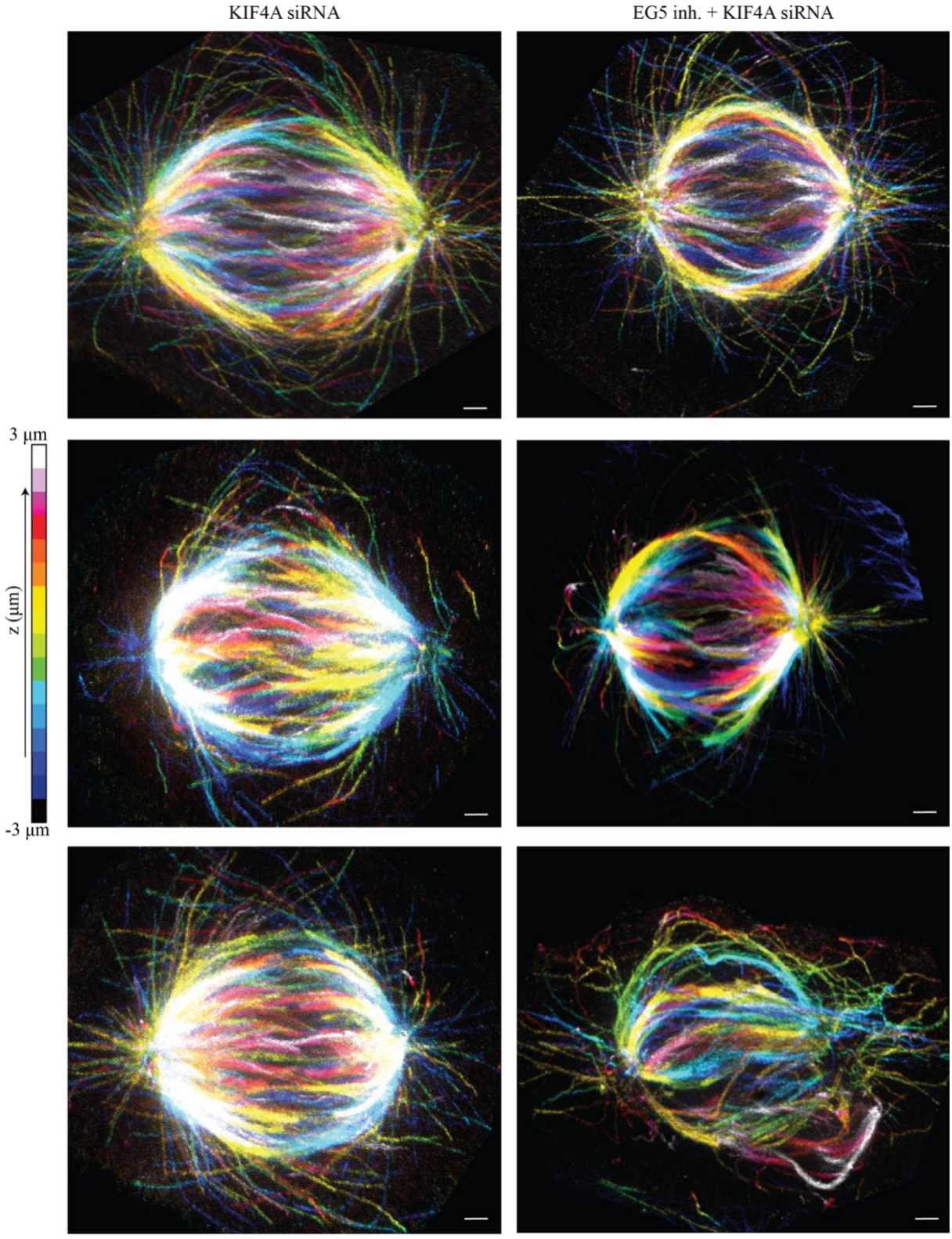

Figure 36. After EG5 inhibition and KIF4A siRNA treatment spindles are shortened but the spindle midzone structure is mostly not impaired. Immunofluorescence images of fixed

KIF4A depleted spindle and EG5 inhibited and KIF4A depleted RPE-1 cells stably expressing CENP-A-GFP and centrin1-GFP (not showed here) and stained with AlexaFluor594 conjugated with α-tubulin antibody (multicolor). Scale bar is 1µm.

Next, as mentioned previously with only EG5 inhibited cells, once again the study turned to kinetochore oscilations to see if there were some abnormal behaviors in EG5 inhibited and KIF4A depleted cells. I tracked kinetochore oscilations of 10 pairs of kinetochores from EG5 inhibited and KIF4A depleted cells. When compared with control and EG5 inhibited cells, oscilations in EG5 inhibited and KIF4A depleted cells were showing much larger oscilations which was surprising (Figure 37). This could be related to much slower bridging fiber flux in this treatment when compared to control and STLC treatment. Also, I measured interkinetochore distance in EG5 inhibited and KIF4A depleted cells and again confirmed what can also be seen in the movies, that EG5 inhibited and KIF4A depleted cells have significantly shorter interkinetochore distance when compared to control ($p<0.0001$) (Figure 37). This again could be due to shorter spindle length in EG5 inhibited cells or it could be caused by the slow bridging fiber flux. When taken together, these results suggest that EG5 and KIF4A work together in metaphase to maintain sliding and without them bridging fiber flux as well as the k-fiber flux is severly impaired.

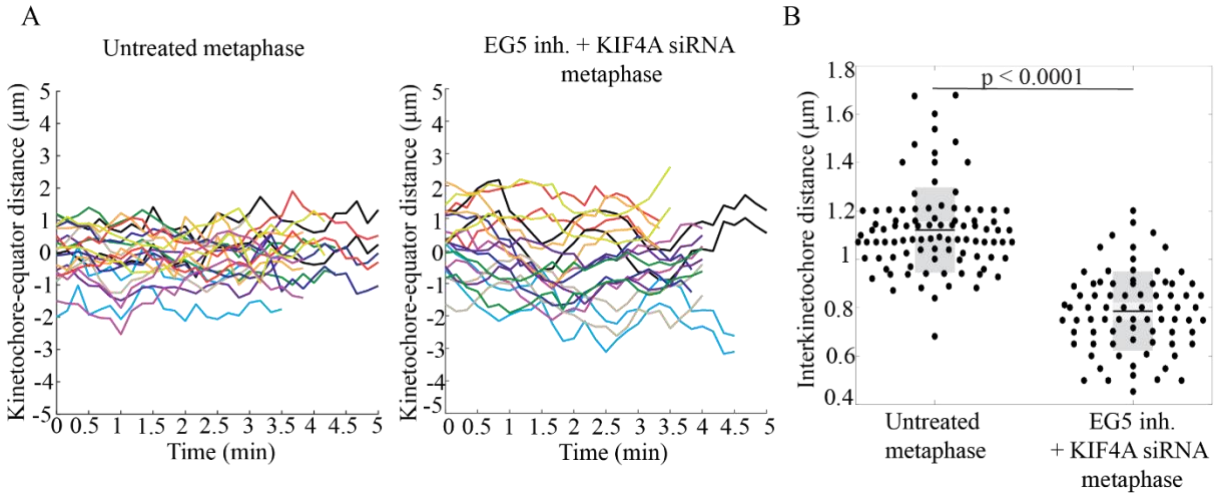

Figure 37. Kinetochore-equator distance tracked in time for control and EG5 inhibited and KIF4A depleted cells is different as well as interkinetochore distance. (A) Kinetochore oscilations are higher for the EG5 inhibited and KIF4A depleted cells when compared to the

control. **(B)** Graph on the right side of the figure is showing interkinetochore distances for control and EG5 inhibited cells. I can notice that EG5 inhibited and KIF4A depleted cells have significantly shorter interkinetochore distances. Each dot corresponds to an individual kinetochore pair. The light and dark area in the boxes mark 95% confidence interval on the mean and standard deviation, respectively; and the black line shows mean value. Statistical analysis, t-test.

4.5 Dynein plays a role in transmission of the sliding forces from bridging to k-fibers

It was observed that force-balancing phenomenon exists in RPE-1 cells, in which EG5 is obviously dominant outward exerting motor since, after its inhibition with STLC, spindles usually tend to collapse very quickly into practically monopolar spindles where two centrosomes are very close to each other, as described earlier by others (Bannigan et al., 2007; Saunders & Hoyt, 1992; Sawin et al., 1992; Sharp et al., 1999; Sturgill et al., 2014). This collapse is presumably mediated by forces exerted by inward directed minus-end motors, primarily dynein, since its depletion restores spindle collapse seen after EG5 inhibition (vanHeesbeen et al., 2014). So I decided to investigate what is the role of dynein in generating poleward flux in the spindle and how dynein inhibition affects poleward flux of individual MTs using speckle microscopy. Usually dynein knockdown experiments are done either with dynein siRNA (vanHeesbeen et al., 2014) or CRISPR-Cas9 method of knockout (Neahring et al., 2021). Both of these methods require several days before imaging of the cells and that is a lot of time in which the cell may find another way to replace dynein role in the spindle. Thus, I wanted to inhibit dynein in an acute way and investigate immediate spindle response. Dynein inhibition is hard to accomplish since most if not all of the dynein inhibitors react with the serum from the cell medium so for this kind of experiment to work it was crucial to replace cell medium around 10 minutes before adding the inhibitor with the cell medium without serum (Opti-MEM). It is important to note that values related to poleward flux, such as speckle-equator velocity, speckle-pole velocity and pole to pole velocity, in Opti-MEM are not different from control cells growing in regular DMEM medium (n = 10 speckles from 5 cells for bridging fiber and n = 12 speckles from 5 cells for k-fibers) (Figure 38). Also, kinetochore oscillations and interkinetochore distance is the same in cells that were in Opti-MEM medium when compared to cells in regular DMEM medium (Figure 39). Inhibitor that I used here is called

Ciliobrevin D. After establishing the dynein inhibition protocol I was able to image immediate response of the spindle when Ciliobrevin D was added using speckle microscopy (Figure 40). Some acute effects that can be seen immediately after adding Ciliobrevin D are splaying of the spindle poles and general splitting of the bundles which is in agreement with previous studies done with this inhibitor (Firestone et al., 2012; Sikirzhytski et al., 2014). Some spindles procedeed to anaphase even with severe pole and MT defects when compared to the untreated metaphase spindles which suggests that inhibitor Ciliobrevin D does not impact regular cell division (Figure 41).

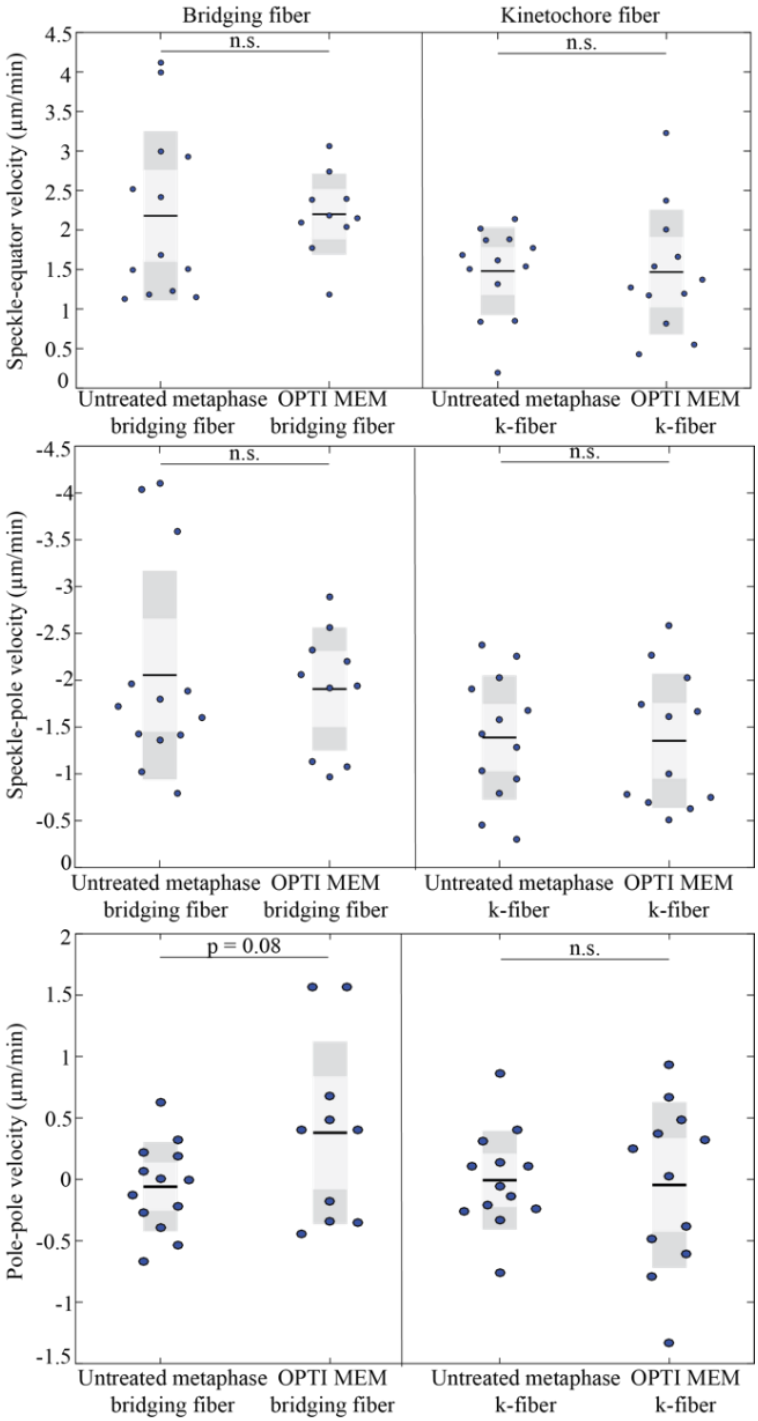

Figure 38. Speckle-equator, speckle-pole and pole-pole velocities in untreated metaphase in DMEM medium and in Opti-MEM medium. Speckle-equator velocity, speckle-pole velocity and pole-pole velocity of the bridging fiber and of the k-fiber is the same for metaphase spindles independent of the medium the cells are in. The light and dark area in the boxes mark 95% confidence interval on the mean and standard deviation, respectively; and the black line shows mean value. Statistical analysis, t-test.

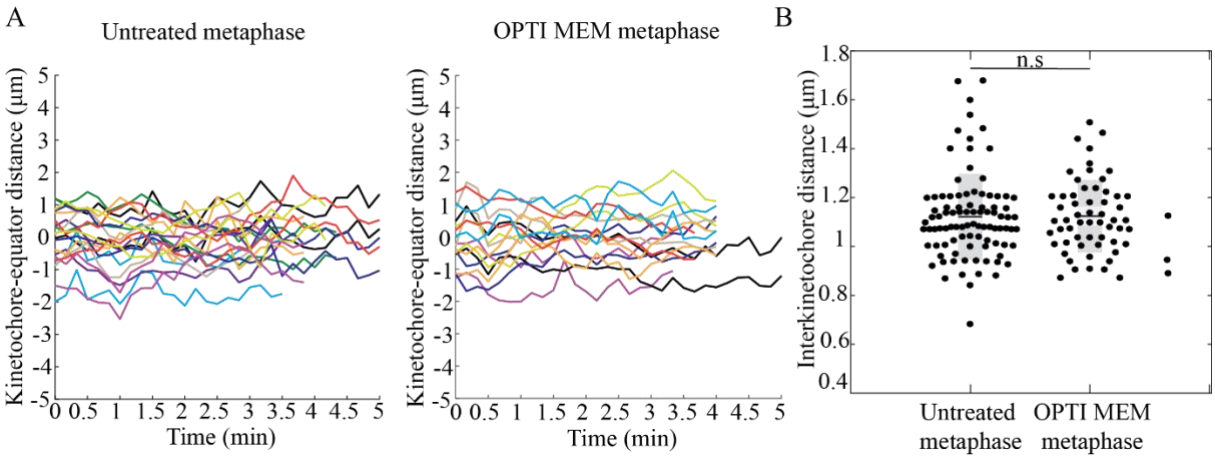

Figure 39. Kinetochore-equator distance tracked in time for untreated metaphase cells in regular DMEM medium and in Opti-MEM medium are similar as well as interkinetochore distance. (A) Kinetochore oscilations are similar for metaphase cells growing in regular DMEM-FBS and metaphase cells in OPTI-MEM medium. **(B)** Graph on the right side of the figure is showing interkinetochore distances for untreated metaphase spindles in DMEM and Opti-MEM. I can notice that interkinetochore distances are the same for both types of cell medium. Each dot corresponds to an individual kinetochore pair. The light and dark area in the boxes mark 95% confidence interval on the mean and standard deviation, respectively; and the black line shows mean value. Statistical analysis, t-test.

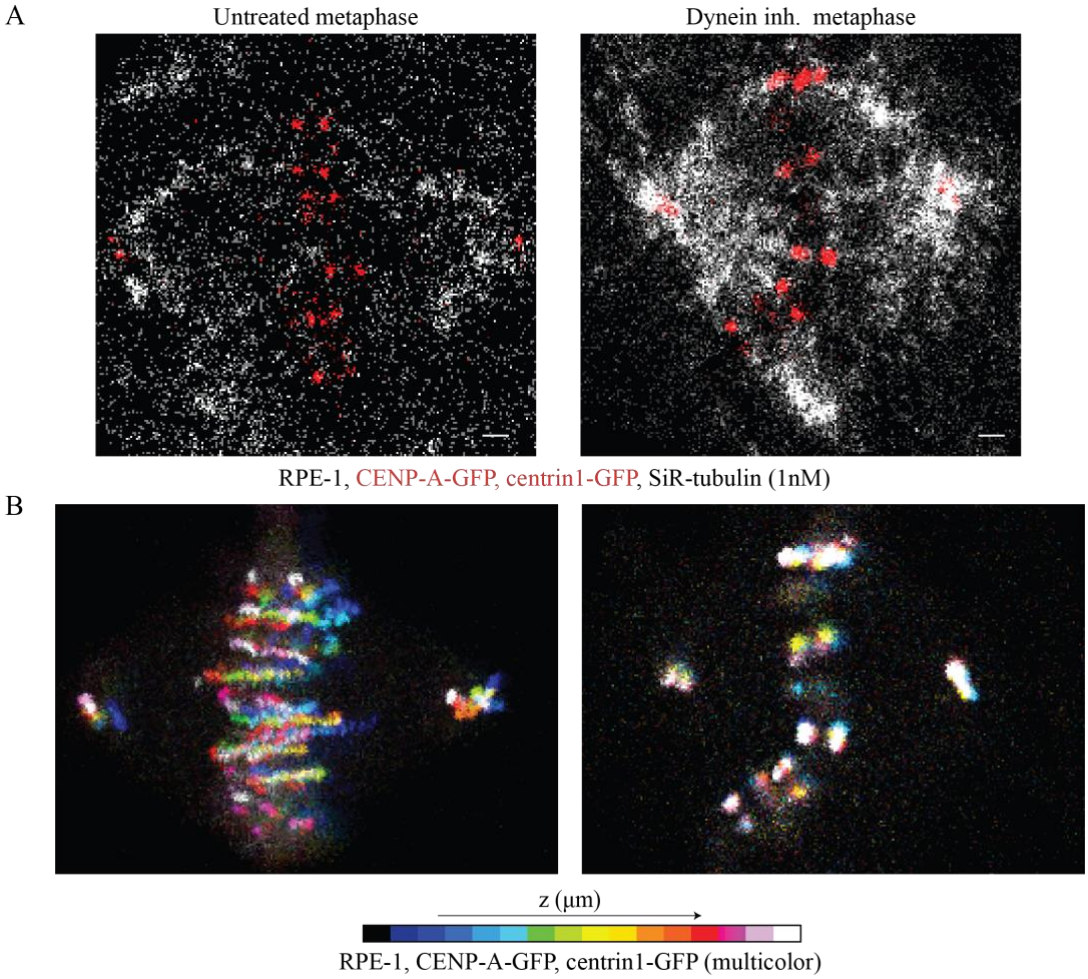

Figure 40. Speckle microscopy assay for measurement of poleward flux of individual MTs. **(A)** Live images of untreated metaphase spindle (left) and dynein inhibited metaphase spindle (right) in a RPE-1 cells stably expressing CENP-A-GFP and centrin1-GFP (red) stained with 1 nM SiR-tubulin dye, which appears as distinct speckles marking individual MTs (white). **(B)** Depth color coded (see color bar) live images of untreated metaphase spindle (left) and dynein inhibited metaphase spindle (right) in a RPE-1 cells stably expressing CENP-A-GFP and centrin1-GFP. After dynein inhibition I can see splaying of the spindle poles and widening of the spindle. Scale bar is 1µm.

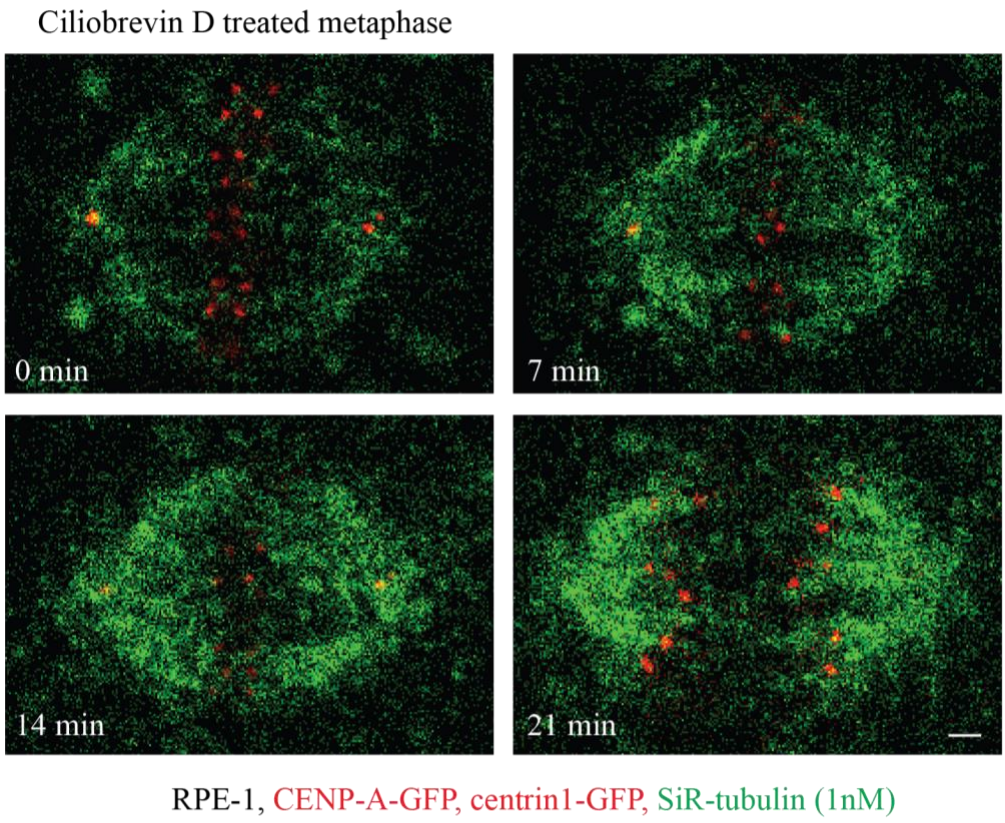

Figure 41. Ciliobrevin D treated metaphase spindles undergo anaphase in most cases. Timelapse of Ciliobrevin D treated metaphase RPE-1 cell imaged using speckle microscopy. After dynein inhibition spindles undergo anaphase. Scale bar is 1µm.

Next, I set out to measure values that will describe MT sliding in dynein inhibited spindles. Distance that poles go trough time of the tracked speckles in dynein inhibited spindles is similar to that of untreated metaphase spindles (Figure 42) which is suggesting that the spindle length is not changing in dynein inhibited spindles. Distance of the speckle and the poles trough time of the tracked speckles is affected by the moving of the poles towards eachother but compared to the control cells is not significantly different for the bridging fiber. On the other hand, for the k-fibers this distance is much shorter than in control cells (Figure 42). Similarly, distance of the speckle from the equator for k-fiber is visibly shorter when compared to control (Figure 42). Pole-pole velocity for dynein inhibited spindles for bridging fibers is – 0.35 ± 0.17 µm/min (n = 10 speckles from 7 cells) and for k-fibers is – 0.26 ± 0.17 µm/min (n = 11 speckles from 6 cells) (Figure 43). Speckle-pole velocity for for dynein inhibited cells for bridging fibers is –

2.14 ± 0.34 µm/min (n = 10 speckles from 7 cells) and for k-fibers is – 0.18 ± 0.17 µm/min (n = 11 speckles from 6 cells) (Figure 43). Speckle-equator velocity for dynein inhibited cells for bridging fibers is 1.44 ± 0.18 µm/min (n = 10 speckles from 7 cells) and for k-fibers is 0.35 ± 0.12 µm/min (n = 11 speckles from 6 cells) (Figure 43). Interestingly, there was no difference between bridging fiber flux in control and in dynein inhibited cells which suggests that the midzone part of the spindle remained active during dynein inhibition. The biggest surprise was that k-fiber sliding was diminished after dynein inhibition, while bridging fiber sliding was similar to untreated metaphase spindles. I can speculate that the transmission of the forces from the bridging fiber to k-fiber was impaired when dynein was inhibited.

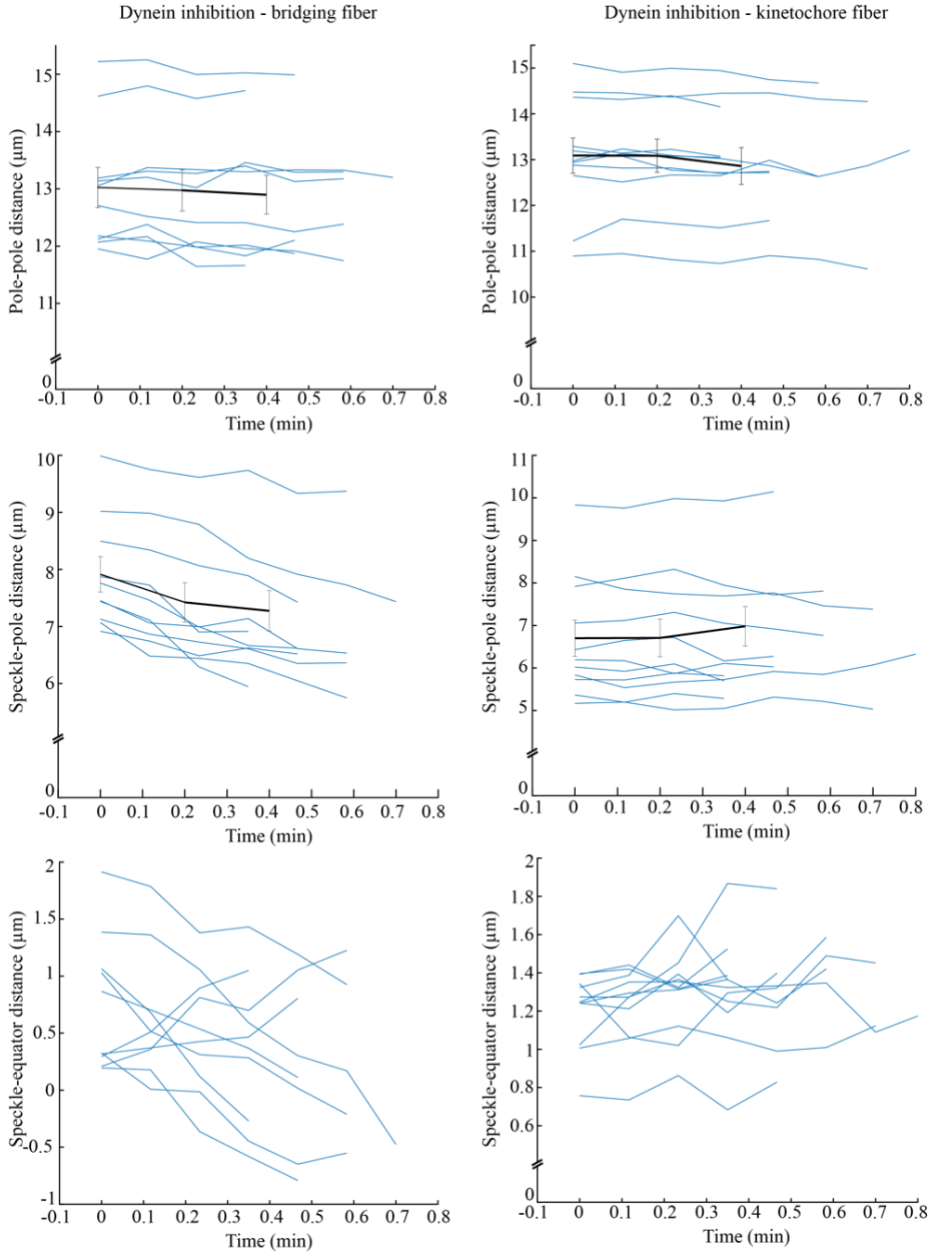

Figure 42. Raw data describing microtubule dynamics in dynein inhibited cells. Here I show the data about pole-pole movement, speckle-pole movement and speckle-equator movement in dynein inhibited cells.

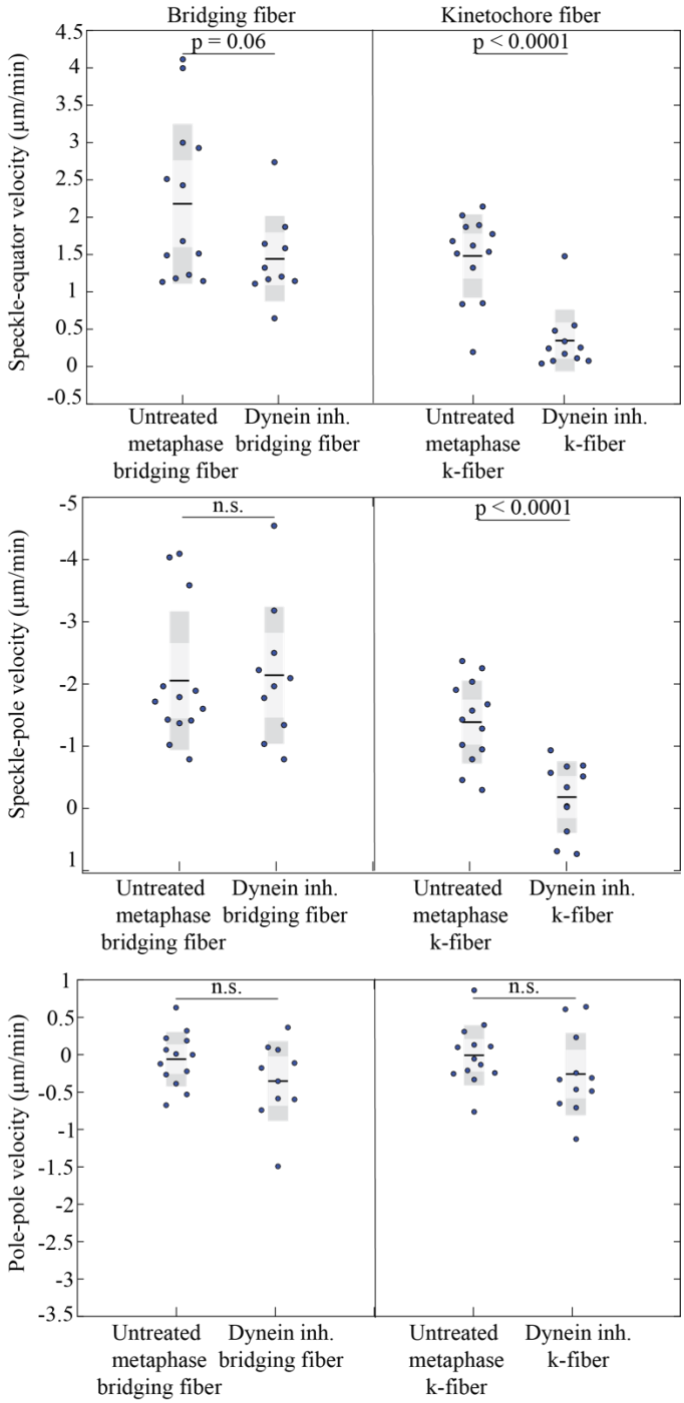

Figure 43. Speckle-equator, speckle-pole and pole-pole velocities in untreated metaphase and dynein inhibited spindles. Speckle-equator velocity of the k-fiber is extremely slower

after dynein inhibition with Ciliobrevin D treatment. Pole to pole velocity after dynein inhibition is similar to untreated metaphase cells. Each dot corresponds to an individual speckle. The light and dark area in the boxes mark 95% confidence interval on the mean and standard deviation, respectively; and the black line shows mean value. Statistical analysis, t-test.

Since speckle-equator velocity of the bridging fiber remained the same as in control metaphase spindle after dynein inhibition, I suggest that the midzone part of the mitotic spindle remains active with all of the sliding motors working properly. What surprised me in this experiment, was that after dynein inhibition k-fiber flux was greatly impaired which suggests that there is a problem in transmission of the sliding from the bridging fiber onto the k-fibers. To test this hypothesis I decided to image previously mentioned RPE-1 cell line with stable expression of PRC1 protein which is the main bundler of antiparallel MTs. Interestingly, after dynein inhibition I observed lower intensity of PRC1 signal in the spindle, specifically PRC1 signal was located only in the short region of the spindle midzone as oposed to longer PRC1 signal in untreated metaphase spindles. I observed splaying of the poles and reduction of the bridging fibers region in the spindles as well as the general splitting of the bundles (Figure 44). After comparing PRC1 signal intensity in the control metaphase and in dynein inhibited spindle, 2 minutes after inhibition, it can be seen that the PRC1 signal is shorter than in control spindles which is in agreement with the images (Figure 44). The length of the PRC1 signal in individual bundles in untreated metaphase RPE-1 cells with stable expression of PRC1 protein is 6.75 ± 0.19 μm (n of bundles = 33 from 10 cells), and in dynein inhibited metaphase spindle the length of the PRC1 bundle is 2.73 ± 0.11 μm (n of bundles = 43 from 9 cells) which is significant ($p < 0.0001$). Also, after dynein inhibition the spindle length did not change as much as it did after EG5 inhibition. Spindle length of untreated metaphase RPE-1 cells with stable expression of PRC1 protein is 12.34 ± 0.40 μm (n = 10 cells) and after dynein inhibition the spindle length is 10.62 ± 0.44 μm (n = 9 cells) which is statistically significant ($p = 0.01$) (Figure 44). In untreated metaphase cells PRC1 signal takes 58% of the entire spindle length and in dynein inhibited cells, PRC1 signal length is 26% of the spindle length which is significantly lower than in untreated metaphase ($p < 0.0001$). Thus, here I show that the PRC1 signal is significantly shortened after dynein inhibition when compared to control and is limited only to the center of the spindle. Taken together, these results suggest that midzone bridging region of the spindle

that consists of antiparallel MTs is shortened after dynein inhibition which could contribute to slower speckle-equator velocity of the k-fibers when compared to control spindles.

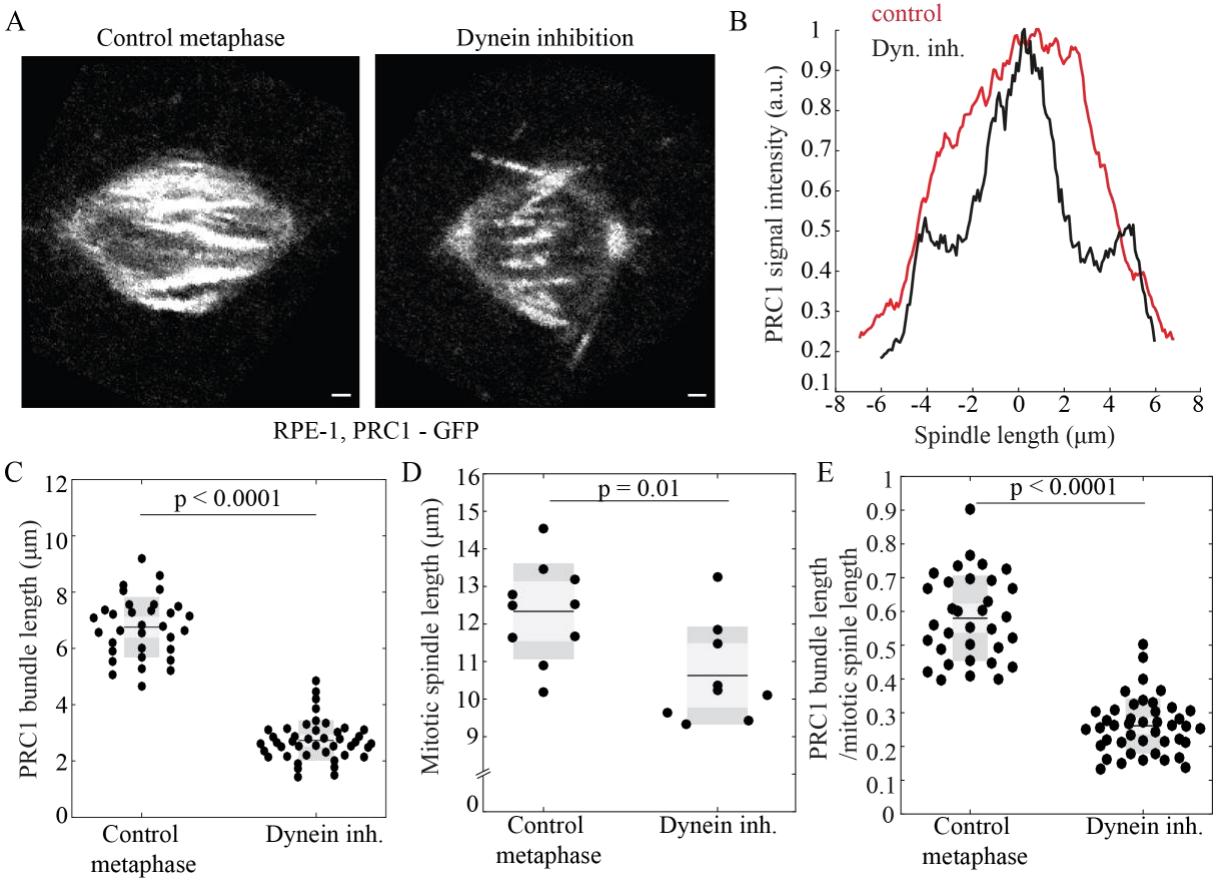

Figure 44. PRC1 signal in RPE-1 cells with stable expression of PRC1-GFP protein is significantly shortened after dynein inhibition. (A) Live images of untreated metaphase and dynein inhibited metaphase RPE-1 cells with stable expression of PRC1-GFP protein (gray) before and after EG5 inhibition. **(B)** After dynein inhibition with Ciliobrevin D, midzone of the spindle with PRC1 signal begins to shorten. **(C)** PRC1 bundle length is significantly shorter 2 minutes after dynein inhibition when compared to control metaphase spindles. **(D)** Mitotic spindle length is smaller after dynein inhibition. **(E)** PRC1 length to spindle length ratio is significantly lower for dynein inhibited cells. Each dot corresponds to an individual PRC1 bundle or cell. Black line; mean. The light and dark area in the boxes mark 95% confidence interval on the mean and standard deviation, respectively; and the black line shows mean value. Statistical analysis, t-test. Scale bar is 1µm.

As mentioned previously, I speculate that the bridging fibers after dynein inhibition remain functional but the transmission of the force to the k-fiber is impaired. To confirm this, I turned to study and compare the structure of the midzone MTs using MT preserving fixation protocol and STED microscopy. Using this approach, I showed that midzone MT organization is similar in control cells and in dynein inhibited cells, but k-fibers on the other hand were shorter than in control cells and extensively curved and twisted (Figure 45). Thus, I suggest that the low speckle-equator velocity of the k-fibers could be the result of impaired k-fiber structure. It is possible that the connection between bridging fibers and k-fibers is weakened by dynein inhibition. I suggest that dynein acts as a general crosslinker in the spindle and has a role in crosslinking bridging and kinetochore fibers, thus after dynein inhibition the connection between them would be damaged. Another dynein inhibition effect that can be seen after super-resolution imaging of MTs is splaying of the poles. This result suggests that dynein has a pole-focusing role in the spindle, as was previously proposed (Goshima et al., 2005). Spindle length shortening was also observed which could suggest that dynein is not sliding in the midzone of the spindle as was previously proposed (vanHeesbeen et al., 2014) because if dynein was actually sliding I would expect to observe longer spindles when compared to the untreated metaphase.

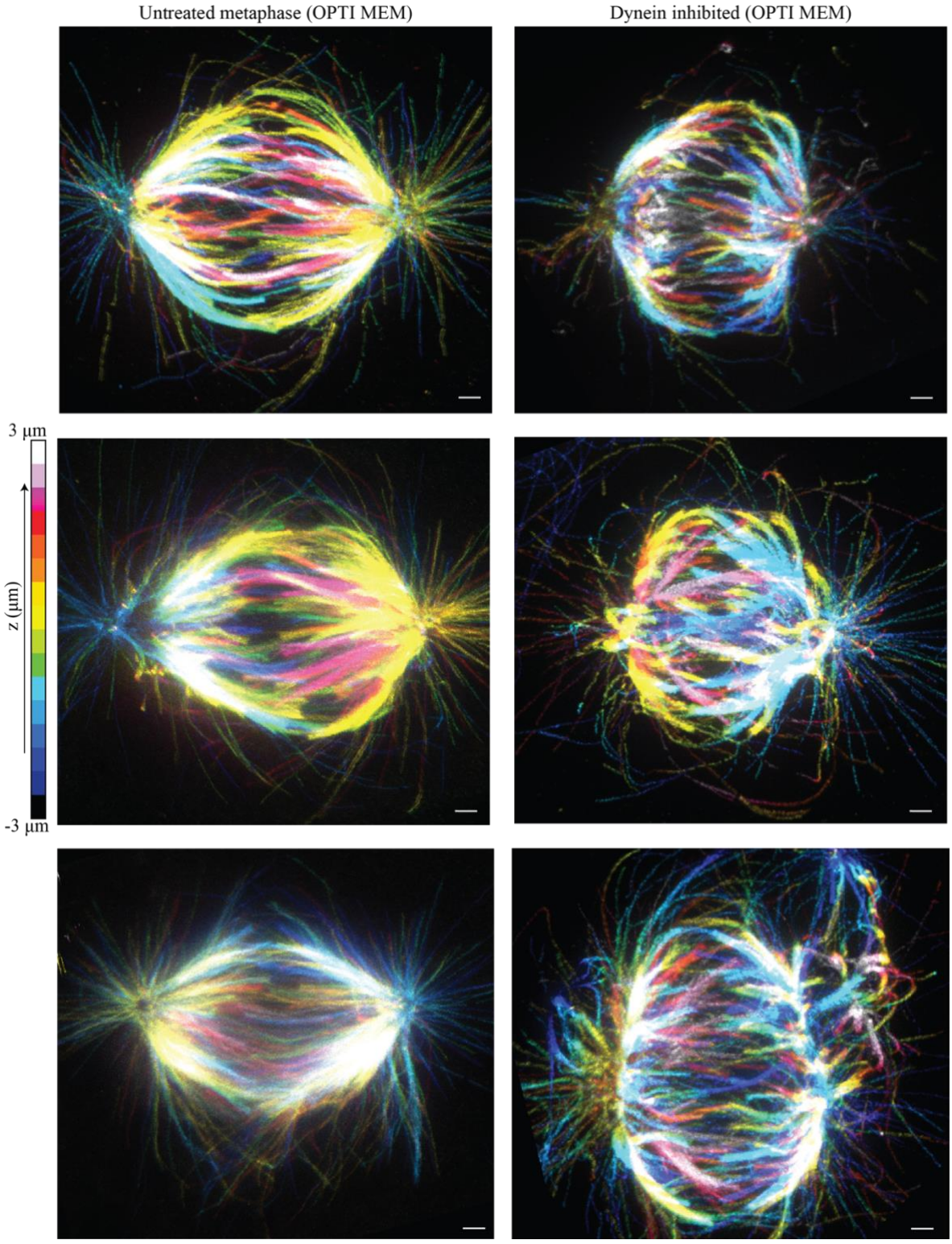

Figure 45. After dynein inhibition spindles are shortened, k-fiber structure is impaired and bridging region is shortened. Immunofluorescence images of fixed control mitotic spindle in Opti-MEM medium and Ciliobrevin D treated RPE-1 cells in OPTI-MEM stably

expressing CENP-A-GFP and centrin1-GFP (not showed here) and stained with AlexaFluor594 conjugated with α-tubulin antibody (multicolor). Scale bar is 1μm

Then, as mentioned previously with EG5 inhibited cells and EG5 inhibited and KIF4A depleted cells, once again I turned to investigating the kinetochore oscilations. I tracked kinetochore oscilations of 9 pairs of kinetochores from dynein inhibited cells and compared it to 10 kinetochore pairs from control. When compared with OPTI-MEM control, oscilations in dynein inhibited cells were similar (Figure 46). This once agains confirms that bridging fibers remain functional after dynein inhibition. Next, I measured interkinetochore distance in dynein inhibited cells and showed that cells with inhibited dynein, as well as all treatments up till this point, have significantly shorter interkinetochore distance when compared to control ($p<0.0001$) (Figure 46). When taken together, these results suggest that dynein works in metaphase as a general crosslinker of bundles that connects bridging fibers with k-fibers. When dynein is inhibited, force transmission from the midzone to the spindle poles is impaired.

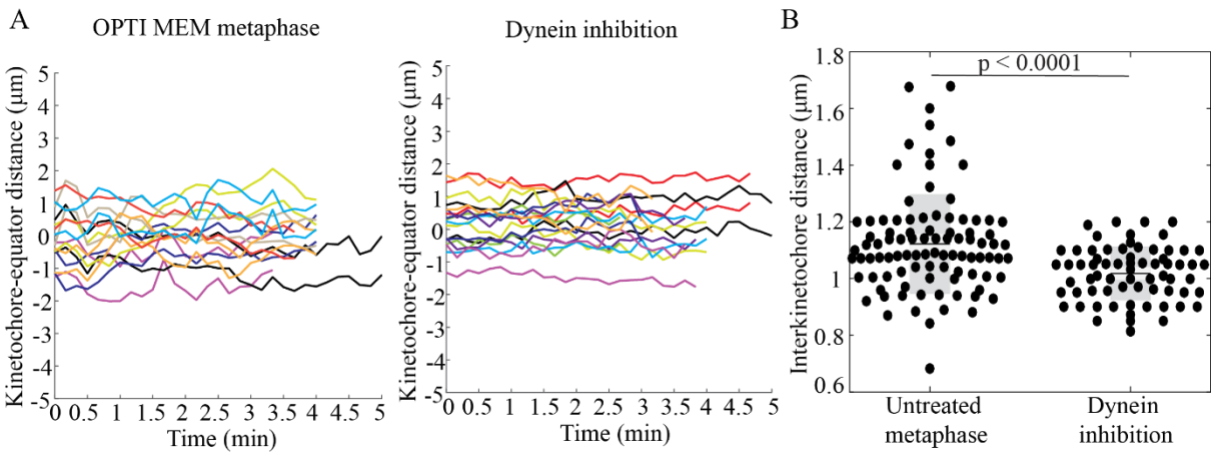

Figure 46. Kinetochore-equator distance tracked in time for control OPTI MEM metaphase and dynein inhibited cells is similar but interkinetochore distance for dynein inhibited cells is significantly shorter than in untreated spindles. (A) Kinetochore oscilations are similar for control cells in OPTI-MEM and dynein inhibited cells which suggests that the midzone part of the mitotic spindle is perserved even after dynein inhibition with Ciliobrevin D treatment. **(B)** Graph on the right side of the figure is showing interkinetochore distances for control and dynein inhibited cells. I can notice that dynein inhibited cells have significantly shorter interkinetochore distances. Each dot corresponds to an individual

kinetochore pair. The light and dark area in the boxes mark 95% confidence interval on the mean and standard deviation, respectively; and the black line shows mean value. Statistical analysis, t-test.

4.6 Double inhibition of dynein and EG5 rescues the bipolarity of the spindle but problems with force transmission remain

After individual inhibitions of dynein and EG5, I decided to inhibit both proteins at the same time. It is known that the most renowned antagonism in human spindles is achieved in metaphase between EG5 as a dominant outward motor, and dynein as a dominant inward motor (Ferenz et al., 2010; Fink et al., 2006; Goshima & Scholey, 2010; Raaijmakers & Medema, 2014), and many showed that dynein inhibition rescues monopolar phenotype of the EG5 inhibited spindles (Neahring et al., 2021; vanHeesbeen et al., 2014). However, it was unknown how the double inhibition of the two main antagonist motors reflects on the poleward flux of the bridging and k-fibers. After establishing the double inhibition protocol I was able to image immediate response of the spindle when Ciliobrevin D together with STLC was added using speckle microscopy (Figure 47). One acute effect that can be seen immediately after adding Ciliobrevin D and STLC is shortening of the spindle length but also there is no splaying of the poles like in dynein only inhibition or monopolar spindles like in EG5 only inhibition. Thus, I confirmed what others also described, that after double inhibition of dynein and EG5 motor, mitotic spindle remains bipolar.

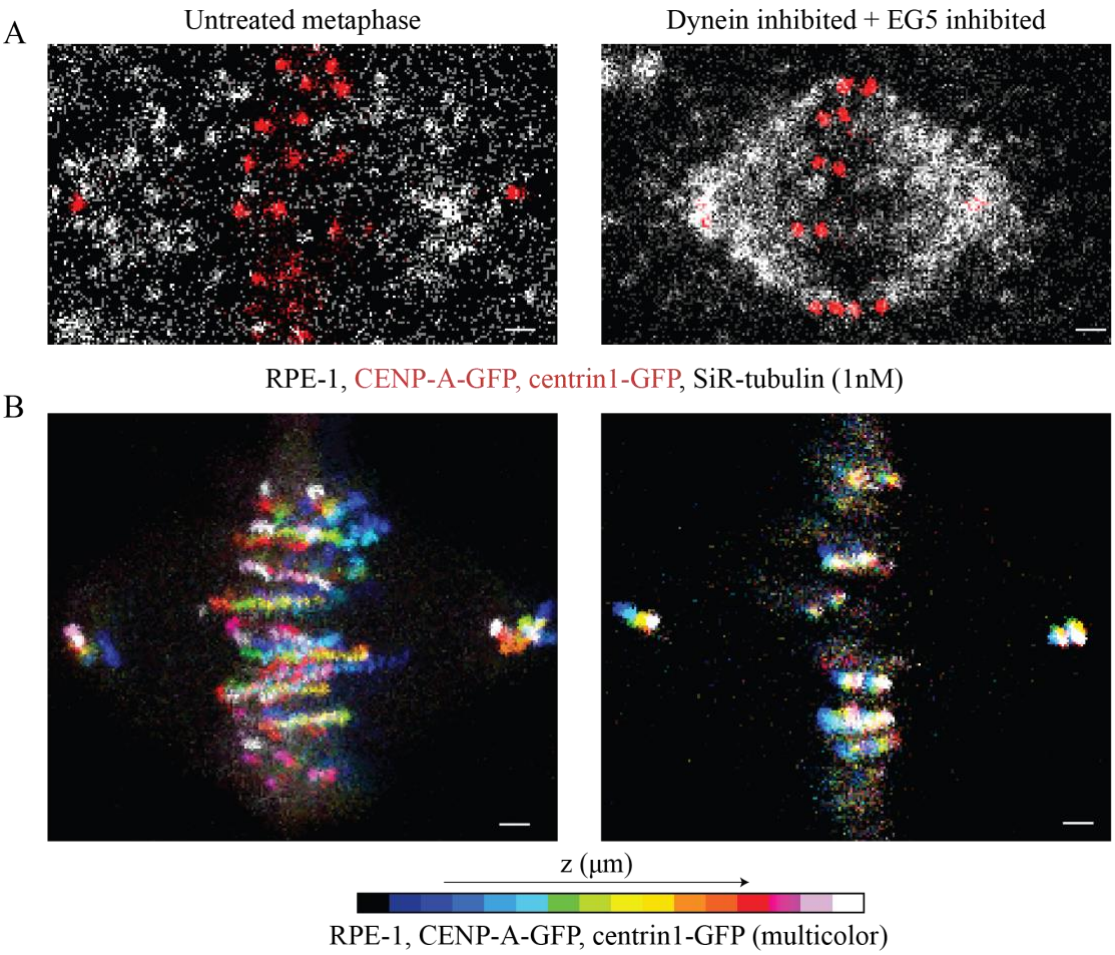

Figure 47. Speckle microscopy assay for measurement of poleward flux of individual MTs. **(A)** Live images of untreated metaphase spindle (left) and dynein and EG5 inhibited metaphase spindle (right) in a RPE-1 cells stably expressing CENP-A-GFP and centrin1-GFP (red) stained with 1 nM SiR-tubulin dye, which appears as distinct speckles marking individual MTs (white). **(B)** Depth color coded images (see color bar) filmed for 2 minute, of untreated metaphase spindle (left) and dynein and EG5 inhibited metaphase spindle (right) in a RPE-1 cells stably expressing CENP-A-GFP and centrin1-GFP. After dynein and EG5 inhibition spindles are shortened but bipolar. Scale bar is 1μm.

Next, just as in previous treatments, I set out to measure values that will describe MT sliding in spindles with inhibited dynein and EG5. Distance that poles go trough time of the tracked speckles is similar to that of untreated metaphase spindles (Figure 48) which is suggesting that the spindle length, at least in the frames that I tracked the speckles, is not drastically changing.

Also slight decrease in length is visible. Distance of the speckle and the poles trough time of the tracked speckles is affected by the moving of the poles towards eachother but compared to the control cells is not significantly different for the bridging fiber. On the other hand, it is clearly visible that for the k-fiber this distance is much shorter than in control cells (Figure 48). Similarly, distance of the speckle from the equator for k-fiber is visibly shorter when compared to control (Figure 48) just as in dynein only inhibition. Pole-pole velocity for dynein and EG5 inhibited spindles for bridging fibers is – 0.25 ± 0.13 μm/min (n = 12 speckles from 6 cells) and for k-fibers is – 0.26 ± 0.17 μm/min (n = 12 speckles from 8 cells) (Figure 49). Speckle-pole velocity for dynein inhibited cells for bridging fibers is – 1.41 ± 0.21 μm/min (n = 12 speckles from 6 cells) and for k-fibers is – 0.34 ± 0.20 μm/min (n = 12 speckles from 8 cells) (Figure 49). Speckle-equator velocity for dynein inhibited cells for bridging fibers is 1.31 ± 0.21 μm/min (n = 12 speckles from 6 cells) and for k-fibers is 0.43 ± 0.11 μm/min (n = 12 speckles from 8 cells) (Figure 49). Interestingly, there was no difference between bridging fiber flux in control and in dynein and EG5 inhibited cells which suggests that the midzone part of the spindle remained active during dynein and EG5 inhibition, same as in dynein only and EG5 only inhibition. Surprisingly, k-fiber flux was diminished as in dynein only inhibition. I can speculate that the transmission of the forces from the bridging fiber to k-fiber was impaired in dynein inhibition independent if EG5 is inhibited in the spindle or not.

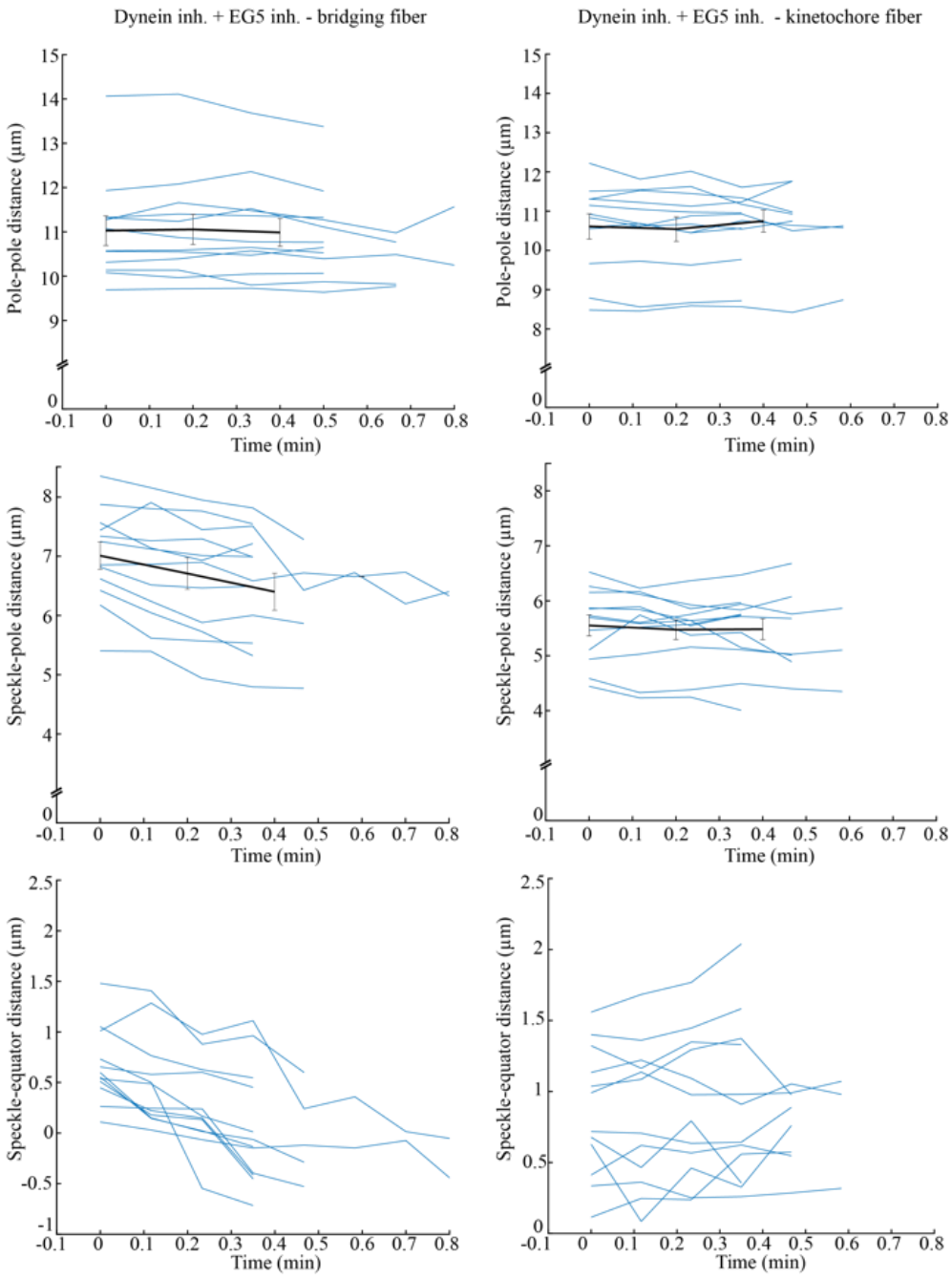

Figure 48. Raw data describing poleward flux in Ciliobrevin D and STLC treated cells. Here I show the data about pole-pole movement, speckle-pole movement and speckle-equator movement in dynein and EG5 inhibited cells.

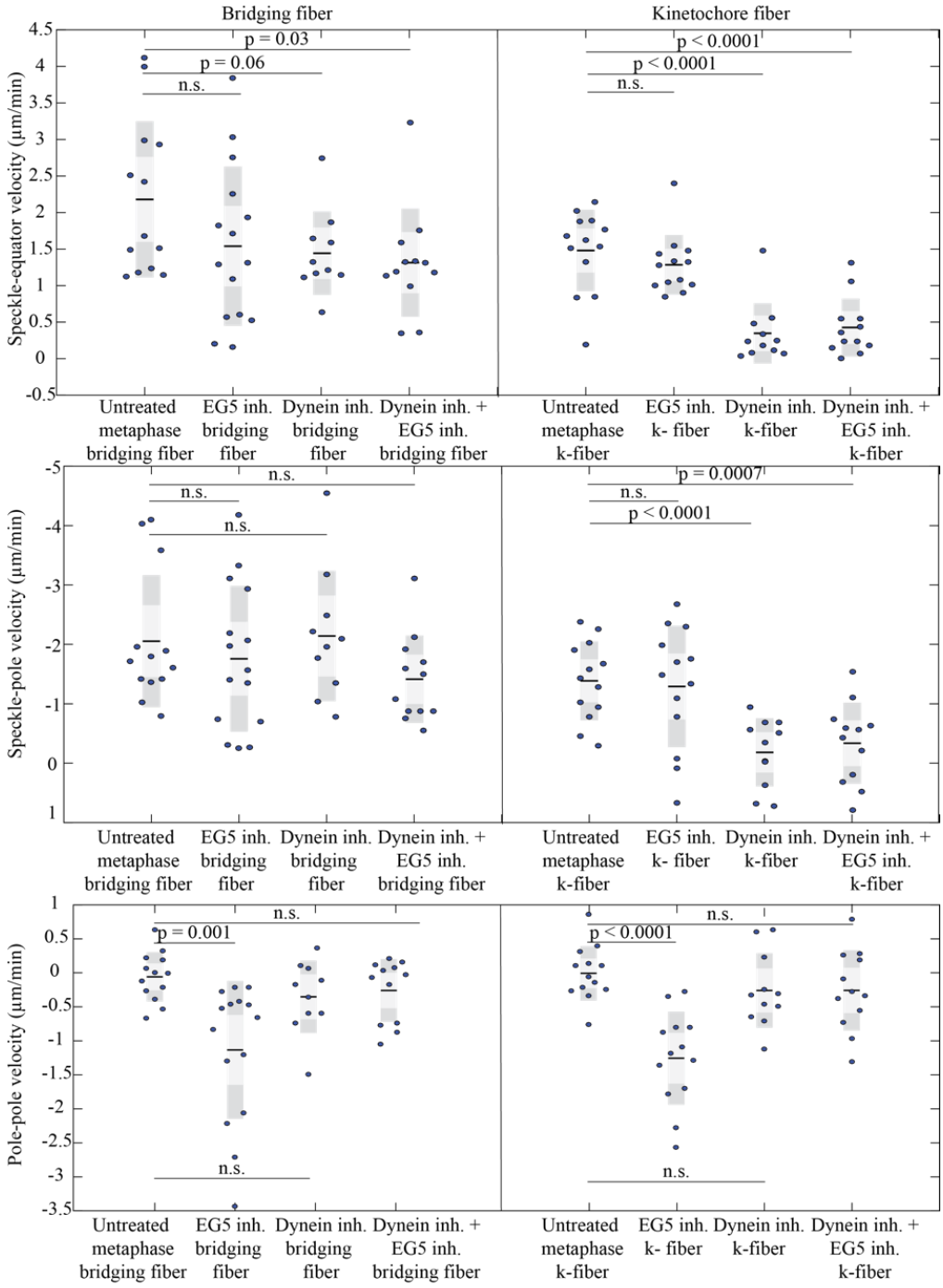

Figure 49. Speckle-equator, speckle-pole and pole-pole velocities in untreated metaphase, EG5 inhibited, dynein inhibited and dynein and EG5 inhibited spindles. Speckle-equator velocity of the k-fiber is extremely lower after dynein inhibition and dynein and EG5 inhibition treatment. Each dot corresponds to an individual speckle. The light and dark area in the boxes

mark 95% confidence interval on the mean and standard deviation, respectively; and the black line shows mean value. Statistical analysis, t-test.

As I mentioned before, I speculate that k-fiber flux is diminished in all of the treatments with Ciliobrevin D when dynein is inhibited because transmission of the force from the midzone of the spindle is impaired. To check the structure of the midzone, I used RPE-1 cell that stably express PRC1 signal to measure the intensity of the PRC1 in the midzone after inhibiting dynein and EG5 together. Interestingly, as the spindle shortens, PRC1 signal is getting reduced to only middle part of the spindle, similarly to the only dynein inhibited spindles which suggests that the midzone region of the spindle is getting reduced and possibly the connection between bridging and k-fibers is damaged (Figure 50). When PRC1 signal is measured in control spindles and EG5 and dynein inhibited spindles, 2 minutes after inhibition, and their signal intensities are compared it is visible that in the EG5 and dynein inhibited spindles bridging fiber region is shortened similar to the only dynein inhibited mitotic spindles (Figure 50). The length of the PRC1 signal in individual bundles in untreated metaphase RPE-1 cells with stable expression of PRC1 protein is 6.75 ± 0.19 μm (n of bundles = 33 from 10 cells), and in dynein and EG5 inhibited metaphase spindles the length of the PRC1 bundles is 3.43 ± 0.19 μm (n of bundles = 19 from 8 cells) which is significant ($p < 0.0001$). Spindle length of untreated metaphase RPE-1 cells with stable expression of PRC1 protein is 12.34 ± 0.40 μm (n = 10 cells) and after dynein and EG5 inhibition the spindle length is 7.54 ± 0.44 μm (n = 8 cells) which is statistically significant ($p < 0.0001$) (Figure 50) and is similar to drastic spindle length shortening in only EG5 inhibited spindles. In untreated metaphase cells PRC1 signal takes 58% of the entire spindle length and in dynein inhibited cells, PRC1 signal length is 45% of the spindle length which is significantly lower than in untreated metaphase ($p = 0.0006$). Thus, here I show that the PRC1 bundles are significantly shortened after dynein and EG5 inhibition and that their localization did not remain same as in control, but is limited only to the center of the spindle similar to only dynein inhibited spindles. Taken together, these results suggest that bridging region of the spindle that consists of PRC1 crosslinked antiparallel MTs is shortened after dynein and EG5 inhibition which could contribute to slower speckle-equator velocity of the briging fibers when compared to control spindles.

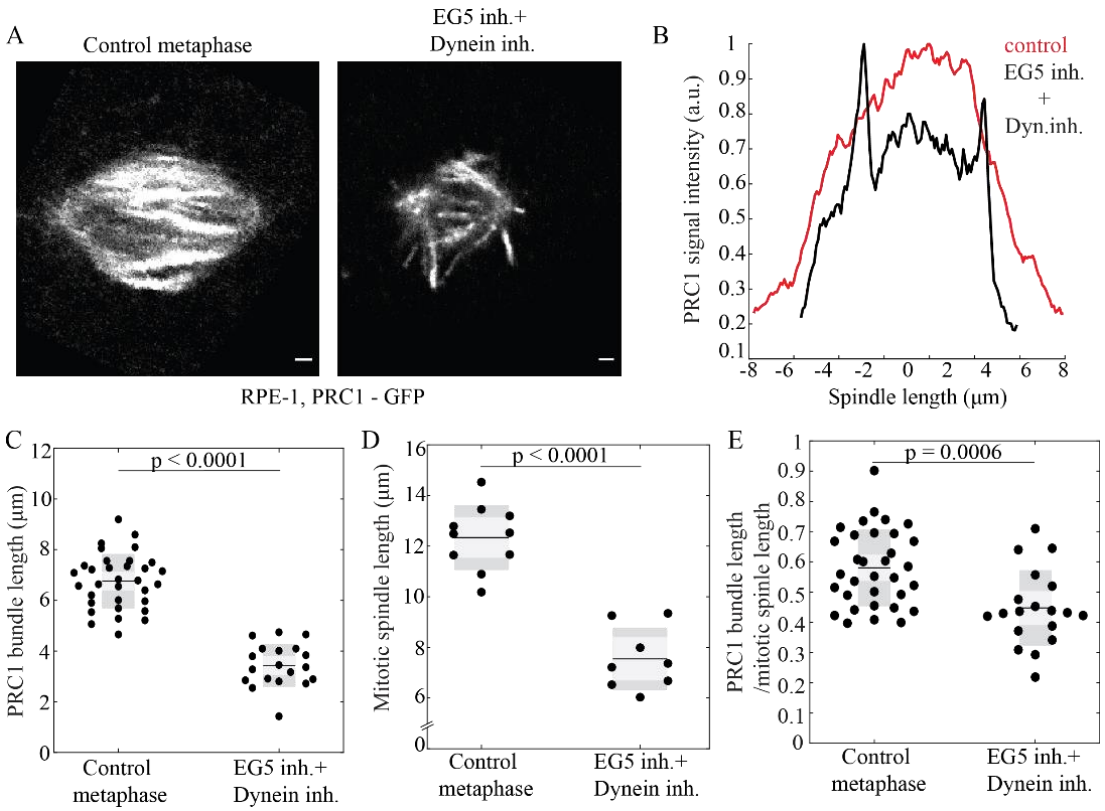

Figure 50. PRC1 signal in RPE-1 cells with stable expression of PRC1-GFP protein is significantly shortened after dynein inhibition. (A) Live images of untreated metaphase and dynein inhibited metaphase RPE-1 cells with stable expression of PRC1-GFP protein (gray) before and after EG5 inhibition. **(B)** After dynein inhibition with Ciliobrevin D, midzone region of the spindle with PRC1 signal begins to shorten. **(C)** PRC1 signal length is significantly shorter after 2 minutes after dynein inhibition when compared to control metaphase spindles, **(D)** as well as spindle length. **(E)** PRC1 length to spindle length ratio is significantly lower for dynein and EG5 inhibited cells (bottom, right). Each dot corresponds to an individual PRC1 bundle or cell. The light and dark area in the boxes mark 95% confidence interval on the mean and standard deviation, respectively; and the black line shows mean value. Statistical analysis, t-test. Scale bar is 1µm.

Finally, I studied kinetochore oscilations to check the kinetochore movements during the double inhibition. I tracked kinetochore oscilations of 9 pairs of kinetochores from Ciliobrevin D and STLC treated cells. When compared with control in Opti-MEM medium, oscilations in Ciliobrevin D and STLC treated cells were similar (Figure 51). This once agains confirms that bridging fibers remain functional after dynein inhibition, and here after dynein and EG5 inhibiton. This is expected since both individual inhibitions had perserved midzone parts of the spindle. Next, I measured interkinetochore distance in Ciliobrevin D and STLC treated cells and showed that cells with inhibited dynein and EG5, as well as all treatments up till this point, have significantly shorter interkinetochore distance when compared to control ($p<0.0001$) (Figure 51). When taken together, these results suggest that dynein works in metaphase as a general crosslinker of bundles that connects bridging fibers with k-fibers. When dynein is inhibited, alone or together with EG5, force transmission from the midzone to the spindle poles is impaired. Dynein inhibition rescues monopolar spindles in EG5 inhibited spindles which is consistent with our hypothesis of their opposing sliding activites in the spindle.

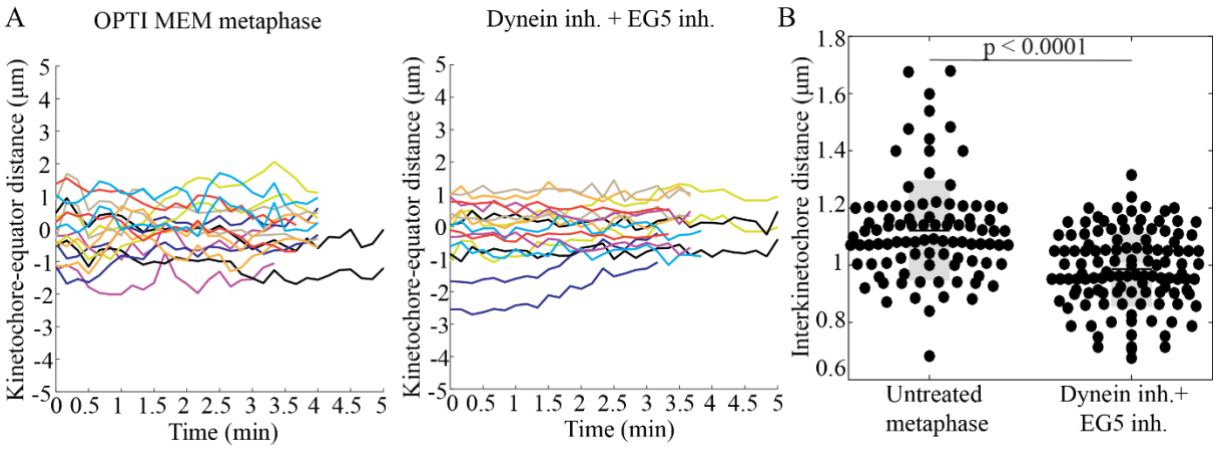

Figure 51. Kinetochore-equator distance tracked in time for OPTI MEM control and dynein and EG5 inhibited cells is similar but interkinetochore distance for dynein and EG5 inhibited cells is significantly shorter than in untreated spindles. (A) Kinetochore oscilations are similar for control in OPTI MEM medium and dynein and EG5 inhibited cells which suggests that the midzone part of the mitotic spindle is perserved even after dynein inhibition with Ciliobrevin D treatment. **(B)** Graph on the right side of the figure is showing interkinetochore distances for control and dynein and EG5 inhibited cells. I can notice that dynein and EG5 inhibited cells have significantly shorter interkinetochore distances. Each dot

corresponds to an individual kinetochore pair. The light and dark area in the boxes mark 95% confidence interval on the mean and standard deviation, respectively; and the black line shows mean value. Statistical analysis, t-test.

Table 1. Measurments of speckle movement parameters in RPE-1 cells. Values are given as mean ± sem. The numbers in brackets denote the number of measurments: number of speckles; number of cells and p-value from a t-test (last column) for a comparison with untreated metaphase cells. NA, not applicable; ND, not determined.

	Pole-pole velocity (µm/min)	**Speckle-pole velocity (µm/min)**	**Speckle-equator velocity (µm/min)**
Untreated anaphase	Bridging fiber: 1.99 ± 0.22 (13, 8, NA) K-fiber: 1.92 ± 0.34 (14, 7, NA)	Bridging fiber: -0.66 ± 0.13 (13, 8, NA) K-fiber: -0.77 ± 0.14 (14, 7, NA)	Bridging fiber: 1.86 ± 0.18 (13, 8, NA) K-fiber: 1.70 ± 0.20 (14, 7, NA)
Untreated metaphase	Bridging fiber: -0.06 ± 0.10 (13, 8, NA) K-fiber: -0.001 ± 0.111 (13, 7, NA)	Bridging fiber: -2.05 ± 0.30 (13, 8, NA) K-fiber: -1.38 ± 0.18 (13, 7, NA)	Bridging fiber: 2.18 ± 0.30 (13, 8, NA) K-fiber: 1.48 ± 0.15 (13, 7, NA)
Untreated metaphase In Opti-MEM	Bridging fiber: 0.38 ± 0.23 (10, 5, 0.08) K-fiber: -0.04 ± 0.19 (12, 5, 0.9)	Bridging fiber: -1.90 ± 0.20 (10, 5, 0.7) K-fiber: -1.35 ± 0.20 (12, 5, 0.9)	Bridging fiber: 2.20 ± 0.16 (10, 5, 1) K-fiber: 1.47 ± 0.22 (12, 5, 1)
EG5 inhibition with STLC	Bridging fiber: -1.13 ± 0.26 (15, 10, 0.0012) K-fiber: -1.13 ± 0.26 (13, 8, <0.0001)	Bridging fiber: -1.76 ± 0.31 (15, 10, 0.5) K-fiber: -1.29 ± 0.28 (13, 8, 0.8)	Bridging fiber: 1.54 ± 0.30 (15, 10, 0.1) K-fiber: 1.28 ± 0.11 (13, 8, 0.3)
EG5 inhibition + KIF4A knockdown using siRNA	Bridging fiber: -0.81 ± 0.15 (10, 5, 0.0004) K-fiber: -0.95 ± 0.20 (10, 7, 0.0004)	Bridging fiber: -1.17 ± 0.21 (10, 5, 0.04) K-fiber: -0.81 ± 0.22 (10, 7, 0.06)	Bridging fiber: 0.80 ± 0.17 (10, 5, 0.001) K-fiber: 0.46 ± 0.13 (10, 7, <0.0001)
Dynein inhibition with Ciliobrevin D	Bridging fiber: -0.35 ± 0.17 (10, 7, 0.1) K-fiber: -0.26 ± 0.17 (11, 6, 0.2)	Bridging fiber: -2.14 ± 0.34 (10, 7, 0.9) K-fiber: -0.18 ± 0.17 (11, 6, <0.0001)	Bridging fiber: 1.44 ± 0.18 (10, 7, 0.06) K-fiber: 0.35 ± 0.12 (11, 6, <0.0001)
Dynein inhibition with Ciliobrevin	Bridging fiber: -0.26 ± 0.13 (12, 6, 0.3) K-fiber:	Bridging fiber: -1.41 ± 0.21 (12, 6, 0.1) K-fiber:	Bridging fiber: 1.31 ± 0.21 (12, 6, 0.03) K-fiber:

D + EG5 inhibition with STLC	-0.26 ± 0.17 (12, 8, 0.2)	-0.34 ± 0.20 (12, 8, 0.0007)	0.43 ± 0.11 (12, 8, <0.0001)

Table 2. Measurments of PRC1, spindle length and kinetochore parameters in RPE-1 cells. Values are given as mean ± sem. The numbers in brackets denote the number of measurments: number of bundles of PRC1 signal; number of cells and p-value from a t-test (last column) for a comparison with untreated metaphase cells. NA, not applicable; ND, not determined.

	PRC1 signal length (µm/)	Mitotic spindle length (µm/)	PRC1 signal/spindle length (%)	Interkinetochore distance (µm/)
Untreated metaphase	6.76 ± 0.19 (33, 10, NA)	12.34 ± 0.40 (10, NA)	58 (33, 10, NA)	1.12 ± 0.02 (94, NA)
KIF4A knockdown using siRNA	7.56 ± 0.20 (46, 10, 0.007)	13.52 ± 0.42 (10, 0.06)	56 (46, 10, 0.6)	ND
EG5 inhibition with STLC	4.85 ± 0.13 (53, 12, <0.0001)	7.81 ± 0.24 (12, <0.0001)	61 (53, 12, 0.2)	1.03 ± 0.02 (68, 0.003)
EG5 inhibition with STLC + KIF4A knockdown using siRNA	5.23 ± 0.15 (18, 8, <0.0001)	8.51 ± 0.26 (8, <0.0001)	62 (18, 8, 0.2)	0.79 ± 0.02 (79, <0.0001)
Dynein inhibition with Ciliobrevin D	2.73 ± 0.11 (43, 9, <0.0001)	10.62 ± 0.44 (9, 0.01)	26 (43, 9, <0.0001)	1.02 ± 0.02 (68, <0.0001)
Dynein inhibition with Ciliobrevin D + EG5 inhibition with STLC	3.43 ± 0.19 (19, 8, <0.0001)	7.54 ± 0.44 (8, <0.0001)	45 (19, 8, 0.0006)	0.99 ± 0.01 (124, <0.0001)

4.7. Putting it all together

After conducting ANOVA and Tukey HSD tests to analyze all of the treatments together for easier summarizing of my results, I decided to put all of the graphs showing velocities related to speckle measurments and PRC1 signal measurements in one section.

Firstly, I will discuss speckle-equator and speckle-pole velocities of the bridging fiber. For speckle-equator velocity of the bridging fibers, one-way ANOVA test showed a significant difference between group means ($p = 0.0002$). Speckle-equator velocity for bridging fibers was significantly different between untreated metaphase spindles and KIF4A depleted and EG5 inhibited spindles ($p = 0.0042$), between OPTI MEM metaphase spindles and KIF4A depleted and EG5 inhibited spindles ($p = 0.0075$) and between KIF4A depleted metaphase spindles and KIF4A depleted and EG5 inhibited spindles ($p = 0.0008$) (Figure 52). When comparing all other treatments there is no difference between them for speckle-equator velocities. Data for KIF4A depleted spindles was obtained by Patrik Risteski (Risteski et al., 2022) and was used in this section for conducting ANOVA test. For speckle-pole velocity of the bridging fibers, one-way ANOVA test showed a significant difference between group means ($p = 0.0118$). Speckle-pole velocity for bridging fibers was significantly different only between KIF4A depleted metaphase spindles and KIF4A depleted and EG5 inihibited spindles ($p = 0.0150$) (Figure 52).

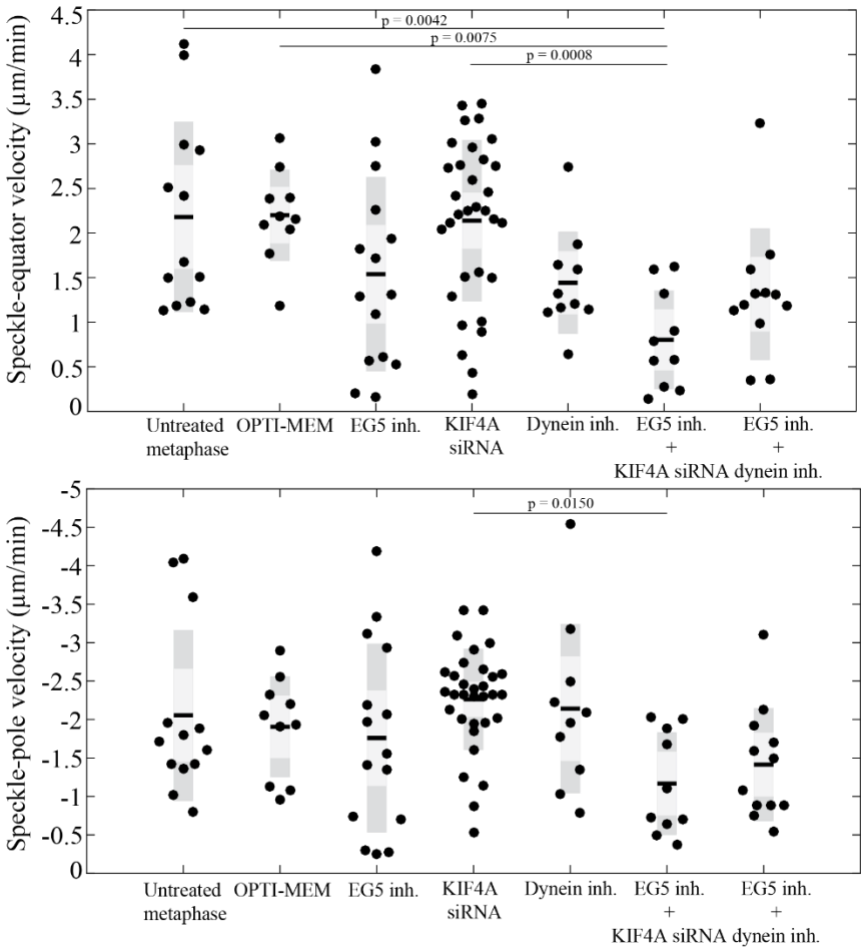

Figure 52. Depletion of KIF4A together with EG5 inhibition slows down speckle-equator velocity of the bridging fibers. Quantification (univariate scatter plot) of speckle-equator velocity (up) and speckle-pole velocity (down) across indicated conditions. Each dot corresponds to an individual speckle. The light and dark area in the boxes mark 95% confidence interval on the mean and standard deviation, respectively; and the black line shows mean value. Statistical analysis, ANOVA and Tukey HSD. One-way ANOVA test showed a significant difference between group means for speckle-equator velocity ($p = 0.0002$) and for speckle-pole velocity ($p = 0.0118$).

For speckle-equator velocity of the k-fibers, one-way ANOVA test showed a significant difference between group means ($p = 6.12 \times 10^{-12}$). Speckle-equator velocity for kinetochore fibers was significantly different between untreated metaphase spindles and dynein inhibited spindles ($p = 0.0009$), between untreated metaphase spindles and dynein and EG5 inhibited

spindles ($p = 0.0018$), between untreated metaphase spindles and KIF4A depleted and EG5 inhibited spindles ($p = 0.0058$), between Opti-MEM metaphase spindles and dynein inhibited spindles ($p = 0.0013$), between Opti-MEM metaphase spindles and dynein and EG5 inhibited spindles ($p = 0.0029$), between Opti-MEM metaphase spindles and KIF4A depleted and EG5 inhibited spindles ($p = 0.0084$), between EG5 inhibited metaphase spindles and dynein inhibited spindles ($p = 0.0110$), between EG5 inhibited metaphase spindles and dynein and EG5 inhibited spindles ($p = 0.0221$), between KIF4A depleted metaphase spindles and dynein inhibited spindles ($p = 1.04 \times 10^{-7}$), between KIF4A depleted spindles and dynein and EG5 inhibited spindles ($p = 3.64 \times 10^{-6}$) and between KIF4A depleted spindles and KIF4A depleted and EG5 inhibited spindles ($p = 2.16 \times 10^{-7}$) (Figure 53).

For speckle-pole velocity of the k-fibers, one-way ANOVA test showed a significant difference between group means ($p = 6.13 \times 10^{-11}$). Speckle-pole velocity for kinetochore fibers was significantly different between untreated metaphase spindles and dynein inhibited spindles ($p = 0.0024$), between untreated metaphase spindles and dynein and EG5 inhibited spindles ($p = 0.010$), between Opti-MEM metaphase spindles and dynein inhibited spindles ($p = 0.0045$), between Opti-MEM metaphase spindles and dynein and EG5 inhibited spindles ($p = 0.0179$), between EG5 inhibited metaphase spindles and dynein inhibited spindles ($p = 0.0070$), between EG5 inhibited metaphase spindles and dynein and EG5 inhibited spindles ($p = 0.0273$), between KIF4A depleted metaphase spindles and dynein inhibited spindles ($p = 1.83 \times 10^{-8}$), between KIF4A depleted spindles and dynein and EG5 inhibited spindles ($p = 1.32 \times 10^{-7}$) and between KIF4A depleted spindles and KIF4A depleted and EG5 inhibited spindles ($p = 0.0026$) (Figure 53).

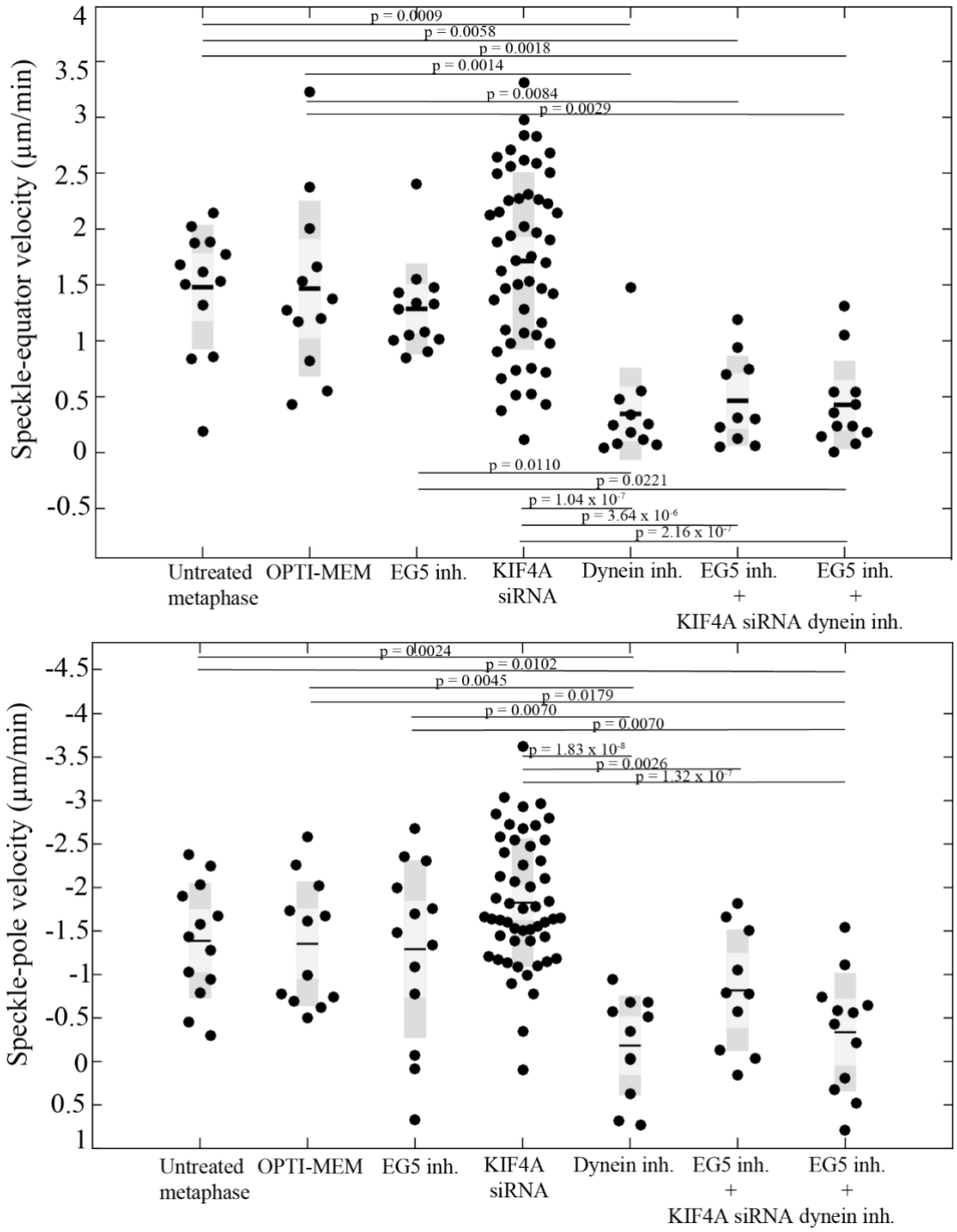

Figure 53. Depletion of KIF4A together with EG5 inhibition, dynein inhibition and dynein and EG5 inhibition significantly slows down speckle-equator velocity of the k-fibers. Quantification (univariate scatter plot) of speckle-equator velocity (up) and speckle-pole velocity (down) across indicated conditions. Each dot corresponds to an individual speckle. The light and dark area in the boxes mark 95% confidence interval on the mean and standard deviation, respectively; and the black line shows mean value. Statistical analysis, ANOVA and

Tukey HSD. One-way ANOVA test showed a significant difference between group means for speckle-equator velocity ($p = 6.12 \times 10^{-12}$) and for speckle-pole velocity ($p = 6.13 \times 10^{-11}$).

For pole-pole velocities of bridging and k-fiber together, one-way ANOVA test did not show a significant difference between group means ($p = 0.1790$) (Figure 54).

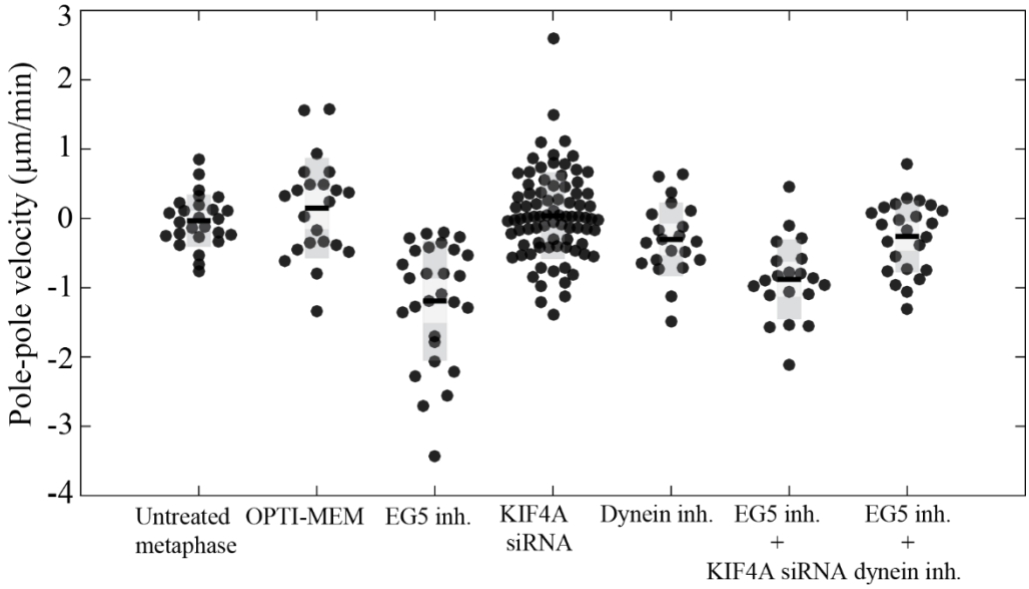

Figure 54. Pole-pole velocity of the bridging and k-fibers is not different across indicated treatments. Quantification (univariate scatter plot) of speckle-equator velocity (up) and speckle-pole velocity (down) across indicated conditions. Each dot corresponds to an individual speckle. The light and dark area in the boxes mark 95% confidence interval on the mean and standard deviation, respectively; and the black line shows mean value. Statistical analysis, ANOVA and Tukey HSD.

For interkinetochore distance, one-way ANOVA test showed a significant difference between group means ($p = 2.22 \times 10^{-16}$). Interkinetochore distance was significantly different between untreated metaphase spindles and EG5 inhibited spindles ($p = 0.0038$), between untreated metaphase spindles and KIF4A depleted and EG5 inhibited spindles ($p = 2.17 \times 10^{-10}$), between untreated metaphase spindles and dynein inhibited spindles ($p = 0.0004$), between untreated metaphase spindles and dynein and EG5 inhibited spindles ($p = 4.14 \times 10^{-9}$), between OPTI MEM metaphase spindles and EG5 inhibited spindles ($p = 0.0112$), between OPTI MEM metaphase spindles and KIF4A depleted and EG5 inhibited spindles ($p = 2.17 \times 10^{-10}$), between

OPTI MEM metaphase spindles and dynein inhibited spindles (p = 0.0017), between OPTI MEM metaphase spindles and dynein and EG5 inhibited spindles (p = 3.97 x 10^{-7}), between EG5 inhibited metaphase spindles and KIF4A depleted and EG5 inhibited spindles (p = 2.17 x 10^{-10}), between KIF4A depleted and EG5 inhibited metaphase spindles and dynein inhibited spindles (p = 2.18 x 10^{-10}) and between KIF4A depleted and EG5 inhibited metaphase spindles and dynein and EG5 inhibited spindles (p = 2.18 x 10^{-10}) (Figure 55).

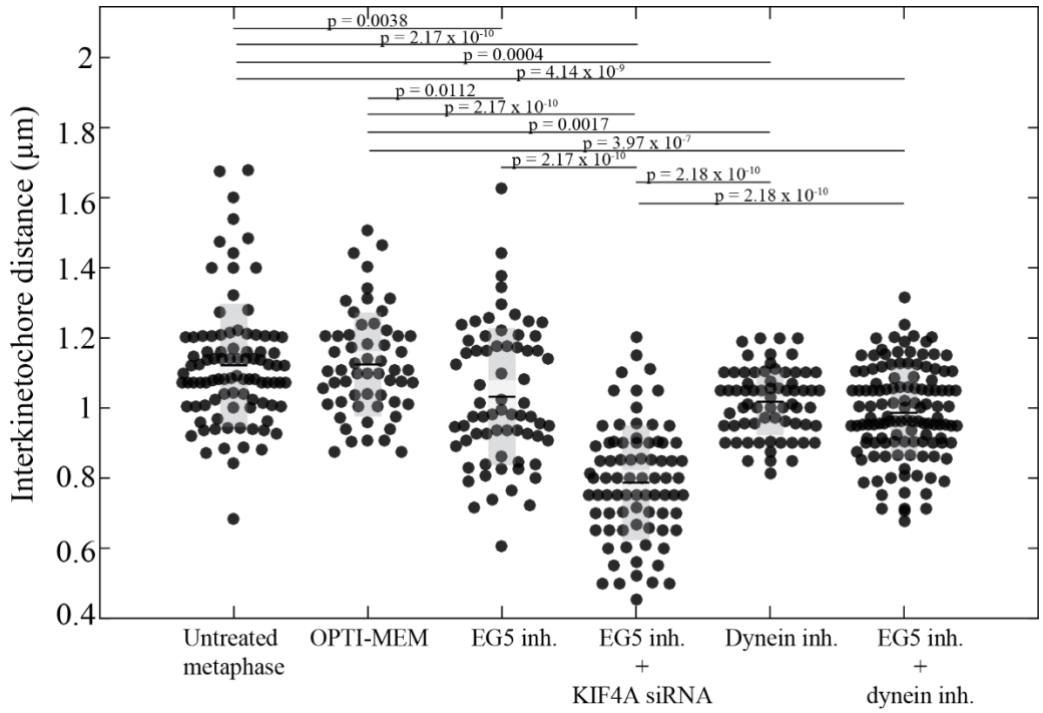

Figure 55. Interkinetochore distance varies troughout different treatments. Quantification (univariate scatter plot) of interkinetochore distance across indicated conditions. Each dot corresponds to an individual kinetochore pair. The light and dark area in the boxes mark 95% confidence interval on the mean and standard deviation, respectively; and the black line shows mean value. Statistical analysis, ANOVA and Tukey HSD. One-way ANOVA test showed a significant difference between group means (p = 2.22 x 10^{-16}).

For PRC1 signal length, one-way ANOVA test showed a significant difference between group means (p = 0). PRC1 signal length was significantly different between untreated metaphase spindles and EG5 inhibited spindles (p = 1.06 x 10^{-10}), between untreated metaphase spindles and dynein inhibited spindles (p = 1.06 x 10^{-10}), between untreated metaphase spindles and

dynein and EG5 inhibited spindles ($p = 1.06 \times 10^{-10}$), between untreated metaphase spindles and KIF4A depleted and EG5 inhibited spindles ($p = 7.95 \times 10^{-6}$), between untreated metaphase spindles and KIF4A depleted spindles ($p = 0.0076$), between EG5 inhibited metaphase spindles and dynein inhibited spindles ($p = 1.06 \times 10^{-10}$), between EG5 inhibited metaphase spindles and dynein and EG5 inhibited spindles ($p = 5.13 \times 10^{-6}$), between EG5 inhibited metaphase spindles and KIF4A depleted spindles ($p = 1.06 \times 10^{-10}$), between dynein inhibited metaphase spindles and KIF4A depleted and EG5 inhibited spindles ($p = 1.06 \times 10^{-10}$), between dynein inhibited metaphase spindles and KIF4A depleted spindles ($p = 1.06 \times 10^{-10}$), between dynein and EG5 inhibited metaphase spindles and KIF4A depleted and EG5 inhibited spindles ($p = 2.57 \times 10^{-6}$), between dynein and EG5 inhibited metaphase spindles and KIF4A depleted spindles ($p = 1.06 \times 10^{-10}$) and between KIF4 depleted and EG5 inhibited metaphase spindles and KIF4A depleted metaphase spindles ($p = 1.06 \times 10^{-10}$) (Figure 56).

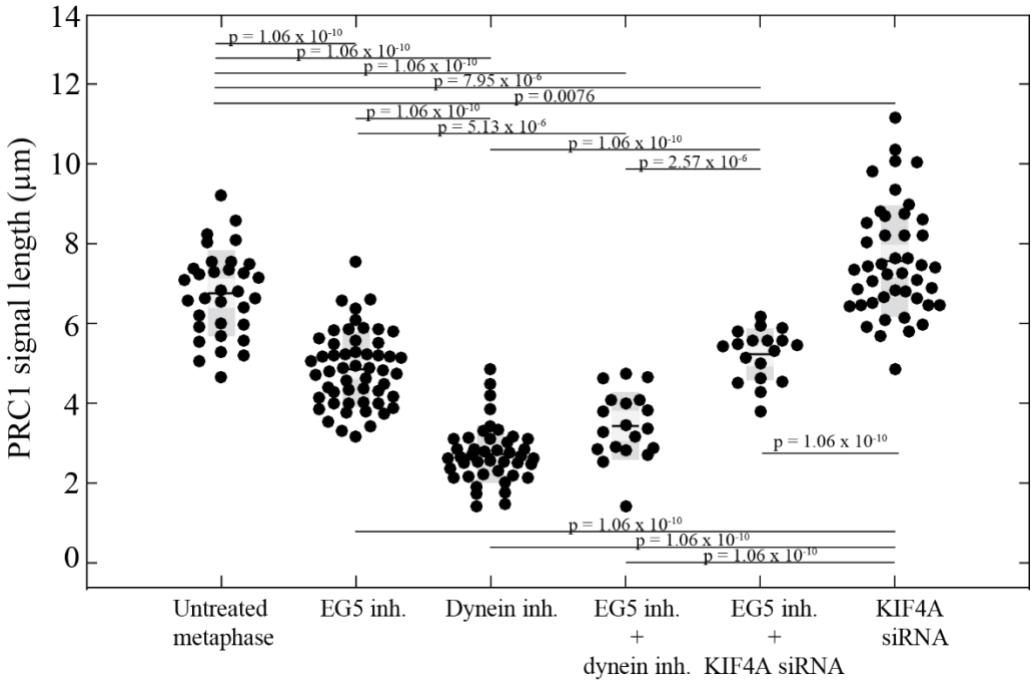

Figure 56. PRC1 signal length varies troughout different treatments. Quantification (univariate scatter plot) of interkinetochore distance across indicated conditions. Each dot corresponds to an individual PRC1 signal. The light and dark area in the boxes mark 95% confidence interval on the mean and standard deviation, respectively; and the black line shows

mean value. Statistical analysis, ANOVA and Tukey HSD. One-way ANOVA test showed a significant difference between group means (p = 0).

For PRC1 signal length and spindle length ratio, one-way ANOVA test showed a significant difference between group means (p = 0). PRC1 signal length/mitotic spindle length ratio was significantly different between untreated metaphase spindles and dynein inhibited spindles ($p = 1.06 \times 10^{-10}$), between untreated metaphase spindles and dynein and EG5 inhibited spindles (p = 0.0004), between EG5 inhibited metaphase spindles and dynein inhibited spindles ($p = 1.06 \times 10^{-10}$), between EG5 inhibited metaphase spindles and dynein and EG5 inhibited spindles ($p = 7.16 \times 10^{-7}$), between dynein and EG5 inhibited metaphase spindles and dynein and KIF4A depleted spindles (p = 0.0013), between dynein and EG5 inhibited metaphase spindles and dynein and KIF4A depleted and EG5 inhibited spindles ($p = 2.13 \times 10^{-5}$), between dynein and EG5 inhibited metaphase spindles and dynein inhibited spindles ($p = 2.23 \times 10^{-8}$), between KIF4A depleted metaphase spindles and dynein inhibited spindles ($p = 1.06 \times 10^{-10}$) and between KIF4A depleted and EG5 inhibited and dynein inhibited spindles ($p = 1.06 \times 10^{-10}$) (Figure 57).

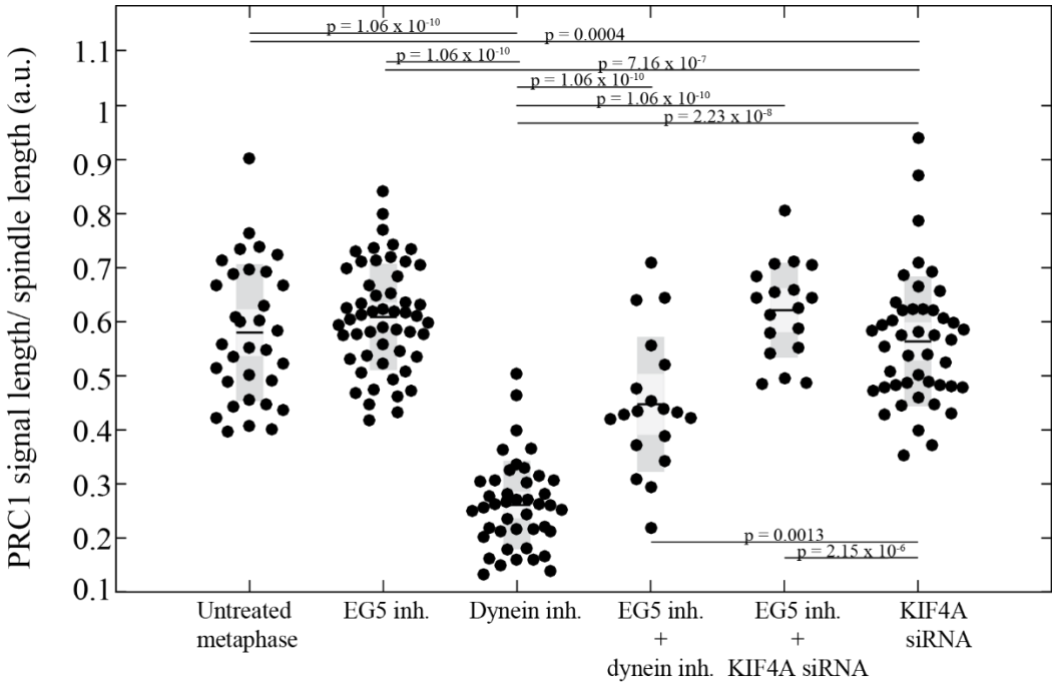

Figure 57. PRC1 signal length/spindle length ratio is the same for untreated metaphase and EG5 inhibited spindles as well as for EG5 inhibited and KIF4A depleted spindles. Quantification (univariate scatter plot) of interkinetochore distance across indicated conditions.

Each dot corresponds to an individual PRC1 signal/spindle length ratio. The light and dark area in the boxes mark 95% confidence interval on the mean and standard deviation, respectively; and the black line shows mean value. Statistical analysis, ANOVA and Tukey HSD. One-way ANOVA test showed a significant difference between group means ($p = 0$).

Also, in this section I wanted to see what is the connection between spindle length, PRC1 signal length and all of the speckle-equator velocities in order to obtain net polymerization and depolymerization velocities for bridging and kinetochore MTs. Spindle length was obtained from pole-pole distance measured while tracking the speckles. In Risteski et al., 2022 it was showed that ratio of PRC1 signal length and spindle length is 48% when measured in fixed RPE-1 cells with GFP-tagged CENP-A and centrin1 while I measured the same ratio in live RPE-1 cells with GFP-tagged PRC1 protein and the same ratio in this cell line is 58%. For my calculations I adapted mentioned ratios to correspond with the cell line that I used for tracking the speckles in and that is live imaged RPE-1 cells with GFP-tagged CENP-A and centrin1 so I used average ratio between the two ratios mentioned previously which is 53%. In untreated metaphase spindles, net polymerization at (+) end of kinetochore MTs is 1.48 μm/min which corresponds to the speckle-equator velocity of the k-fiber. Net depolymerization at (-) end of kinetochore MTs also corresponds to the speckle-equator velocity of the k-fiber since the poles did not move. Polymerization at the (+) end of the bridging MTs in untreated metaphase cells is same as the speckle-equator velocity for bridging MTs which is 2.18 μm/min since metaphase is a stable state (Figure 58).

By using data for KIF4A depleted spindles that was obtained by Patrik Risteski (Risteski et al., 2022) I was able to calculate net polymerization at the (+) end of kinetochore MTs which corresponds with speckle-equator velocity of the k-fibers and it is 1.71 μm/min while net depolymerization at the (-) end of kinetochore MTs is 1.85 μm/min which is speckle-pole velocity. Since after KIF4A depletion, the spindle is at a stable state same as untreated metaphase spindles and there are no changes in spindle length and PRC1 signal length, speckle-equator velocity of the bridging fiber corresponds to the net polymerization at the (+) end of bridging MTs which is 2.14 μm/min (Figure 58).

I wondered what are the possible outcomes of different protein inhibitions during metaphase, for example is polymerization of bridging MTs active after EG5 inhibition or is depolymerization of MTs at the poles main force behind spindle shortening. I calculated net

polymerization at the (+) ends of bridging MTs by supstracting change in PRC1 signal length (which is positive by definition) from speckle-equator velocity of the bridging fiber (which is positive by definition). After calculating net polymerization at the (+) ends of bridging MTs for all of the noted treatments, the fastest polymerization of bridging MTs is in the KIF4A depleted spindles and it is 2.14 µm/min, then untreated metaphase spindles (2.18 µm/min), after that EG5 inhibited spindles (1.24 µm/min), dynein and EG5 inhibited spindles (0.91 µm/min), EG5 inhibited spindles and KIF4A depleted spindles (0.6 µm/min) and the slowest net polymerization at the (+) ends of bridging MTs had dynein inhibited spindles which is 0.44 µm/min. I can conclude that the polymerization exists at the plus end of bridging fibers after all of the treatments but the velocity of the polymerization varies between the treatments dependent of the PRC1 signal length and sliding velocites (Figure 58).

Out of all of the treatments which resulted in spindle collapse (EG5 inh., EG5 inh. + KIF4A depl., dyn inh., dyn. and EG5 inh.), the fastest depolymerization at the (-) ends of kinetochore MTs had KIF4A depleted spindles (1.85 µm/min), then untreated metaphase spindles (1.48 µm/min), EG5 inhibited spindles (1.29 µm/min), EG5 inhibited spindles and KIF4A depleted spindles (0.81 µm/min), dynein and EG5 inhibited spindles (0.34 µm/min) and the slowest net depolymerization at the (-) ends of kinetochore MTs had dynein inhibited spindles which is 0.18 µm/min (Figure 58).

Finally, the net polymerization at the (+) end of the kinetochore MTs corresponds to the speckle-equator velocities of the k-fibers. Fastest polymerization at the (+) end of the kinetochore MTs can be seen in KIF4A depleted spindles (1.71 µm/min), then in untreated metaphase spindles (1.48 µm/min), then EG5 inhibited spindles (1.28 µm/min), EG5 inhibited and KIF4A depleted spindles (0.46 µm/min), dynein and EG5 inhibited spindles (0.43 µm/min) and the slowest net polymerization at the (+) ends of kinetochore MTs had dynein inhibited spindles which is 0.35 µm/min (Figure 58).

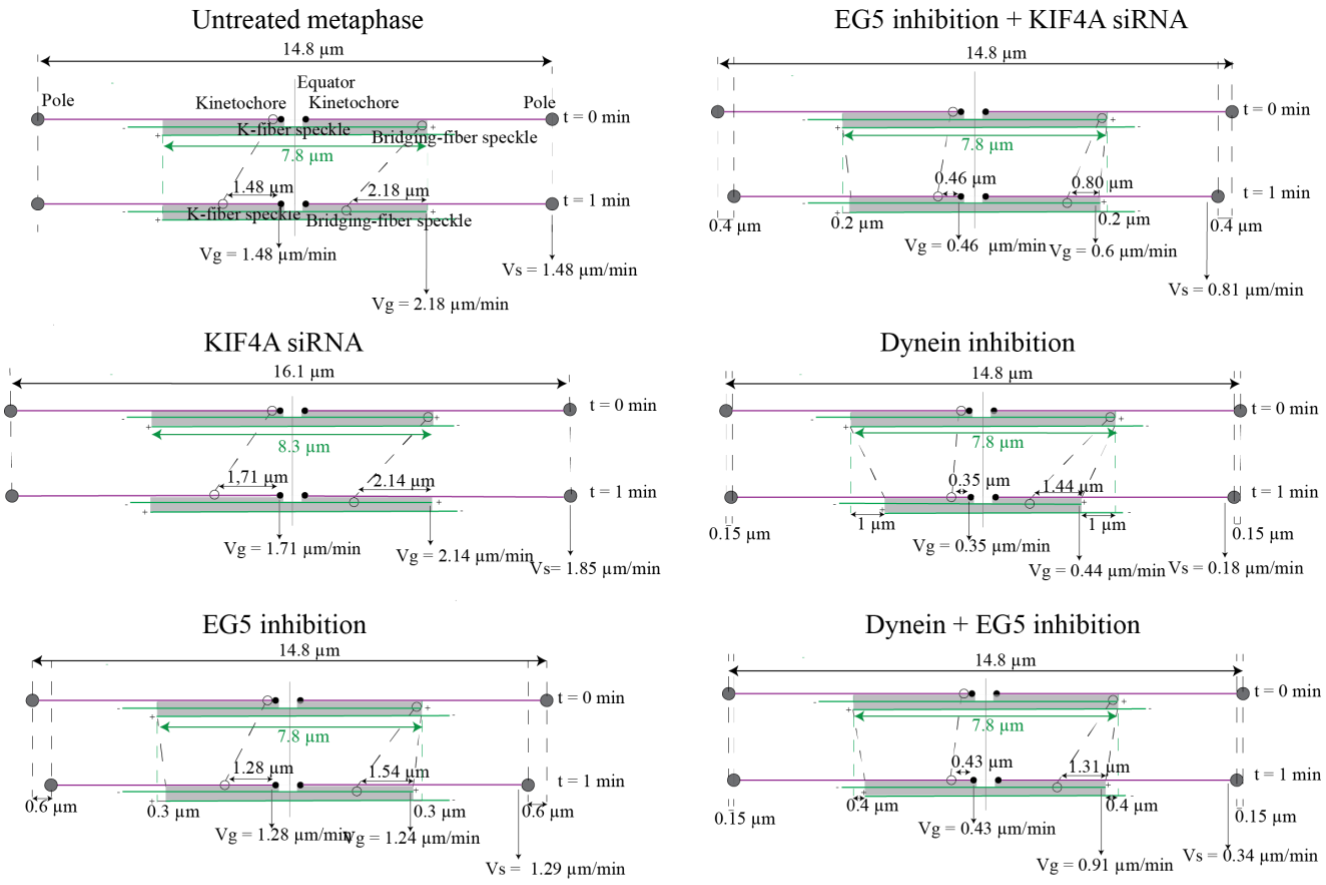

Vg = net polymerization at (+) end of kinetochore or bridging microtubules
Vs = net depolymerization at (-) end of kinetochore microtubules

Figure 58. Simplified models for calculation of net polymerization and depolymerization velocities after noted treatments in RPE-1 cells. Schemes show movement of speckles along kinetochore (pink) and bridging (green) MTs at the start of tracking of the speckle and after 1 minute. Polymerization at the (+) end of bridging MTs is active after all of the noted treatments but varies between treatmens dependent of PRC1 signal length and speckle-equator velocities. Polymerization at the (+) end of kinetochore MTs corresponds with speckle-equator velocities of the kinetochore MTs and depolymerization at the (-) end of the kinetochore MTs coresponds to poleward flux of kinetochore MTs.

5 DISCUSSION

5.1. Differences of sliding in metaphase and anaphase

The dynamic mitotic spindle, a complex micromolecular machine that drives chromosome segregation is still one of the main subjects of investigation in the field of molecular biology. Fascinating property of the MTs, their dynamics, is a challenging question in the mitosis field. The foundation of the understanding of dynamics of the MTs is based on the proper characterization of all structures in the mitotic spindle that are contributing to their constant movement. Thanks to the recently optimized speckle-microscopy assay (Risteski et al., 2022) I was able to study individual flux of different types of MTs in the spindle.

In accordance to the previous study using speckle-microscopy in metaphase (Risteski et al., 2022) and using a new measure for speckle movement called speckle-equator velocity, I confirmed that the bridging fibers flux at a higher rate than the k-fibers in metaphase. Moreover, a slower flux of kinetochore MTs than non-kinetochore ones was also observed in Xenopus egg extracts (Jang et al., 2008; Maddox et al., 2003) and crane-fly spermatocytes (LaFountain et al., 2004), from which I can speculate that this relationship between bridging and k-fiber flux is conserved in many organisms whose spindles have MT flux. Interestingly, after measuring speckle movement in anaphase I concluded that there is no difference in the sliding of the bridging and k-fibers and that k-fibers undergo sliding at the same velocity as the bridging fiber in anaphase which is in accordance with previous photoactivation experiments (Vukušić et al., 2017). This could be explained by less tension from the chromosomes in anaphase then there is in metaphase so the transmission of the force from the midzone to the k-fibers is more efficient in anaphase thus the velocities of MTs in the bridging and k-fibers are similar. In metaphase, the tension between sister kinetochores is present because they are linked by chromatin, but in anaphase this link vanishes.

5.2. Role of EG5 in sliding of the antiparallel microtubules in metaphase

To investigate the role of one of the most studied kinesin members, EG5, a motor protein with the motor domain located at the N-terminus which has a capacity to move toward MT plus-ends (Kenneth E. Sawin & Mitchison, 1995) I decided to inhibit EG5 in metaphase using small molecule drug inhibitor STLC (Skoufias et al., 2006). It was hypothesized by many to be the

primary sliding motor in various circumstances during mitosis (Gayek & Ohi, 2014; Hoyt, 1994; Kapoor et al., 2000; Mann & Wadsworth, 2019; Saunders & Hoyt, 1992; Straight et al., 1998). It is known that purified vertebrate EG5 walks processively toward the plus-ends of MTs with relatively short run lengths (~8 steps) (Kapitein et al., 2005; Valentine et al., 2006). Additionally, because they from bipolar homotetramers, EG5 protein family use both their motor domains and non-motor tail domains to crosslink and simultaneously walk on two MTs, showing a preference for MTs in the antiparallel configuration (Kapitein et al., 2005), effectively resulting in relative MTs sliding. In HeLa cell line it was previously shown that Kif15 is not required for spindle bipolarity in cells with full EG5 activity but becomes essential when EG5 is partially inhibited (Tanenbaum et al., 2009). Furthermore, in U2OS cells stably co-expressing PA-GFP-α-tubulin and mCherry-α-tubulin it was shown that combined action of EG5 and KIF15 support MT-flux driving activities of CENP-E and KIF4A (Steblyanko et al., 2020b) which means that to get monopolar spindles it is necessary to inhibit the action of both EG5 and KIF15. However in RPE-1 cell line, EG5 inhibition in metaphase leads to immediate spindle collapse into monopolar spindle (Gayek & Ohi, 2014). Here I show that during spindle collapse after EG5 inhibition, bridging and k-fibers flux at the similar rate as in untreated metaphase cells which is in accordance with previous photoactivation experiments (Steblyanko et al., 2020b; Vukušić et al., 2021). Moreover, there is a fraction of RPE-1 cells that after EG5 inhibition with STLC, enter anaphase and proceed with normal spindle elongation even after spindles are shortened to 7-8 μm (Vukušić et al., 2021) which would suggest that antiparallel overlaps remain the same length in untreated metaphase spindles and in short EG5 inhibited spindles. Here I showed that the PRC1 overlaps are significantly shorter in EG5 inhibited spindles but what is interesting is that they still take 61% of spindle length which is similar as in untreated metaphase spindles where PRC1 length takes 58% of the spindle length. This could suggest that this shorter antiparallel overlap is still sufficient for motors to slide at the similar rate as in longer overlaps because the PRC1 length to spindle length ratio is the same for untreated and EG5 inhibited spindles. However, even though it is not significant, change of around 30% slower speckle-equator velocity can be noticed after EG5 inhibition. When comparing speckle-equator velocity or sliding to poleward flux I can conclude that the change in sliding is larger than in poleward flux after EG5 inhibition when compared to the untreated metaphase which suggests that sliding of the antiparallel MTs is perturbed after EG5 inhibition.

5.3. Role of EG5 on the pole

Sliding could be connected to depolymerization at the spindle poles which was previously suggested by Miyamoto et al. (2004) and Brust-Mascher et al. (2009). This would suggest that the spindle during the EG5 collapse is actually collapsing from the poles inward and not the other way around. Poles are most likely where most of the minus-end directed motors, like dynein, exert their forces (vanHeesbeen et al., 2014; She & Yang, 2017). To further explore depolymerization at the poles it would be interesting to explore how perturbations of proteins that are regulators of MT dynamic ends would be affecting sliding in EG5 inhibited spindles. Those would include proteins members of kinesin-13 family like depolymerases KIF2A and mitotic centromere-associated kinesin (MCAK, KIF2C) that are localized at the poles or at the kinetochores (Goshima & Scholey, 2010). Furthermore, it was shown previously that in a cloud of short MTs, EG5 can first condense the MTs into bundles and subsequently sort them apart according to orientation, possibly aligning the plus ends of parallel MTs (Kapitein et al., 2005). Such a process might operate around the centrosomes in the initial phase of spindle morphogenesis, and might also contribute to the formation of MT bundles important for chromosome–spindle attachment (Kapitein et al., 2005) thus that could be one of the roles of EG5 at the spindle poles. Since after EG5 inhibition there was no change in poleward flux when compared to the untreated metaphase spindles I suggest that the role of EG5 at the poles is not essential for the spindle shortening after inhibition of EG5.

5.4. Kinesins EG5 and KIF4A together drive sliding in the metaphase

The plus-end-directed motor kinesin-4 KIF4A is one of the proteins that PRC1 recruits in human cells (Kurasawa et al., 2004; Powers et al., 2004; Vernos et al., 1995; Zhu & Jiang, 2005) which is also known to regulate the length of central antiparallel MT overlaps in the anaphase spindle (Hu et al., 2011; Kurasawa et al., 2004; Zhu & Jiang, 2005). KIF4A moves along the MTs towards their plus ends and upon its accumulation at the plus end, reduces MT polymerisation and depolymerisation dynamics (Bieling et al., 2010; Bringmann et al., 2004). According to Hu et al. (2011), KIF4 depletion results in aberrant central spindle elongation and misdirected MT overlaps. Since we previoulsy showed that in anaphase after EG5 inhibition and KIF4A depletion, anaphase stops and sliding is abolished (Vukušić et al., 2021), it was

expected that in metaphase this would be similar. This is supported by previous studies by Steblyanko et al. (2020) where it was showed that in U2OS cells combined action of EG5 and KIF15 support MT flux driving activites od CENP-E and KIF4A. Here, I show that after EG5 inhibition and KIF4A depletion, bridging fiber flux as well as the k-fiber flux is significantly slower than in untreated metaphase cells. I conclude that EG5 and KIF4A are the main drivers of sliding and force producing proteins in the spindle midzone in metaphase and that without these two motors, sliding in the midzone in metaphase is severely impaired. In live imaging of PRC1 labeled RPE-1 spindles it could be seen that, similarly to the only EG5 inhibited spindles, antiparallel bundles extent at the same percent of the spindle length even in drastically short spindles which suggests that the structure of the spindle midzone is preserved. Normal midzone structure could also be seen with super-resolution imaging of immunofluorescently labeled MTs which is in agreement with our previous studies (Vukušić et al., 2021). When this all is taken together I can speculate that the abolished MT sliding of the bridging and k-fiber is only due to main motors not sliding in the midzone.

5.5. Role of dynein in sliding of the antiparallel microtubules in metaphase

Furthermore, it is known that the most renowned antagonism in human spindles is achieved in metaphase between EG5 as a dominant outward motor, and dynein as a dominant inward motor (Goshima & Scholey, 2010). Recent experiments were done either with dynein knockdown using transfection with siRNA (vanHeesbeen et al., 2014) or dynein knockout using CRISPR-Cas9 method (Neahring et al., 2021) to show that spindles without dynein show splaying of the poles or unfocused poles. Here, I show that by using Ciliobrevin D inhitibitor to inhibit dynein (Firestone et al., 2012; Sikirzhytski et al., 2014) I can observe acute effects of dynein inhibition on the mitotic spindle and measure dynamic properties of the MTs. I show that after dynein inhibition, k-fiber flux is significantly reduced when compared to untreated metaphase spindles but bridging fibers flux at the similar rate as bridging fibers in untreated cells. This suggests that after dynein inhibition, midzone part of the spindle remains preserved but the connection with the k-fiber is impaired and so is the force transmission between the two. Furthermore, this was confirmed in RPE-1 cell line with stable expression of the PRC1 protein and tubulin preservation fixation protocol imaged on STED microscope where I can notice structural

changes on the k-fibers while midzone of the spindle looks similar to the untreated metaphase spindles.

However, some researchers proposed that dynein could drive the antiparallel MT inward sliding in the spindle midzone which they mostly explain by spindle length increase after dynein inhibition (Ferenz et al., 2010; Tanenbaum et al., 2013). Here, I showed that after dynein inhibition spindle length decreases when compared to the untreated metaphase spindles which would then suggest that dynein is not sliding antiparallel MTs in the midzone. The discrepancy between these results could be explained by different methods used to inhibit dynein. Namely, Ferenz et al. (2010) and Tanenbaum et al. (2013) used siRNA while I used inhibitor Ciliobrevin D. When using siRNA there is usually 48 to 72 hours before imaging of the cells thus cells have time to develop other mechanisms to bypass dynein deficiency while inhibition with Ciliobrevin D shows acute effects and imaging is done immediately.

Moreover, here I show that after double inhibition of dynein and EG5, bipolarity of the spindle is rescued, as previously shown (Neahring et al., 2021; vanHeesbeen et al., 2014). After studying poleward flux in spindles without EG5 and dynein I show that similarly to only dynein inhibited spindles, bridging fiber flux is preserved but k-fiber flux is diminished. Recently it was shown that without these opposing motor activities, spindles are more fragile when mechanically challenged in metaphase (Neahring et al., 2021) thus I suggest that impaired k-fiber poleward flux might be behind this. Our conclusion relies on a connection between the bridging fiber and k-fibers, which is created by parallel non-motor cross-linkers, in addition to the motor proteins. It was demonstrated that MTs in a k-fiber are connected by parallel cross-linkers known as "the mesh" (Nixon et al., 2015). Yet, in the areas where their parallel overlaps, these proteins could potentially crosslink k-fiber MTs and bridging MTs. Similarly, the bridging fibers include the antiparallel cross-linker PRC1 (Kajtez et al., 2016a; Polak et al., 2017). Here I show that one of these essential general crosslinkers in the mitotic spindle could be dynein. Crosslinking between k-fibers and interpolar MTs in metaphase and anaphase has been discussed in several works (Goode, 1981; Maiato & Lince-Faria, 2010; Matos et al., 2009; Mitchison et al., 2005). Yet, the role of dynein and other proteins as crosslinkers have not been directly tested and it would be interesting to test this in the future experiments.

5.6. The spindle consists of two mechanically distinct parts, the midzone and the pole-proximal part

Here I propose that the spindle consists of two mechanically distinct parts, the midzone part which remains functional during collapse, and the pole-proximal part of the spindle which is shortened during spindle collapse (Figure 59). After EG5 inhibition I suggest that the midzone part of the spindle remains structurally intact but sliding is showing about 30% decrease when compared to the untreated metaphase. Since poleward flux did not change after EG5 inhibition it is unlikely that any changes are happening at the spindle pole after EG5 inhibition. After EG5 inhibition in KIF4A depleted cells I speculate that the spindle midzone has preserved structure as in only EG5 inhibited spindles, but the main motor drivers are not sliding thus the bridging and k-fiber speckle-equator velocities are close to zero. Since after dynein inhibition there is almost non-existent speckle-equator velocity of the k-fibers I suggest that the connection between the bridging and k-fibers is impaired. It would be interesting in the future to explore possible redundancies between dynein and other motor proteins in the midzone during metaphase but also anaphase as well as to investigate differences between poleward flux of infividual MTs in normal and tumor human cells.

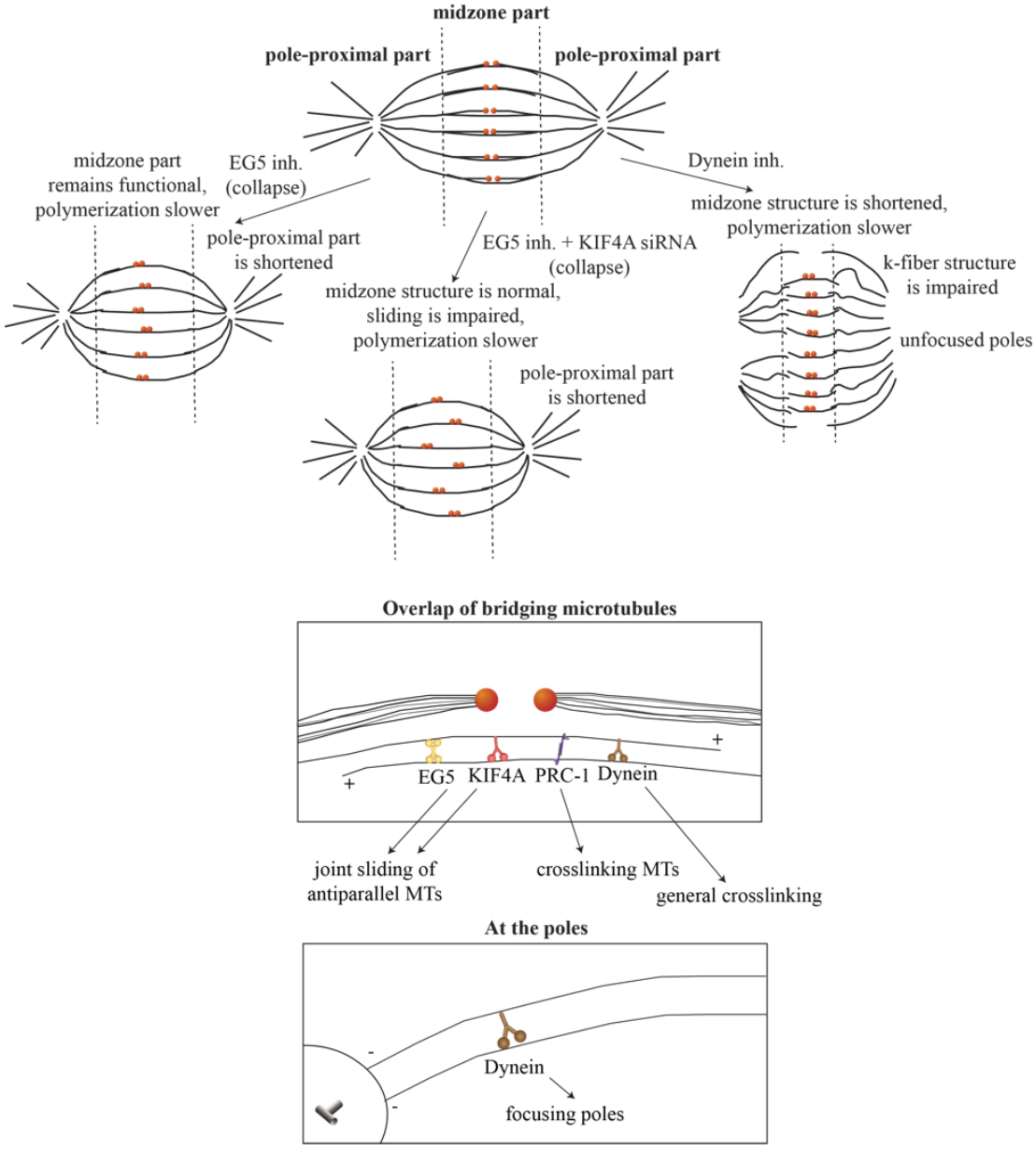

Figure 59. Simplified model of midzone and proximal parts of the spindle after different inhibitions of motor proteins in the mitotic spindle. I suggest that dynein acts as a general crosslinker in the spindle connecting bridging fibers and k-fiber and also that dynein doesn't slide in the midzone. It was previously shown as well as in this paper that dynein is essential for pole focusing. On the other hand, EG5 together with KIF4 slides antiparallel MTs in the midzone. Role of EG5 at the spindle poles remains unknown.

6 CONCLUSION

After measuring speckle movement in anaphase I concluded that there is no difference in the sliding velocity of the bridging and k-fibers and that k-fibers undergo sliding at the same velocity as the bridging fiber in anaphase. Here I show that during spindle collapse after EG5 inhibition, briding and k-fibers slide at the similar rate as in untreated metaphase cells which is in accordance with previous photoactivation experiments. However, slight decrease in sliding of the bridging fibers can be noticed after EG5 inhibition. Using tubulin preservation protocol I show that the spindle midzone remains the same after EG5 inhibition when compared to the untreated metaphase cells. Furthermore, I conclude that EG5 and KIF4A are the main sliders in the spindle midzone in metaphase. Next, I show that after dynein inhibition, k-fiber sliding is significantly reduced when compared to untreated metaphase spindles but bridging fiber sliding velocity is similar as bridging fibers in untreated cells. In spindles without EG5 and dynein I show that same as in only dynein inhibited spindles, bridging fiber sliding is preserved but k-fiber sliding is diminished. Here I propose that the spindle consists of two mechanically distinct parts, the midzone part which remains functional during collapse, and the pole-proximal part of the spindle which is shortened during spindle shortening.

7 LITERATURE

Akhmanova, A., & Steinmetz, M. O. (2008). Tracking the ends: a dynamic protein network controls the fate of microtubule tips. *Nature Reviews Molecular Cell Biology 2008 9:4*, *9*(4), 309–322. https://doi.org/10.1038/nrm2369

Alberts, B., Johnson, A., Lewis, J., Morgan, D., Raff, M., Roberts, K., and Walter, P. (2014). Molecular biology of the cell, 6th edn (Garland Science, New York).

Asbury, C. L. (2017). Anaphase A: Disassembling Microtubules Move Chromosomes toward Spindle Poles. *Biology*, *6*(1). https://doi.org/10.3390/BIOLOGY6010015

Asashima, M., Ikeuchi, M., Ishiura, S., Ide, T., Irimura, T., Ohya, Y., Kamimura, S., Kodama, T., Komazaki, S., Sasagawa, N., et al. (2010). Fundamental Concept of Biology. In A comprehensive approach to Life Science, C.T.U.o. Tokio, ed.

Asthana, J., Cade, N. I., Normanno, D., Lim, W. M., & Surrey, T. (2021). Gradual compaction of the central spindle decreases its dynamicity in PRC1 and EB1 gene-edited cells. *Life Science Alliance*, *4*(12). https://doi.org/10.26508/LSA.202101222

Balchand, S. K., Mann, B. J., & Wadsworth, P. (2016). Using fluorescence microscopy to study mitosis. *Methods in Molecular Biology*, *1413*, 3–14. https://doi.org/10.1007/978-1-4939-3542-0_1/COVER

Bannigan, A., Scheible, W. R., Lukowitz, W., Fagerstrom, C., Wadsworth, P., Somerville, C., & Baskin, T. I. (2007). A conserved role for kinesin-5 in plant mitosis. *Journal of Cell Science*, *120*(16), 2819–2827. https://doi.org/10.1242/JCS.009506

Barnum, K. J., & O'Connell, M. J. (2014). Cell cycle regulation by checkpoints. *Methods in Molecular Biology*, *1170*, 29–40. https://doi.org/10.1007/978-1-4939-0888-2_2/COVER

Belar, K. (1929). Beitrage zur Kausalanalyse der Mitose : II. Untersuchungen an den Spermatocyten von Chorthippus (Stenobothrus) lineatus Panz. Wilhelm Roux Arch Entwickl Mech Org 118, 359-484.

Bieling, P., Telley, I. A., & Surrey, T. (2010). A Minimal Midzone Protein Module Controls Formation and Length of Antiparallel Microtubule Overlaps. *Cell*, *142*(3), 420–432. https://doi.org/10.1016/J.CELL.2010.06.033

Braun, M., Lansky, Z., Fink, G., Ruhnow, F., Diez, S., & Janson, M. E. (2011). Adaptive braking by Ase1 prevents overlapping microtubules from sliding completely apart. *Nature Cell Biology*, *13*(10), 1259–1264. https://doi.org/10.1038/NCB2323

Bringmann, H., Skiniotis, G., Spilker, A., Kandels-Lewis, S., Vernos, I., & Surrey, T. (2004). A kinesin-like motor inhibits microtubule dynamic instability. *Science (New York, N.Y.)*, *303*(5663), 1519–1522. https://doi.org/10.1126/SCIENCE.1094838

Brust-Mascher, I., Sommi, P., Cheerambathur, D. K., & Scholey, J. M. (2009). Kinesin-5–dependent Poleward Flux and Spindle Length Control in Drosophila Embryo Mitosis. *Molecular Biology of the Cell*, *20*(6), 1749. https://doi.org/10.1091/MBC.E08-10-1033

Buđa, R., Vukušić, K., & Tolić, I. M. (2017). Dissection and characterization of microtubule bundles in the mitotic spindle using femtosecond laser ablation. *Methods in Cell Biology*, *139*, 81–101. https://doi.org/10.1016/bs.mcb.2016.11.007

Cai, S., O'Connell, C. B., Khodjakov, A., & Walczak, C. E. (2009). Chromosome Congression in the Absence of K-Fibres. *Nature Cell Biology*, *11*(7), 832. https://doi.org/10.1038/NCB1890

Cameron, L. A., Yang, G., Cimini, D., Canman, J. C., Kisurina-Evgenieva, O., Khodjakov, A., Danuser, G., & Salmon, E. D. (2006). Kinesin 5–independent poleward flux of kinetochore microtubules in PtK1 cells. *The Journal of Cell Biology*, *173*(2), 173. https://doi.org/10.1083/JCB.200601075

Civelekoglu-Scholey, G., & Scholey, J. M. (2010). Mitotic force generators and chromosome segregation. *Cellular and Molecular Life Sciences 2010 67:13*, *67*(13), 2231–2250. https://doi.org/10.1007/S00018-010-0326-6

Cross, R. A., & McAinsh, A. (2014). Prime movers: the mechanochemistry of mitotic kinesins. *Nature Reviews Molecular Cell Biology 2014 15:4*, *15*(4), 257–271. https://doi.org/10.1038/nrm3768

Debonis, S., Skoufias, D. A., Lebeau, L., Lopez, R., Robin, G., Margolis, R. L., Wade, R. H., & Kozielski, F. (2004). In vitro screening for inhibitors of the human mitotic kinesin Eg5 with antimitotic and antitumor activities. *Mol Cancer Ther*, *3*(9), 1079–1090. http://dtp.nci.nih.gov/branches/dscb/diversity_explanation.html.

Desai, A., & Mitchison, T. J. (2003). MICROTUBULE POLYMERIZATION DYNAMICS. *Https://Doi.Org/10.1146/Annurev.Cellbio.13.1.83*, *13*, 83–117. https://doi.org/10.1146/ANNUREV.CELLBIO.13.1.83

Downing, K. H., & Nogales, E. (1999). Crystallographic Structure of Tubulin : Implications for Dynamics and Drug Binding. *Cell Structure and Function*, *24*(5), 269–275. https://doi.org/10.1247/CSF.24.269

Drechsler, H., McHugh, T., Singleton, M. R., Carter, N. J., & McAinsh, A. D. (2014). The Kinesin-12 Kif15 is a processive track-switching tetramer. *ELife*, *2014*(3). https://doi.org/10.7554/ELIFE.01724

Dujardin, D. L., & Vallee, R. B. (2002). Dynein at the cortex. *Current Opinion in Cell Biology*, *14*(1), 44–49. https://doi.org/10.1016/S0955-0674(01)00292-7

Dumont, J., & Desai, A. (2012). Acentrosomal spindle assembly and chromosome segregation during oocyte meiosis. *Trends in Cell Biology*, *22*(5), 241–249. https://doi.org/10.1016/J.TCB.2012.02.007

Dumont, S., & Mitchison, T. J. (2009). Force and Length in the Mitotic Spindle. *Current Biology : CB*, *19*(17), R749. https://doi.org/10.1016/J.CUB.2009.07.028

Ferenz, N. P., Gable, A., & Wadsworth, P. (2010). Mitotic functions of kinesin-5. *Seminars in Cell & Developmental Biology*, *21*(3), 255–259. https://doi.org/10.1016/J.SEMCDB.2010.01.019

Fink, G., Schuchardt, I., Colombelli, J., Stelzer, E., & Steinberg, G. (2006). Dynein-mediated pulling forces drive rapid mitotic spindle elongation in Ustilago maydis. *The EMBO Journal*, *25*(20), 4897. https://doi.org/10.1038/SJ.EMBOJ.7601354

Firestone, A. J., Weinger, J. S., Maldonado, M., Barlan, K., Langston, L. D., O'Donnell, M., Gelfand, V. I., Kapoor, T. M., & Chen, J. K. (2012). Small-molecule inhibitors of the AAA+ ATPase motor cytoplasmic dynein. *Nature*, *484*(7392), 125. https://doi.org/10.1038/NATURE10936

Florian, S., & Mayer, T. U. (2012). The Functional Antagonism between Eg5 and Dynein in Spindle Bipolarization Is Not Compatible with a Simple Push-Pull Model. *Cell Reports*, *1*(5), 408–416. https://doi.org/10.1016/J.CELREP.2012.03.006

Forer, A. (1965). LOCAL REDUCTION OF SPINDLE FIBER BIREFRINGENCE IN LIVING NEPHROTOMA SUTURALIS (LOEW) SPERMATOCYTES INDUCED BY ULTRAVIOLET MICROBEAM IRRADIATION. *The Journal of Cell Biology*, *25*(1), 95–117. https://doi.org/10.1083/JCB.25.1.95

Forth, S., Hsia, K. C., Shimamoto, Y., & Kapoor, T. M. (2014). Asymmetric Friction of Nonmotor MAPs Can Lead to Their Directional Motion in Active Microtubule Networks. *Cell*, *157*(2), 420–432. https://doi.org/10.1016/J.CELL.2014.02.018

Foster, P. J., Furthauer, S., Shelley, M. J., & Needleman, D. J. (2015). Active contraction of microtubule networks. *ELife*, *4*(DECEMBER2015).

https://doi.org/10.7554/ELIFE.10837

Fu, C., Yan, F., Wu, F., Wu, Q., Whittaker, J., Hu, H., Hu, R., & Yao, X. (2007). Mitotic phosphorylation of PRC1 at Thr470 is required for PRC1 oligomerization and proper central spindle organization. *Cell Research*, *17*(5), 449–457. https://doi.org/10.1038/CR.2007.32

Fu, J., Bian, M., Xin, G., Deng, Z., Luo, J., Guo, X., Chen, H., Wang, Y., Jiang, Q., & Zhang, C. (2015). TPX2 phosphorylation maintains metaphase spindle length by regulating microtubule flux. *Journal of Cell Biology*, *210*(3), 373–383. https://doi.org/10.1083/JCB.201412109/VIDEO-6

Gaetz, J., & Kapoor, T. M. (2004). Dynein/dynactin regulate metaphase spindle length by targeting depolymerizing activities to spindle poles. *Journal of Cell Biology*, *166*(4), 465–471. https://doi.org/10.1083/JCB.200404015/VIDEO-6

Gaglio, T., Saredi, A., Bingham, J. B., Hasbani, M. J., Gill, S. R., Schroer, T. A., & Compton, D. A. (1996). Opposing motor activities are required for the organization of the mammalian mitotic spindle pole. *The Journal of Cell Biology*, *135*(2), 399–414. https://doi.org/10.1083/JCB.135.2.399

Galderisi, U., Jori, F. P., & Giordano, A. (2003). Cell cycle regulation and neural differentiation. *Oncogene 2003 22:33*, *22*(33), 5208–5219. https://doi.org/10.1038/sj.onc.1206558

Ganem, N. J., Upton, K., & Compton, D. A. (2005). Efficient Mitosis in Human Cells Lacking Poleward Microtubule Flux. *Current Biology*, *15*(20), 1827–1832. https://doi.org/10.1016/J.CUB.2005.08.065

Gayek, A. S., & Ohi, R. (2014). Kinetochore-microtubule stability governs the metaphase requirement for Eg5. *Molecular Biology of the Cell*, *25*(13), 2051. https://doi.org/10.1091/MBC.E14-03-0785

Glotzer, M. (2004). Cleavage furrow positioning. *The Journal of Cell Biology*, *164*(3), 347. https://doi.org/10.1083/JCB.200310112

Goode, D. (1981). Microtubule turnover as a mechanism of mitosis and its possible evolution. *Bio Systems*, *14*(3–4), 271–287. https://doi.org/10.1016/0303-2647(81)90034-4

Goodman, S.R. (2008). The Cell Cycle and Cancer. In Medical Cell Biology S.R. Goodman, ed. (Academic Press), pp. 273-289.

Goshima, G., Nédélec, F., & Vale, R. D. (2005). Mechanisms for focusing mitotic spindle

poles by minus end–directed motor proteins. *The Journal of Cell Biology*, *171*(2), 229. https://doi.org/10.1083/JCB.200505107

Goshima, G., & Scholey, J. M. (2010). Control of Mitotic Spindle Length. *Annual Review of Cell and Developmental Biology*, *26*(1), 21–57. https://doi.org/10.1146/annurev-cellbio-100109-104006

Heilemann, M., Van De Linde, S., Schüttpelz, M., Kasper, R., Seefeldt, B., Mukherjee, A., Tinnefeld, P., & Sauer, M. (2008). Subdiffraction-resolution fluorescence imaging with conventional fluorescent probes. *Angewandte Chemie - International Edition*, *47*(33), 6172–6176. https://doi.org/10.1002/anie.200802376

Howell, B. J., McEwen, B. F., Canman, J. C., Hoffman, D. B., Farrar, E. M., Rieder, C. L., & Salmon, E. D. (2001). Cytoplasmic dynein/dynactin drives kinetochore protein transport to the spindle poles and has a role in mitotic spindle checkpoint inactivation. *The Journal of Cell Biology*, *155*(7), 1159. https://doi.org/10.1083/JCB.200105093

Hoyt, M. A. (1994). Cellular roles of kinesin and related proteins. *Current Opinion in Cell Biology*, *6*(1), 63–68. https://doi.org/10.1016/0955-0674(94)90117-1

Hu, C. K., Coughlin, M., Field, C. M., & Mitchison, T. J. (2011). KIF4 Regulates Midzone Length during Cytokinesis. *Current Biology : CB*, *21*(10), 815. https://doi.org/10.1016/J.CUB.2011.04.019

Hueschen, C. L., Kenny, S. J., Xu, K., & Dumont, S. (2017). NuMA recruits dynein activity to microtubule minus-ends at mitosis. *ELife*, *6*. https://doi.org/10.7554/ELIFE.29328

Jang, C. Y., Wong, J., Coppinger, J. A., Seki, A., Yates, J. R., & Fang, G. (2008). DDA3 recruits microtubule depolymerase Kif2a to spindle poles and controls spindle dynamics and mitotic chromosome movement. *The Journal of Cell Biology*, *181*(2), 255. https://doi.org/10.1083/JCB.200711032

Janson, M. E., Loughlin, R., Loïodice, I., Fu, C., Brunner, D., Nédélec, F. J., & Tran, P. T. (2007). Crosslinkers and Motors Organize Dynamic Microtubules to Form Stable Bipolar Arrays in Fission Yeast. *Cell*, *128*(2), 357–368. https://doi.org/10.1016/J.CELL.2006.12.030

Jiang, K., Rezabkova, L., Hua, S., Liu, Q., Capitani, G., Altelaar, A. F. M., Heck, A. J. R., Kammerer, R. A., Steinmetz, M. O., & Akhmanova, A. (2017). Microtubule minus-end regulation at spindle poles by an ASPM-katanincomplex. *Nature Cell Biology*, *19*(5), 480. https://doi.org/10.1038/NCB3511

Jiang, W., Jimenez, G., Wells, N. J., Hope, T. J., Wahl, G. M., Hunter, T., & Fukunaga, R. (1998). PRC1: A human mitotic spindle-associated CDK substrate protein required for cytokinesis. *Molecular Cell*, *2*(6), 877–885. https://doi.org/10.1016/s1097-2765(00)80302-0

Kajtez, J., Solomatina, A., Novak, M., Polak, B., Vukušić, K., Rüdiger, J., Cojoc, G., Milas, A., Šumanovac Šestak, I., Risteski, P., Tavano, F., Klemm, A. H., Roscioli, E., Welburn, J., Cimini, D., Glunčić, M., Pavin, N., & Tolić, I. M. (2016a). Overlap microtubules link sister k-fibres and balance the forces on bi-oriented kinetochores. *Nature Communications*, *7*(1), 1–11. https://doi.org/10.1038/ncomms10298

Kajtez, J., Solomatina, A., Novak, M., Polak, B., Vukušić, K., Rüdiger, J., Cojoc, G., Milas, A., Šumanovac Šestak, I., Risteski, P., Tavano, F., Klemm, A. H., Roscioli, E., Welburn, J., Cimini, D., Glunčić, M., Pavin, N., & Tolić, I. M. (2016b). Overlap microtubules link sister k-fibres and balance the forces on bi-oriented kinetochores. *Nature Communications*, *7*. https://doi.org/10.1038/NCOMMS10298

Kapitein, L. C., Janson, M. E., van den Wildenberg, S. M. J. L., Hoogenraad, C. C., Schmidt, C. F., & Peterman, E. J. G. (2008). Microtubule-driven multimerization recruits ase1p onto overlapping microtubules. *Current Biology : CB*, *18*(21), 1713–1717. https://doi.org/10.1016/J.CUB.2008.09.046

Kapitein, L. C., Peterman, E. J. G., Kwok, B. H., Kim, J. H., Kapoor, T. M., & Schmidt, C. F. (2005). The bipolar mitotic kinesin Eg5 moves on both microtubules that it crosslinks. *Nature 2005 435:7038*, *435*(7038), 114–118. https://doi.org/10.1038/nature03503

Kapoor, T. M., Mayer, T. U., Coughlin, M. L., & Mitchison, T. J. (2000). Probing Spindle Assembly Mechanisms with Monastrol, a Small Molecule Inhibitor of the Mitotic Kinesin, Eg5. *The Journal of Cell Biology*, *150*(5), 975. https://doi.org/10.1083/JCB.150.5.975

Kardon, J. R., & Vale, R. D. (2009). Regulators of the cytoplasmic dynein motor. *Nature Reviews. Molecular Cell Biology*, *10*(12), 854. https://doi.org/10.1038/NRM2804

Kashina, A. S., Scholey, J. M., Leszyk, J. D., & Saxton, W. M. (1996). An essential bipolar mitotic motor. *Nature 1996 384:6606*, *384*(6606), 225–225. https://doi.org/10.1038/384225a0

Kellogg, E. H., Howes, S., Ti, S. C., Ramírez-Aportela, E., Kapoor, T. M., Chacón, P., & Nogales, E. (2016). Near-atomic cryo-EM structure of PRC1 bound to the microtubule.

Proceedings of the National Academy of Sciences of the United States of America, *113*(34), 9430–9439. https://doi.org/10.1073/PNAS.1609903113/SUPPL_FILE/PNAS.1609903113.SM01.MP4

Kiyomitsu, T., & Cheeseman, I. M. (2012). Chromosome and spindle pole-derived signals generate an intrinsic code for spindle position and orientation. *Nature Cell Biology*, *14*(3), 311. https://doi.org/10.1038/NCB2440

Kurasawa, Y., Earnshaw, W. C., Mochizuki, Y., Dohmae, N., & Todokoro, K. (2004). Essential roles of KIF4 and its binding partner PRC1 in organized central spindle midzone formation. *The EMBO Journal*, *23*(16), 3237–3248. https://doi.org/10.1038/SJ.EMBOJ.7600347

LaFountain, J. R., Cohan, C. S., Siegel, A. J., & LaFountain, D. J. (2004). Direct Visualization of Microtubule Flux during Metaphase and Anaphase in Crane-Fly Spermatocytes. *Molecular Biology of the Cell*, *15*(12), 5724. https://doi.org/10.1091/MBC.E04-08-0750

Lane, N. (2015). The unseen world: reflections on Leeuwenhoek (1677) 'Concerning little animals.' *Philosophical Transactions of the Royal Society B: Biological Sciences*, *370*(1666), 20140344. https://doi.org/10.1098/RSTB.2014.0344

Lee, K. Y., Davies, T., & Mishima, M. (2012). Cytokinesis microtubule organisers at a glance. *Journal of Cell Science*, *125*(15), 3495–3500. https://doi.org/10.1242/JCS.094672/-/DC1

Liu, M., Ran, J., & Zhou, J. (2018). Non-canonical functions of the mitotic kinesin Eg5. *Thoracic Cancer*, *9*(8), 904. https://doi.org/10.1111/1759-7714.12792

Lodish, H.E.A. et al. (2014). Molecular cell biology, 7th ed. (W. H. Freeman and Company, New York).

Lukinavičius, G., Reymond, L., D'Este, E., Masharina, A., Göttfert, F., Ta, H., Güther, A., Fournier, M., Rizzo, S., Waldmann, H., Blaukopf, C., Sommer, C., Gerlich, D. W., Arndt, H. D., Hell, S. W., & Johnsson, K. (2014). Fluorogenic probes for live-cell imaging of the cytoskeleton. *Nature Methods 2014 11:7*, *11*(7), 731–733. https://doi.org/10.1038/nmeth.2972

Maddox, P., Straight, A., Coughlin, P., Mitchison, T. J., & Salmon, E. D. (2003). Direct observation of microtubule dynamics at kinetochores in Xenopus extract spindles:

implications for spindle mechanics. *The Journal of Cell Biology*, *162*(3), 377. https://doi.org/10.1083/JCB.200301088

Maffini, S., Maia, A. R. R., Manning, A. L., Maliga, Z., Pereira, A. L., Junqueira, M., Shevchenko, A., Hyman, A., Yates, J. R., Galjart, N., Compton, D. A., & Maiato, H. (2009). Motor-Independent Targeting of CLASPs to Kinetochores by CENP-E Promotes Microtubule Turnover and Poleward Flux. *Current Biology*, *19*(18), 1566–1572. https://doi.org/10.1016/J.CUB.2009.07.059

Magidson, V., O'Connell, C. B., Lončarek, J., Paul, R., Mogilner, A., & Khodjakov, A. (2011). The spatial arrangement of chromosomes during prometaphase facilitates spindle assembly. *Cell*, *146*(4), 555. https://doi.org/10.1016/J.CELL.2011.07.012

Maiato, H., Khodjakov, A., & Rieder, C. L. (2005). Drosophila CLASP is required for the incorporation of microtubule subunits into fluxing kinetochore fibres. *Nature Cell Biology*, *7*(1), 42. https://doi.org/10.1038/NCB1207

Maiato, H., & Lince-Faria, M. (2010). The perpetual movements of anaphase. *Cellular and Molecular Life Sciences 2010 67:13*, *67*(13), 2251–2269. https://doi.org/10.1007/S00018-010-0327-5

Maiato, H., Rieder, C. L., & Khodjakov, A. (2004). Kinetochore-driven formation of kinetochore fibers contributes to spindle assembly during animal mitosis. *The Journal of Cell Biology*, *167*(5), 831. https://doi.org/10.1083/JCB.200407090

Malumbres, M. (2020). Control of the Cell Cycle. In Abeloff's Clinical Oncology N. J.E., A. J.O., K. M.B., D. J.H., and T. J.E., eds., pp. 56-73.e55.

Mann, B. J., & Wadsworth, P. (2019). Kinesin-5 Regulation and Function in Mitosis. *Trends in Cell Biology*, *29*(1), 66–79. https://doi.org/10.1016/J.TCB.2018.08.004

Matos, I., Pereira, A. J., Lince-Faria, M., Cameron, L. A., Salmon, E. D., & Maiato, H. (2009). Synchronizing chromosome segregation by flux-dependent force equalization at kinetochores. *The Journal of Cell Biology*, *186*(1), 11. https://doi.org/10.1083/JCB.200904153

Mazumdar, M., & Misteli, T. (2005). Chromokinesins: multitalented players in mitosis. *Trends in Cell Biology*, *15*(7), 349–355. https://doi.org/10.1016/J.TCB.2005.05.006

Mazumdar, M., Sundareshan, S., & Misteli, T. (2004). Human chromokinesin KIF4A functions in chromosome condensation and segregation. *The Journal of Cell Biology*, *166*(5), 613–620. https://doi.org/10.1083/JCB.200401142

McDonald, K. L., O'Toole, E. T., Mastronarde, D. N., & McIntosh, J. R. (1992). Kinetochore microtubules in PTK cells. *The Journal of Cell Biology*, *118*(2), 369. https://doi.org/10.1083/JCB.118.2.369

McEwen, B. F., Heagle, A. B., Cassels, G. O., Buttle, K. F., & Rieder, C. L. (1997). Kinetochore Fiber Maturation in PtK1 Cells and Its Implications for theMechanisms of Chromosome Congression and Anaphase Onset. *The Journal of Cell Biology*, *137*(7), 1567. https://doi.org/10.1083/JCB.137.7.1567

McIntosh, J. R., Hepler, P. K., & Van Wie, D. G. (1969). Model for Mitosis. *Nature*, *224*(5220), 659–663. https://doi.org/10.1038/224659A0

McIntosh, J. Richard, Molodtsov, M. I., & Ataullakhanov, F. I. (2012). Biophysics of mitosis. *Quarterly Reviews of Biophysics*, *45*(2), 147–207. https://doi.org/10.1017/S0033583512000017

Mitchison, T., Evans, L., Schulze, E., & Kirschner, M. (1986). Sites of microtubule assembly and disassembly in the mitotic spindle. *Cell*, *45*(4), 515–527. https://doi.org/10.1016/0092-8674(86)90283-7

Mitchison, T. J. (1989). Polewards microtubule flux in the mitotic spindle: evidence from photoactivation of fluorescence. *The Journal of Cell Biology*, *109*(2), 637. https://doi.org/10.1083/JCB.109.2.637

Mitchison, T. J. (2005). Mechanism and function of poleward flux in Xenopus extract meiotic spindles. *Philosophical Transactions of the Royal Society B: Biological Sciences*, *360*(1455), 623. https://doi.org/10.1098/RSTB.2004.1616

Mitchison, T. J., Maddox, P., Gaetz, J., Groen, A., Shirasu, M., Desai, A., Salmon, E. D., & Kapoor, T. M. (2005). Roles of Polymerization Dynamics, Opposed Motors, and a Tensile Element in Governing the Length of Xenopus Extract Meiotic Spindles. *Molecular Biology of the Cell*, *16*(6), 3064. https://doi.org/10.1091/MBC.E05-02-0174

Mitchison, T., & Kirschner, M. (1984). Dynamic instability of microtubule growth. *Nature 1984 312:5991*, *312*(5991), 237–242. https://doi.org/10.1038/312237a0

Miyamoto, D. T., Perlman, Z. E., Burbank, K. S., Groen, A. C., & Mitchison, T. J. (2004a). The kinesin Eg5 drives poleward microtubule flux in Xenopus laevis egg extract spindles. *The Journal of Cell Biology*, *167*(5), 813. https://doi.org/10.1083/JCB.200407126

Miyamoto, D. T., Perlman, Z. E., Burbank, K. S., Groen, A. C., & Mitchison, T. J. (2004b).

The kinesin Eg5 drives poleward microtubule flux in Xenopus laevis egg extract spindles. *The Journal of Cell Biology*, *167*(5), 813. https://doi.org/10.1083/JCB.200407126

Mollinari, C., Kleman, J. P., Jiang, W., Schoehn, G., Hunter, T., & Margolis, R. L. (2002). PRC1 is a microtubule binding and bundling protein essential to maintain the mitotic spindle midzone. *Journal of Cell Biology*, *157*(7), 1175–1186. https://doi.org/10.1083/jcb.200111052

Musacchio, A., & Desai, A. (2017). A Molecular View of Kinetochore Assembly and Function. *Biology 2017, Vol. 6, Page 5*, *6*(1), 5. https://doi.org/10.3390/BIOLOGY6010005

Musacchio, A., & Salmon, E. D. (2007). The spindle-assembly checkpoint in space and time. *Nature Reviews Molecular Cell Biology 2007 8:5*, *8*(5), 379–393. https://doi.org/10.1038/nrm2163

Neahring, L., Cho, N. H., & Dumont, S. (2021). Opposing motors provide mechanical and functional robustness in the human spindle. *Developmental Cell*, *56*(21), 3006-3018.e5. https://doi.org/10.1016/J.DEVCEL.2021.09.011

Nixon, F. M., Gutiérrez-Caballero, C., Hood, F. E., Booth, D. G., Prior, I. A., & Royle, S. J. (2015). The mesh is a network of microtubule connectors that stabilizes individual kinetochore fibers of the mitotic spindle. *ELife*, *4*(JUNE2015). https://doi.org/10.7554/ELIFE.07635

O'Toole, E., Morphew, M., & Richard McIntosh, J. (2020). Electron tomography reveals aspects of spindle structure important for mechanical stability at metaphase. *Molecular Biology of the Cell*, *31*(3), 184–195. https://doi.org/10.1091/MBC.E19-07-0405/ASSET/IMAGES/LARGE/MBC-31-184-G008.JPEG

Ohi, H., Fujita, Y., Miyao, M., Saguchi, K. I., Murayama, N., & Higuchi, S. (2003). Molecular cloning and expression analysis of the aryl hydrocarbon receptor of Xenopus laevis. *Biochemical and Biophysical Research Communications*, *307*(3), 595–599. https://doi.org/10.1016/S0006-291X(03)01244-0

ÖSTERGREN, G. (1951). THE MECHANISM OF CO-ORIENTATION IN BIVALENTS AND MULTIVALENTS: THE THEORY OF ORIENTATION BY PULLING. *Hereditas*, *37*(1–2), 85–156. https://doi.org/10.1111/J.1601-5223.1951.TB02891.X

Pavin, N., & Toli´ctoli´c, I. M. (2016). *Self-Organization and Forces in the Mitotic Spindle*.

https://doi.org/10.1146/annurev-biophys-062215-010934

Pellman, D., Bagget, M., Tu, H., & Fink, G. R. (1995). Two microtubule-associated proteins required for anaphase spindle movement in Saccharomyces cerevisiae [published erratum appears in J Cell Biol 1995 Oct;131(2):561]. *The Journal of Cell Biology*, *130*(6), 1373. https://doi.org/10.1083/JCB.130.6.1373

Pfarr, C. M., Coue, M., Grissom, P. M., Hays, T. S., Porter, M. E., & McIntosh, J. R. (1990). Cytoplasmic dynein is localized to kinetochores during mitosis. *Nature 1990 345:6272*, *345*(6272), 263–265. https://doi.org/10.1038/345263a0

Pfister, K. K., Shah, P. R., Hummerich, H., Russ, A., Cotton, J., Annuar, A. A., King, S. M., & Fisher, E. M. C. (2006). Genetic Analysis of the Cytoplasmic Dynein Subunit Families. *PLOS Genetics*, *2*(1), e1. https://doi.org/10.1371/JOURNAL.PGEN.0020001

Polak, B., Risteski, P., Lesjak, S., & Tolić, I. M. (2017). PRC 1-labeled microtubule bundles and kinetochore pairs show one-to-one association in metaphase . *EMBO Reports*, *18*(2), 217–230. https://doi.org/10.15252/embr.201642650

Powers, J., Rose, D. J., Saunders, A., Dunkelbarger, S., Strome, S., & Saxton, W. M. (2004). Loss of KLP-19 polar ejection force causes misorientation and missegregation of holocentric chromosomes. *The Journal of Cell Biology*, *166*(7), 991. https://doi.org/10.1083/JCB.200403036

Raaijmakers, J. A., & Medema, R. H. (2014). Function and regulation of dynein in mitotic chromosome segregation. *Chromosoma*, *123*(5), 407–422. https://doi.org/10.1007/S00412-014-0468-7/METRICS

Raaijmakers, Jonne A., Tanenbaum, M. E., & Medema, R. H. (2013). Systematic dissection of dynein regulators in mitosis. *The Journal of Cell Biology*, *201*(2), 201–215. https://doi.org/10.1083/JCB.201208098

Rath, O., & Kozielski, F. (2012). Kinesins and cancer. *Nature Reviews Cancer 2012 12:8*, *12*(8), 527–539. https://doi.org/10.1038/nrc3310

Renda, F., Pellacani, C., Strunov, A., Bucciarelli, E., Naim, V., Bosso, G., Kiseleva, E., Bonaccorsi, S., Sharp, D. J., Khodjakov, A., Gatti, M., & Somma, M. P. (2017). The Drosophila orthologue of the INT6 onco-protein regulates mitotic microtubule growth and kinetochore structure. *PLOS Genetics*, *13*(5), e1006784. https://doi.org/10.1371/JOURNAL.PGEN.1006784

Richard Mcintosh, J. (2016). Mitosis. *Cold Spring Harbor Perspectives in Biology*, *8*(9).

https://doi.org/10.1101/CSHPERSPECT.A023218

Rieder, C. L., & Salmon, E. D. (n.d.). *Mini-Review Motile Kinetochores and Polar Ejection Forces Dictate Chromosome Position on the Vertebrate Mitotic Spindle*.

Risteski, P., Božan, D., Jagrić, M., Bosilj, A., Pavin, N., & Tolić, I. M. (2022). Length-dependent poleward flux of sister kinetochore fibers promotes chromosome alignment. *Cell Reports*, *40*(5), 111169. https://doi.org/10.1016/J.CELREP.2022.111169

Rogers, G. C., Rogers, S. L., Schwimmer, T. A., Ems-McClung, S. C., Walczak, C. E., Vale, R. D., Scholey, J. M., & Sharp, D. J. (2003). Two mitotic kinesins cooperate to drive sister chromatid separation during anaphase. *Nature 2004 427:6972*, *427*(6972), 364–370. https://doi.org/10.1038/nature02256

Rogers, G. C., Rogers, S. L., Schwimmer, T. A., Ems-McClung, S. C., Walczak, C. E., Vale, R. D., Scholey, J. M., & Sharp, D. J. (2004). Two mitotic kinesins cooperate to drive sister chromatid separation during anaphase. *Nature*, *427*(6972), 364–370. https://doi.org/10.1038/NATURE02256

Rogers, G. C., Rogers, S. L., & Sharp, D. J. (2005). Spindle microtubules in flux. *Journal of Cell Science*, *118*(Pt 6), 1105–1116. https://doi.org/10.1242/JCS.02284

Sacristan, C., & Kops, G. J. P. L. (2015). *Joined at the hip: kinetochores, microtubules, and spindle assembly checkpoint signaling*. https://doi.org/10.1016/j.tcb.2014.08.006

Saunders, W. S., & Hoyt, M. A. (1992). Kinesin-related proteins required for structural integrity of the mitotic spindle. *Cell*, *70*(3), 451–458. https://doi.org/10.1016/0092-8674(92)90169-D

Sawin, K. E., Mitchison, T. J., & Wordeman, L. G. (1992). Evidence for kinesin-related proteins in the mitotic apparatus using peptide antibodies. *Journal of Cell Science*, *101*(2), 303–313. https://doi.org/10.1242/JCS.101.2.303

Sawin, Kenneth E., & Mitchison, T. J. (1995). Mutations in the kinesin-like protein Eg5 disrupting localization to the mitotic spindle. *Proceedings of the National Academy of Sciences*, *92*(10), 4289–4293. https://doi.org/10.1073/PNAS.92.10.4289

Scholey, J. M., Civelekoglu-Scholey, G., & Brust-Mascher, I. (2016). Anaphase B. *Biology 2016, Vol. 5, Page 51*, *5*(4), 51. https://doi.org/10.3390/BIOLOGY5040051

Sekine, Y., Okada, Y., Noda, Y., Kondo, S., Aizawa, H., Takemura, R., & Hirokawa, N. (1994). A novel microtubule-based motor protein (KIF4) for organelle transports, whose expression is regulated developmentally. *The Journal of Cell Biology*, *127*(1), 187.

https://doi.org/10.1083/JCB.127.1.187

Sharp, D. J., McDonald, K. L., Brown, H. M., Matthies, H. J., Walczak, C., Vale, R. D., Mitchison, T. J., & Scholey, J. M. (1999). The bipolar kinesin, KLP61F, cross-links microtubules within interpolar microtubule bundles of Drosophila embryonic mitotic spindles. *The Journal of Cell Biology*, *144*(1), 125–138. https://doi.org/10.1083/JCB.144.1.125

Sharp, D. J., Rogers, G. C., & Scholey, J. M. (2000). Microtubule motors in mitosis. *Nature*, *407*(6800), 41–47. https://doi.org/10.1038/35024000

She, Z. Y., Wei, Y. L., Lin, Y., Li, Y. L., & Lu, M. H. (2019). Mechanisms of the Ase1/PRC1/MAP65 family in central spindle assembly. *Biological Reviews*, *94*(6), 2033–2048. https://doi.org/10.1111/BRV.12547

She, Z. Y., & Yang, W. X. (2017). Molecular mechanisms of kinesin-14 motors in spindle assembly and chromosome segregation. *Journal of Cell Science*, *130*(13), 2097–2110. https://doi.org/10.1242/JCS.200261

Sikirzhytski, V., Magidson, V., Steinman, J. B., He, J., Le Berre, M., Tikhonenko, I., Ault, J. G., McEwen, B. F., Chen, J. K., Sui, H., Piel, M., Kapoor, T. M., & Khodjakov, A. (2014). Direct kinetochore–spindle pole connections are not required for chromosome segregation. *The Journal of Cell Biology*, *206*(2), 231. https://doi.org/10.1083/JCB.201401090

Skoufias, D. A., DeBonis, S., Saoudi, Y., Lebeau, L., Crevel, I., Cross, R., Wade, R. H., Hackney, D., & Kozielski, F. (2006). S-Trityl-L-cysteine Is a Reversible, Tight Binding Inhibitor of the Human Kinesin Eg5 That Specifically Blocks Mitotic Progression. *Journal of Biological Chemistry*, *281*(26), 17559–17569. https://doi.org/10.1074/JBC.M511735200

Steblyanko, Y., Rajendraprasad, G., Osswald, M., Eibes, S., Jacome, A., Geley, S., Pereira, A. J., Maiato, H., & Barisic, M. (2020a). Microtubule poleward flux in human cells is driven by the coordinated action of four kinesins. *The EMBO Journal*, *39*(23), e105432. https://doi.org/10.15252/EMBJ.2020105432

Steblyanko, Y., Rajendraprasad, G., Osswald, M., Eibes, S., Jacome, A., Geley, S., Pereira, A. J., Maiato, H., & Barisic, M. (2020b). Microtubule poleward flux in human cells is driven by the coordinated action of four kinesins. *The EMBO Journal*, *39*(23). https://doi.org/10.15252/EMBJ.2020105432

Steuer, E. R., Wordeman, L., Schroer, T. A., & Sheetz, M. P. (1990). Localization of cytoplasmic dynein to mitotic spindles and kinetochores. *Nature 1990 345:6272*, *345*(6272), 266–268. https://doi.org/10.1038/345266a0

Straight, A. F., Sedat, J. W., & Murray, A. W. (1998). Time-Lapse Microscopy Reveals Unique Roles for Kinesins during Anaphase in Budding Yeast. *The Journal of Cell Biology*, *143*(3), 687. https://doi.org/10.1083/JCB.143.3.687

Sturgill, E. G., Das, D. K., Takizawa, Y., Shin, Y., Collier, S. E., Ohi, M. D., Hwang, W., Lang, M. J., & Ohi, R. (2014). Kinesin-12 Kif15 Targets Kinetochore Fibers through an Intrinsic Two-Step Mechanism. *Current Biology*, *24*(19), 2307–2313. https://doi.org/10.1016/J.CUB.2014.08.022

Subramanian, R., Ti, S. C., Tan, L., Darst, S. A., & Kapoor, T. M. (2013). Marking and measuring single microtubules by PRC1 and kinesin-4. *Cell*, *154*(2), 377. https://doi.org/10.1016/J.CELL.2013.06.021

Subramanian, R., Wilson-Kubalek, E. M., Arthur, C. P., Bick, M. J., Campbell, E. A., Darst, S. A., Milligan, R. A., & Kapoor, T. M. (2010). Insights into Antiparallel Microtubule Crosslinking by PRC1, a Conserved Nonmotor Microtubule Binding Protein. *Cell*, *142*(3), 433–443. https://doi.org/10.1016/J.CELL.2010.07.012

Tanenbaum, M. E., Macůrek, L., Galjart, N., & Medema, R. H. (2008). Dynein, Lis1 and CLIP-170 counteract Eg5-dependent centrosome separation during bipolar spindle assembly. *The EMBO Journal*, *27*(24), 3235–3245. https://doi.org/10.1038/EMBOJ.2008.242

Tanenbaum, M. E., Macůrek, L., Janssen, A., Geers, E. F., Alvarez-Fernández, M., & Medema, R. H. (2009). Kif15 Cooperates with Eg5 to Promote Bipolar Spindle Assembly. *Current Biology*, *19*(20), 1703–1711. https://doi.org/10.1016/J.CUB.2009.08.027

Tanenbaum, M. E., & Medema, R. H. (2010a). Mechanisms of centrosome separation and bipolar spindle assembly. *Developmental Cell*, *19*(6), 797–806. https://doi.org/10.1016/J.DEVCEL.2010.11.011

Tanenbaum, M. E., & Medema, R. H. (2010b). Mechanisms of Centrosome Separation and Bipolar Spindle Assembly. *Developmental Cell*, *19*(6), 797–806. https://doi.org/10.1016/J.DEVCEL.2010.11.011

Tanenbaum, M. E., Vale, R. D., & McKenney, R. J. (2013). Cytoplasmic dynein crosslinks

and slides anti-parallel microtubules using its two motor domains. *ELife*, *2013*(2). https://doi.org/10.7554/ELIFE.00943

Tolić, I. M. (2018). Mitotic spindle: kinetochore fibers hold on tight to interpolar bundles. *European Biophysics Journal : EBJ*, *47*(3), 191–203. https://doi.org/10.1007/S00249-017-1244-4

Trupinić, M., Kokanović, B., Ponjavić, I., Barišić, I., Šegvić, S., Ivec, A., & Tolić, I. M. (2022). The chirality of the mitotic spindle provides a mechanical response to forces and depends on microtubule motors and augmin. *Current Biology*, *32*(11), 2480. https://doi.org/10.1016/J.CUB.2022.04.035

Uzman, A., Lodish, H., Berk, A., Zipursky, L., & Baltimore, D. (2000). Molecular Cell Biology (4th edition) New York, NY, 2000, ISBN 0-7167-3136-3. *Biochemistry and Molecular Biology Education*, *29*(3), Section 1.2The Molecules of Life. https://doi.org/10.1016/S1470-8175(01)00023-6

Valentine, M. T., Fordyce, P. M., Krzysiak, T. C., Gilbert, S. P., & Block, S. M. (2006). Individual dimers of the mitotic kinesin motor Eg5 step processively and support substantial loads in vitro. *Nature Cell Biology*, *8*(5), 470. https://doi.org/10.1038/NCB1394

vanHeesbeen, R. G. H. P., Tanenbaum, M. E., & Medema, R. H. (2014). Balanced Activity of Three Mitotic Motors Is Required for Bipolar Spindle Assembly and Chromosome Segregation. *Cell Reports*, *8*(4), 948–956. https://doi.org/10.1016/J.CELREP.2014.07.015

Vanneste, D., Takagi, M., Imamoto, N., & Vernos, I. (2009). The Role of Hklp2 in the Stabilization and Maintenance of Spindle Bipolarity. *Current Biology*, *19*(20), 1712–1717. https://doi.org/10.1016/J.CUB.2009.09.019

Varma, D., Monzo, P., Stehman, S. A., & Vallee, R. B. (2008). Direct role of dynein motor in stable kinetochore-microtubule attachment, orientation, and alignment. *The Journal of Cell Biology*, *182*(6), 1045. https://doi.org/10.1083/JCB.200710106

Vernos, I., Raats, J., Hirano, T., Heasman, J., Karsenti, E., & Wylie, C. (1995). *Xklpl, a Chromosomal Xenopus Kinesin-like Protein Essential for Spindle Organization and Chromosome Positioning 3Institute for Human Genetics 6Departments of Cell Biology and Neuroanatomy 8Department of Pediatrics*. *81*, 117–127.

Vukušić, K., Buđa, R., Bosilj, A., Milas, A., Pavin, N., & Tolić, I. M. (2017). Microtubule

Sliding within the Bridging Fiber Pushes Kinetochore Fibers Apart to Segregate Chromosomes. *Developmental Cell*, *43*(1), 11-23.e6. https://doi.org/10.1016/j.devcel.2017.09.010

Vukušić, K., Ponjavić, I., Buđa, R., Risteski, P., & Tolić, I. M. (2021). Microtubule-sliding modules based on kinesins EG5 and PRC1-dependent KIF4A drive human spindle elongation. *Developmental Cell*, *56*(9), 1253-1267.e10. https://doi.org/10.1016/J.DEVCEL.2021.04.005

Waitzman, J. S., & Rice, S. E. (2014). Mechanism and Regulation of Kinesin-5, an essential motor for the mitotic spindle. *Biology of the Cell / under the Auspices of the European Cell Biology Organization*, *106*(1), 1. https://doi.org/10.1111/BOC.201300054

Walczak, C. E., Cai, S., & Khodjakov, A. (2010). Mechanisms of chromosome behaviour during mitosis. *Nature Reviews. Molecular Cell Biology*, *11*(2), 91. https://doi.org/10.1038/NRM2832

Wang, S. Z., & Adler, R. (1995). Chromokinesin: a DNA-binding, kinesin-like nuclear protein. *The Journal of Cell Biology*, *128*(5), 761–768. https://doi.org/10.1083/JCB.128.5.761

Waterman-Storer, C. M., & Salmon, E. D. (1998). How microtubules get fluorescent speckles. *Biophysical Journal*, *75*(4), 2059. https://doi.org/10.1016/S0006-3495(98)77648-9

Waters, J. C., & Salmon, E. D. (1997). Pathways of spindle assembly. *Current Opinion in Cell Biology*, *9*(1), 37–43. https://doi.org/10.1016/S0955-0674(97)80149-4

Wayne, R. (2010). In Plant Cell Biology, R. Wayne, ed. (Academic Press), pp. 319-338.

Wendell, K. L., Wilson, L., & Jordan, M. A. (1993). Mitotic block in HeLa cells by vinblastine: Ultrastructural changes in kinetochore-mcirotubule attachment and in centrosomes. *Journal of Cell Science*, *104*(2), 261–274.

Wiese, C., & Zheng, Y. (2006). Microtubule nucleation: γ-tubulin and beyond. *Journal of Cell Science*, *119*(20), 4143–4153. https://doi.org/10.1242/JCS.03226

Yanagida, M. (2014). The Role of Model Organisms in the History of Mitosis Research. *Cold Spring Harbor Perspectives in Biology*, *6*(9), a015768. https://doi.org/10.1101/CSHPERSPECT.A015768

Yu, C. H., Redemann, S., Wu, H. Y., Kiewisz, R., Yoo, T. Y., Conway, W., Farhadifar, R., Müller-Reichert, T., & Needleman, D. (2019). A Highlights from MBoC Selection:

Central-spindle microtubules are strongly coupled to chromosomes during both anaphase A and anaphase B. *Molecular Biology of the Cell*, *30*(19), 2503. https://doi.org/10.1091/MBC.E19-01-0074

Zhou, Q., Lee, K. J., Kurasawa, Y., Hu, H., An, T., & Li, Z. (2018). Faithful chromosome segregation in Trypanosoma brucei requires a cohort of divergent spindle-associated proteins with distinct functions. *Nucleic Acids Research*, *46*(16), 8216–8231. https://doi.org/10.1093/NAR/GKY557

Zhu, C., & Jiang, W. (2005). Cell cycle-dependent translocation of PRC1 on the spindle by Kif4 is essential for midzone formation and cytokinesis. *Proceedings of the National Academy of Sciences of the United States of America*, *102*(2), 343–348. https://doi.org/10.1073/PNAS.0408438102

Zhu, C., Lau, E., Schwarzenbacher, R., Bossy-Wetzel, E., & Jiang, W. (2006). Spatiotemporal control of spindle midzone formation by PRC1 in human cells. *Proceedings of the National Academy of Sciences of the United States of America*, *103*(16), 6196. https://doi.org/10.1073/PNAS.0506926103

8 AUTHOR BIOGRAPHY

Ivana Ponjavić graduated in Education of Biology and Chemistry from the Department of Biology at the Faculty of Science in Zagreb in 2018. Before starting her PhD research under the supervision of prof, Iva M Tolić at the Laboratory of Cell Biophysics, Division of Molecular Biology, Ruđer Bošković Institute, Ivana was a research intern in the same lab since 2017. In 2019 she has enrolled in the postgraduate study of Biology at Faculty of Science, University of Zagreb. During her research career, Ivana published two first/co-first authored papers (Ponjavić et al., *Methods in Cell Biology* 2020; Vukušić, Ponjavić et al., *Dev Cell* 2021) and one co-authored paper (Trupinić et al., *Curr Biol* 2022). She participated in 3 international conferences as a first author on posters (*Mitotic Spindle: From Living and Synthetic Systems to Theory,* 2019*, EMBO / EMBL Symposium: Microtubules: From Atoms to Complex Systems Heidelberg, Njemačka,* 2020 and *Mitotic Spindle: From Living and Synthetic Systems to Theory,* 2023). During her research career she participated in several events related to popularization of science such as *Znanost u prolazu,* 2022, *Znanost za mlade u Vukovaru,* 2022, *Bioteka* workshop, 2022, *Open days of Ruđer Bošković Institute,* 2022.

Publications:

1. Ponjavić, Ivana; Vukušić, Kruno; Tolić, Iva M. Expansion microscopy of the mitotic spindle. *Methods Cell Biol*, 161:247-274. (2021)
2. Vukušić, Kruno*; Ponjavić, Ivana*; Buđa, Renata; Risteski, Patrik; Tolić, Iva M. Microtubule-sliding modules based on kinesins EG5 and PRC1-dependent KIF4A drive human spindle elongation. *Dev Cell*. 56(9):1253-1267. (2021)
3. Trupinić, Monika; Kokanović, Barbara; Ponjavić, Ivana; Barišić, Ivan; Šegvić, Siniša; Ivec, Arian; Tolić, Iva M. The chirality of the mitotic spindle provides a mechanical response to forces and depends on microtubule motors and augmin. *Curr Biol,* 32:2480-2493. (2022)

* These authors contributed equally.